SYNTHESIS AND CHARACTERIZATION OF Mg-Al-LAYERED DOUBLE HYDROXIDES INTERCALATED BY BORATE ANIONS

BORAT ANYONLARI İÇEREN Mg-Al-TABAKALI ÇİFT HİDROKSİTLERİN SENTEZİ VE KARAKTERİZASYONU

AHMET NEDİM AY

Submitted to Institute of Sciences of
Hacettepe University as a partial fullfilment
to the requirements for the award of the degree of
DOCTOR OF PHILOSOPHY
in
CHEMISTRY

2007

Graduated School of Natural and Applied Sciences,

This is to certify that we have read this thesis and that in our opinion it is fully adequate, in scope and quality, as a thesis for degree of **Doctor of Philosophy** in **Chemistry**.

Head : .....
Prof. Dr. Yavuz İMAMOĞLU

Member : .....
Prof. Dr. Saim ÖZKAR

Member (Advisor) : .....
Prof. Dr. Birgül KARAN

Member : .....
Prof. Dr. Abidin TEMEL

Member : .....
Assoc. Prof. Dr. Nurşen ALTUNTAŞ ÖZTAŞ

APPROVAL

This thesis has been certified as a thesis for the Degree of Doctor of Philosophy by the above Examining Committee Members on ...../...../2007.

...../...../2007
Prof. Dr. Erdem YAZGAN
Director of the Graduate School of
Natural and Applied Sciences

BORAT ANYONLARI İÇEREN Mg-Al-TABAKALI ÇİFT HİDROKSİTLERİN SENTEZİ VE KARAKTERİZASYONU

Ahmet Nedim Ay

ÖZET

Doktora tezi olarak hazırlanan bu çalışmada; birlikte çöktürme, iyon-değişimi ve havanda öğütme yöntemleriyle sentezlenen tabakalı çift hidroksitlere (TÇH) borat anyonlarının tutuklanabilirliği incelenmiştir. Elde edilen ürünlerin yapısal özellikleri toz X-ışınları kırınımı, FTIR, ^{11}B MAS NMR, ^{27}Al NMR ve ^{13}C MAS NMR yöntemleri ile; ısısal kararlılıkları TGA/DTA yöntemleri ile ve yüzey özellikleri ise yüzey alan ölçümü, taramalı elektron mikroskop teknikleri ile karakterize edilmiştir.

Anyonik killer sınıfına giren bu sentetik TÇH lerin, borik asit ve amonyum tetraborat çözeltilerindeki borlu anyonların tutuklanması için uygun malzemeler olduğu anlaşılmıştır. En iyi kristal yapısına sahip borlu TÇH yapılarının tetraborat çözeltilerinden iyon-değişimi tekniği kullanılarak hazırlanabileceği bulunmuştur. Borik asit çözeltilerindeki borlu anyonların, tabakalar arasındaki boşlukta pH a bağlı olmaksızın poliborat iyonlarına dönüştüğü ilk kez gösterilmiştir.

Basit bir mekanokimyasal yöntem olarak ilk kez geliştirilen havanda öğütme yöntemiyle hazırlanan TÇH lerin klasik yöntemler ile hazırlanan TÇH ler ile aynı özellikleri taşıdığı bulunmuştur. Çevre dostu bir yöntem olarak sunulan bu yöntem ile elde edilen TÇH ler, borat anyonlarının tabakalar arasına tutuklanmasında başarıyla kullanılmıştır. Çözücü, ısı ve inert atmosfer gerektirmeyen bu yöntem, gelecekte daha geniş uygulama alanları bulabilecektir.

Nitratlı-TÇH lerin, borlu suların arıtılması amacıyla kullanılabilirliği araştırılmıştır. Karbondioksit içermeyen ortamda hazırlanan, yüksek anyon değişim kapasitesine sahip TÇH ler ile %95'den fazla adsorpsiyon değerine ulaşılmıştır. Bor adsorpsiyonu mekanizmasının, yüzey adsorbsiyonu yerine borlu anyonların nitrat iyonları ile yer değiştirerek tabakalar arasında hapsedilmesi şeklinde olduğu gösterilmiştir.

Anahtar Kelimeler: Tabakalı Çift Hidroksitler, Bor, Borat, Tutuklanma, Kalsinasyon, Hidrotalsit, Anyonik Killer.

Danışman: Prof. Dr. Birgül Karan, Hacettepe Universitesi, Fen Fakültesi, Kimya Bölümü, Anorganik Kimya Anabilim Dalı

SYNTHESIS AND CHARACTERIZATION OF Mg-Al-LAYERED DOUBLE HYDROXIDES INTERCALATED BY BORATE ANIONS

Ahmet Nedim Ay

ABSTRACT

In this study presented as a PhD thesis, the intercalation of borate anions into layered double hydroxides (LDHs) synthesized by co-precipitation, ion-exchange and manual grinding in a mortar were studied. The structural properties of the products were characterized by PXRD, FTIR, ^{11}B MAS NMR, ^{27}Al NMR and ^{13}C MAS NMR techniques, thermal properties were analyzed by TGA/DTA and surface properties were investigated by BET surface area measurements and SEM images.

These synthetic LDHs, that belong to the class of anionic clays, have been demonstrated as suitable host materials for the intercalation of borate anions from boric acid and ammonium tetraborate solutions. Well-crystalline borate-intercalated LDHs were obtained from tetraborate solutions by ion-exchange. The borate ions present in boric acid solutions, were shown to transform pH-independently into polyborate species, in the interlayer space, for the first time.

The LDHs prepared by simply grinding the reactants in a mortar, presented as a novel method in this work, were found to possess the same characteristic properties as with the LDHs prepared by classical methods. This environment-friendly method, was successfully applied in the intercalation of borate anions. The method without the needs of a solvent, heat nor inert atmosphere will find potential features for future applications.

Nitrate-LDHs were examined for their usage in the treatment of boronated waters. More than 95 % adsorption could be achieved by using a carbonate-free, Mg-Al-NO_3-LDH with a high anion exchange capacity. The boron uptake mechanism was shown to proceed via intercalation of borate anions by exchanging with the interlayer nitrate ions rather than surface adsorption.

Keywords: Layered Double Hydroxides, Boron, Borate, Intercalation, Calcination, Hydrotalcite, Anionic Clays.

Advisor: Prof. Dr. Birgül Karan, Hacettepe University, Faculty of Science, Department of Chemistry, Inorganic Chemistry Division

ACKNOWLEDGEMENT

I would like to express my gratitude to Prof. Dr. Birgül Karan for her everending guidance and motivation throughout my studies.

I would like to thank to Turkish Scientific and Technological Research Center for granting me a research fellowship in Salamanca and Aveiro Universities. I particularly thank to Prof. Dr. Vicente Rives and Prof. Dr. Margarita del Arco from Salamanca University, Spain; to Prof. Dr. Joao Rocha and Dr. Luis Mafra from Aveiro University, Portugal for providing me their laboratory equipments; and to Prof. Dr. Abidin Temel from Hacettepe University for the extensive PXRD analyses.

I would like to thank to Hacettepe University Scientific Research Unit for funding part of this work.

I am also thankful to all the members of Inorganic Chemistry Division for their cooperativeness and for the friendly working atmosphere.

I wish to express my sincere thanks to my colleagues Barış Temelli, Halil Erdoğan, Sertan Aytaç, Ömer Faruk Öztürk and Dursun Ali Köse for their helps during my studies.

I would like to thank to Prof.Dr. Canan Ünaleroğlu for her kind interest in my work and for providing me her laboratory facilities.

I would like to thank to Prof. Dr. Filiz Ercan for some PXRD analysis, to Evren Çubukçu for collecting SEM images and to Dr. Abdullah Obut for the BET measurements.

My great gratitude and appreciations are devoted to my wife M.D. Saime Ay, my parents Emine and Hamit Ay, and my sister Afife Arslan for their love, encouragement and patience.

dedicated to my family...

aileme...

CONTENTS

FIGURES

TABLES

SCHEMES

ABREVIATIONS

AD	Adipic Acid
BA	Boric Acid
BET	Brunauer-Emmett-Teller
CA-LDH	Calcined LDH
DrTGA	Derivative Thermal Gravimetric Analysis
DTA	Differential Thermal Analysis
FTIR	Fourier Transform Infrared Spectroscopy
HT	Hydrotalcite
ICP-OES	Inductively Coupled Plasma Optical Emission Spectrometer
LDH	Layered Double Hydroxide
LDHs	Layered Double Hydroxides
MAS NMR	Magic Angle Spinning Nuclear Magnetic Resonance
MQ MAS NMR	Multiple-Quantum Magic Angle Spinning Nuclear Magnetic Resonance
PILC	Pillared Clay
PXRD	Powder X-Ray Diffraction
SEM	Scanning Electron Microscopy
TB	Tetra Borate Anion
TÇH	Tabakalı Çift Hidroksit
TGA	Thermal Gravimetric Analysis
XRD	X-Ray Diffraction
2D	Two-dimentional

1. INTRODUCTION

The synthesis and characterization of synthetic inorganic materials with well-defined cavities and surfaces may create new opportunities to solve today's environmental and industrial problems. The open-framework structures can adsorb a wide variety of organic molecules on their intracrystalline surfaces where organic transformations can occur with unique efficiency into specific reaction products. In addition, they exhibit adsorption and ion-exchange properties useful for a range of advanced technological processes, including environmental pollution control, the design of new structural composites and novel electronic, optical and magnetic devices.

Owing to their nanoscale periodicity, ionic lamellar solids give rise to very large intracrystalline surface areas of several hundred square meters per gram or more. In several classes of lamellar solids, layered double hydroxides are of particular interest since they qualitatively resemble the conventional intercalation compounds but with complete charge separation between gallery ions and layers which is a distinguishing feature of their structure. Since Karl Fredenhagen and Gustav Cadenbach described the uptake of potassium vapour into graphite in 1926, intercalation reactions have fascinated inorganic, organic and organometallic chemists and to date thousands of scientific papers have been published describing the synthesis, reactivity and physical characteristics of inorganic intercalation compounds. Numerous nanoporous materials can be prepared in which the chemical functionality is designed into the layered host, the intercalated guest, or both. This flexibility in synthetic strategy greatly extends the compositional diversity of layered double hydroxides for a variety of materials applications.

This study focuses on the preparation and complete characterization of layered double hydroxides intercalated with borate ions by adapting mild mechanochemical and solvothermal methods. The motivation of the choice of the topic comes from the current interest in miscellaneous applications of boron containing materials and also its potential importance for Turkey. The main point of the present work is to supply information to the scientific arena on the preparation

and characterization of borate-intercalated Mg,Al-layered double hydroxides. The investigations carried on the boron uptake behavior and mechanism of the synthesized materials may additionally provide insight into the evaluation of aqueous boron wastes.

2. GENERAL INFORMATION

Layered double hydroxides (LDH's), also known as anionic clays, are a family of synthetic compounds that have attracted considerable attention in recent years because of their interesting properties and potential applications. The structure of most of them corresponds to that of the mineral hydrotalcite. Hydrotalcite (HT), is a natural magnesium-aluminum hydroxycarbonate, $Mg_6Al_2(OH)_{16}CO_3.4H_2O$, that can be easily ground to a white powder similar to talc. Partial Mg^{2+}/Al^{3+} substitution in the structure gives rise to positively charged layers that are neutralized by carbonate anions located between the layers together with the water molecules. The electric charge of the layers and the interlayer ions are just the opposite that found in silicate clays (cationic clays), and therefore these materials are usually known as "layered double hydroxides", "anionic clays" or "hydotalcite-like materials".

2.1. Hydrotalcite-Like LDHs

HT was first discovered in Sweden around 1842 and this discovery was followed in time with other mixed hydroxycarbonates. The name "layered double hydroxide" is derived from the early works of Feitknecht and Gerber (1942) who hypothesized a structure with intercalated hydroxide layers but this idea was refuted by Allmann (1968; 1970) and Taylor (1969) with the X-ray analysis that the two cations are localized in the same layer and only the carbonate ions and the water are located between the metal hydroxide layers.

For a long time, these materials were mainly the object of mineralogical studies and only after 1970 they appeared in the patent and open literature referring to the applications in new and unexpected fields. Numerous compounds of this type have been synthesized with a wide range of applications. The general formula used for representing the chemical composition of the layered double hydroxides is $[M^{II}_{1-x}M^{III}_x(OH)_2]^{x+}[A^{n-}_{x/n}.yH_2O]^{x-}$ where M^{II} and M^{III} are divalent and trivalent metal cations respectively, A^{n-} is an n-valent anion. These compounds have layered crystal structures with wide variations in the nature of the cations and M^{II}/M^{III} molar ratios, as well as in the type of anions. Only a few of these variations are found in the nature where carbonate is the preferred anion. A very high number of variables have been reported for synthetic HT-like materials. Table 2.1 shows the factors

which make it possible to produce tailor-made materials for applications in different areas.

Structural variables	**Preparation variables**
Cation size	pH
Value of x [i.e., the $M^{III}/(M^{III}+M^{II})$ratio]	Precipitation method
Cation stereochemistry	Precipitation temperature
Cation mixture (nature and ratio)	Reagent concentration
Nature of balancing anions	Aging
Amount of interlayer water	Washing and drying
Crystal morphology and size	Presence of impurities

Table 2.1. Factors influencing the properties of LDHs (Vaccari, 1999).

The bonding of most of the anions between the layers is relatively weak and these anions can be exchanged with different anions under proper ion-exchange conditions. This property is very useful in many applications of LDHs.

2.1.1. Structural Properties of LDHs

The structures of the LDHs are very similar with the structure of brucite, $Mg(OH)_2$. Mg^{2+} ions are octahedrally surrounded by six OH^- and the different octahedra share edges to form infinite sheets (Figure 2.1). These sheets are stacked on top of each other in a layer type lattice as a consequence of the presence of relatively small, divalent, positively charged cations in close proximity to the non-spherosymmetrical and highly polarizable OH^- ions. The layers are held together by weak interactions through hydrogen bonds (Vaccari, 1998). If some Mg^{2+} cations are substituted by other cations with higher charge but similar radius, the sheets become positively charged and the anions located in the interlayer spaces maintain charge neutrality.

Cations such as Be^{2+} are too small for octahedral coordination in the layers while Ba^{2+} ions are too large (Miyata and Kumura, 1973). Almost all metal cations with divalent positive charge from Mg^{2+} to Mn^{2+}, except Cu^{2+} owing to the Jahn-Teller

effect, can form LDHs. All trivalent metal cations, except Ti^{3+}, can form LDHs (Khan and O'Hare, 2002).

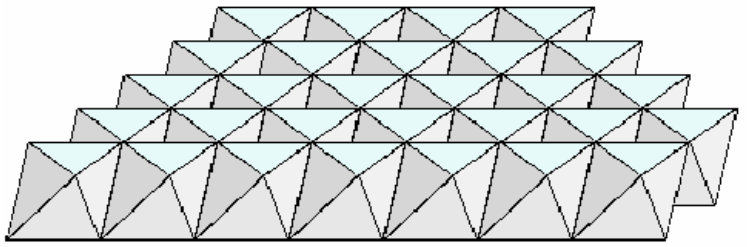

(a)

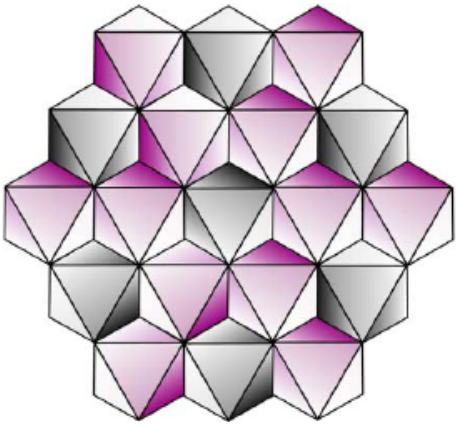

(b)

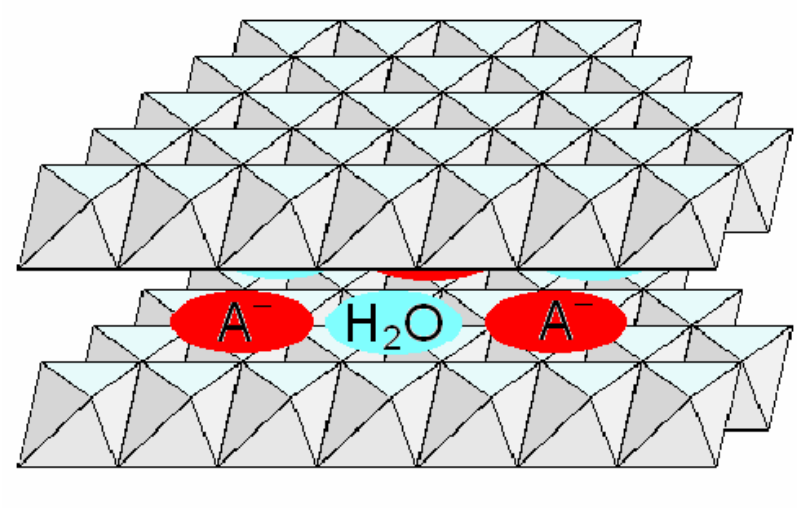

(c)

Figure 2.1. Brucite lattice, a; side and b; top views and c; layer structure (Bravo-Suarez et al., 2004).

Layered double hydroxides are found in two different polymorphic forms in nature; rhombohedral and hexagonal (Figure 2.2). Most of the natural LDHs are rhombohedral where the lattice parameter *c* is equal to three times the interlayer spacing {*c*=3*c'* (*c'*= thickness of one layer + one spacing between the layers)}, the *c* parameter of the hexagonal is equal to twice the interlayer space.

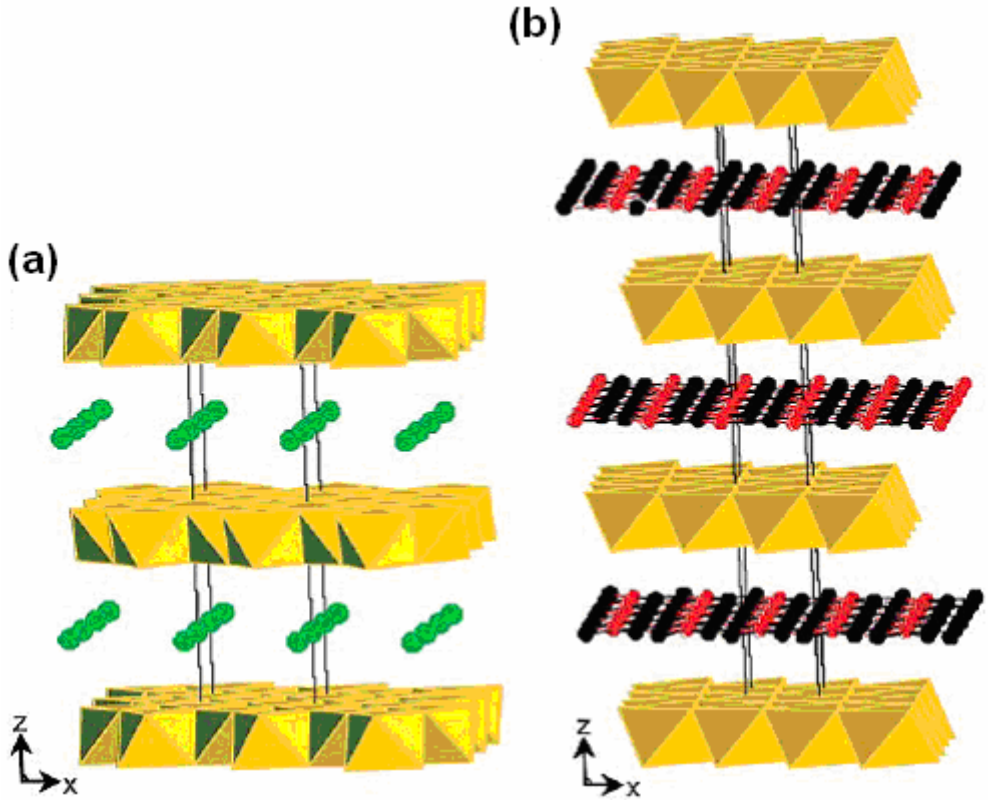

Figure 2.2. Hexagonal (a) and rhombohedral (b) structure of a LDH (Khan and O'Hare., 2002).

The crystal parameter *a* for Mg, Al containing LDHs is a function of x. The *a* parameter decreases with increasing x (increasing Al^{3+} substitution) because the radius of Al^{3+} is smaller than Mg^{2+} (Cavani et al., 1991). For x> 0.33, *a* is constant related to the fact that repulsion between octahedral Al^{3+} compensates for further decrease in *a* itself (Kooli et al., 1996; Cavani et al., 1991). According to Kooli, it is possible to obtain LDHs with Mg/Al ratios between 1 and 5.

The interlayer region contains not only the charge compensating interlayer anions but also interlayer water molecules which are connected to both the interlayer anions and the layers through hydrogen bonding. These hydrogen bonds in the

interlayer space is dynamic, they continuously break and reform. The continuous flux state of the interlayer water molecules has been supported by NMR experiments (Khan and O'Hare, 2002).

Layered double hydroxides have higher particle sizes than those claimed for clay minerals and this reflects on the surface area value. The surface areas of dried LDHs are generally lower than 100 m^2/g. These values refer only to the external area since high charge density of the layers creates strong electrostatic forces between the layers and the interlayer anions thus making the measurement of the internal area by swelling difficult (Vaccari, 1998).

2.1.2. Anion Exchange Properties of LDHs

LDHs have good anion exchange capacities. Their real use is as anion exchangers and adsorbents for ecologically undesirable anions from dilute and aqueous waste streams. LDHs can be used in medical applications, for example stomach acid (~0.1 N HCl) reacts rapidly with Mg-Al-carbonate-LDH by ion-exchange to yield the chloride form of the clay. The order of stability for the interlayer anions is approximately: $OH^->F^->Cl^->Br^->NO_3^->I^-$ and $CO_3^{2-}>SO_4^{2-}$ (Reichle, 1986). LDHs are reluctant to high temperature ion-exchange, thus they find applications in treatment of the cooling water of the nuclear reactors (Vaccari, 1998). The selectivity of the LDHs towards anions increases with increasing anion charge density, multiply charged anions and compounds are preferred. The pH of the solution is also very important in favouring or preventing the ion-exchange procedure.

2.1.3. Intercalation and Pillaring Properties of LDHs

The term *intercalation* refers to the insertion of mobile guest species (atoms, molecules or ions) into a crystalline host lattice that contains an interconnected system of empty lattice sites of appropriate size. Intercalation reactions are usually reversible, the structural integrity of the host lattice is formally conserved in the course of formal and reverse reactions. Typically, these reactions occur near room temperature which is in sharp contrast to most conventional solid state synthetic procedures that often require temperatures in excess of 600 °C (Cheng, 1999).

An important feature of intercalation reactions is that the geometrical, chemical and electronic environment of the guest and host may be controlled and tailored to meet the specific requirements of modern materials. A great number of intercalated LDH compounds have been synthesized and investigated for miscellaneous applications. The applications are growing in many unexpected areas because, the chemical, magnetic, adsorption, catalytic, electronic and optical properties of the LDHs greatly change by intercalation.

The dimensions and the functional groups of the intercalant molecules are very important. Not only the size, orientation and the number of the guest anions but also the interactions between the negatively charged guest molecules and the positively charged host layers are the critical factors in the intercalation process (Cavani et.al. 1991). In some cases, intercalation leads to *pillared* LDH structures. Pillar means "literal column" for supporting part of a structure. Pillared clays (PILC's) are nanocomposite materials with open and rigid structure obtained by linking robust, three-dimensional species to a layered host. Pillars prevent the complete collapse of the galleries after the solvating medium is removed and therefore pillared materials are thermally stable. PILC's can have very large intracrystalline surface areas more than 100 m^2/g.

There are three important criteria for describing the PILC's, firstly, in order to provide vertical expansion of the interlayer galleries, the gallery species should be sufficiently robust. Secondly, the pillars must allow for interpillar access by small molecules like N_2, CO_2, water and small anions. Finally, the host layers must be sufficiently rigid to sustain the desired layered structure (Pinnavaia, 1995). Intercalation of large molecules is preferred for giving access to produce new LDHs for new applications like catalysts, catalyst supports, ion-exchange materials, sorbents, absorbers, pharmaceuticals and to store and deliver biologically active materials *in vivo*.

The intercalation chemistry of LDH hosts is extensive. To date, the incorporation of

- simple inorganic and organic anions,
- isopolyanions (isopolyoxometalates) and heteropolyanions (heteropolyoxometalates),

- transition metal coordination compounds

have been reported (Cavani et al. 1991; Rives and Ulibarri, 1999). Figure 2.3. representatively shows the structure of a Mo-oxo complex intercalated by a Zn/Al-LDH. The product has been obtained by anionic exchange of the LDH in its nitrate form and the measured basal spacing for the (001) reflection is 17.6Å. The calculated free interlayer space (13 Å) is consistent with the intercalation of the complex with its C_2 axis parallel to the brucite-like layers (the size of the anion perpendicular to its C_2 axis is 12.6 Å). The complex is active for thiophenol oxidation to disulphide by dioxygen.

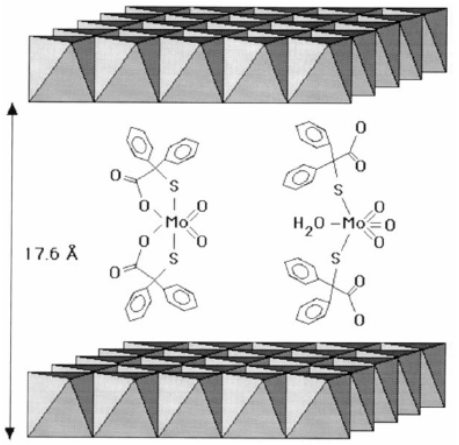

Figure 2.3. Structure of LDH intercalated with $[Mo^{VI}O_2(O_2CC(S)Ph_2)_2]^{2-}$ (Rives and Ulibarri, 1999).

The synthesis of LDH nanocomposites with polymeric guest molecules are possible by

- *in situ* polymerization of an intercalated monomer (Figure 2.4a),
- direct intercalation of a high molecular weight macromolecule by ion-exchange or using the co-precipitation method (Figure 2.4b),
- the reconstruction method, (Figure 2.4c).

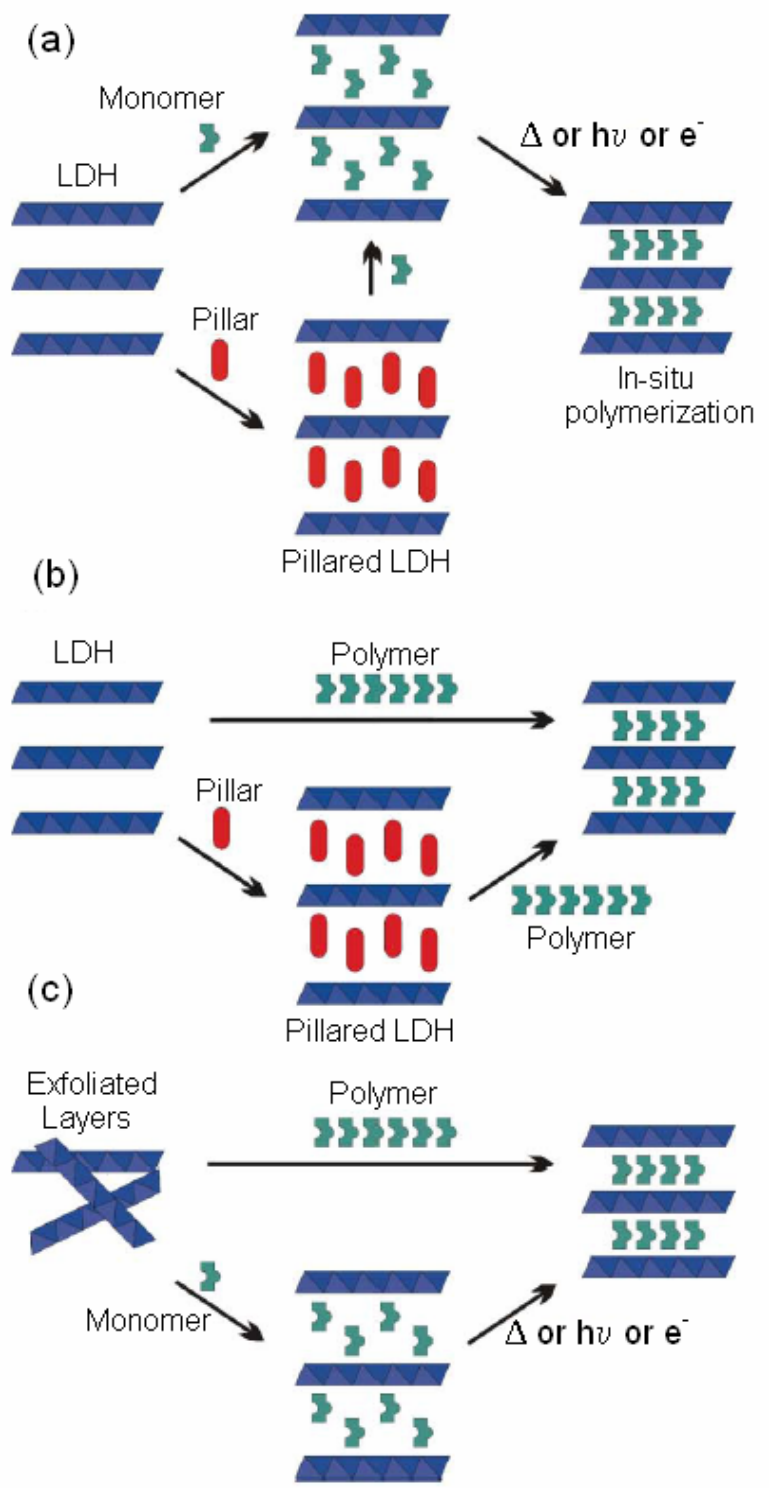

Figure 2.4. Schematic representation of the synthesis of polymer-LDH nanocomposites by: (a) in situ polymerization, (b) direct intercalation; by ion-exchange or co-precipitation and (c) reconstruction method (Leroux and Besse, 2001, Khan and O'hare, 2002).

Most recently, the interest has focused on the intercalation of biologically active materials such as:

- porphyrins, drugs, vitamins, amino acids, fatty acids, and
- macro-biological molecules (DNA, ATP and nucleosides) (Choy et al., 2000).

These bio-LDH-nanohybrids may greatly enhance the transfer of active biomolecules into mammalian cells or organs as illustrated in Figure 2.5. Once inside the cells, some of the LDH which is unstable in acidic conditions, is dissolved by lisosomes resulting in the release of the intercalant molecule.

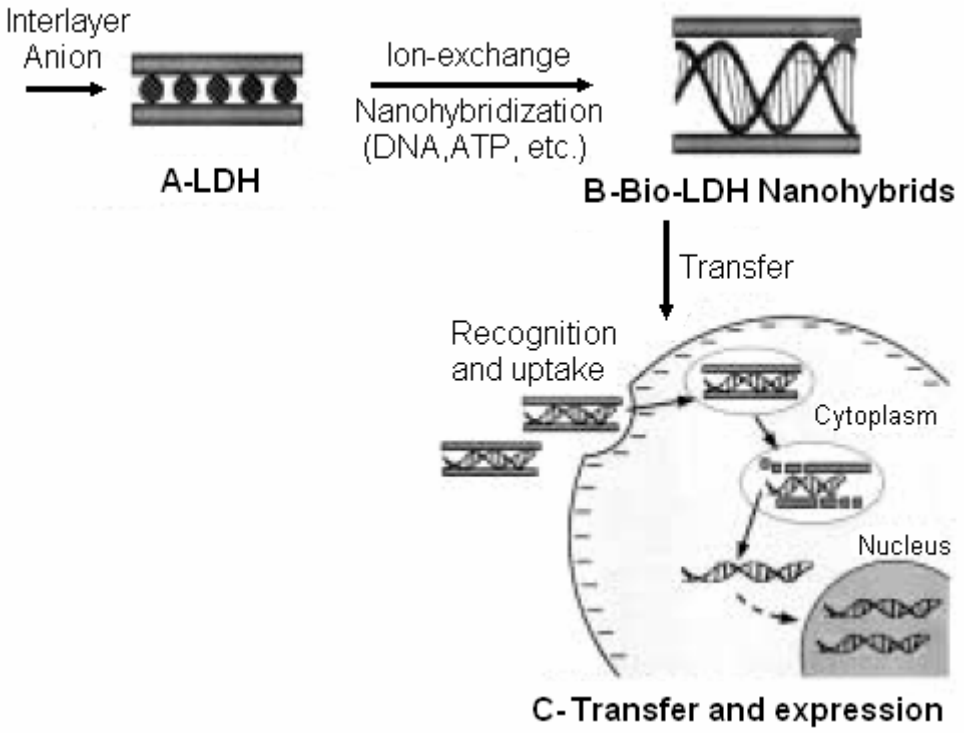

Figure 2.5. Schematic illustration of bio-molecule intercalation and the expected transfer mechanism of the bio-LDH into the cell (Choy et al., 2000).

Certain LDHs exhibit selective, shape-selective or stereo-selective intercalation reactions. This property has great potential for the intercalation of biologically active guests (Khan and O'Hare, 2002).

2.1.4. Adsorption Properties of LDHs

Adsorption properties of the LDHs depend on their composition and the treatments that they are exposed to after their synthesis. Adsorption takes place mainly in the interlayer space rather than on the surface however surface adsorption also takes place to some extent. Interlayer adsorption occurs in two different ways, ion-exchange and the reconstruction of the calcined LDHs.

The sorption of anions by anion exchange occurs if the interlayer anions (i.e. nitrate, chloride etc.) of the precursor are electrostatically weakly held and the substituting anions have higher charge densities.

The sorption of anions through the reconstruction method, the so-called “memory effect”, is mainly based on calcining the LDH structure first and then reestablishing the original layered structure by exposing the mixed oxides obtained by calcination to rehydration in water or an anionic solution. This process is very effective due to the lack of electroneutrality in the calcined structure and is accompanied by an increase in the solution pH value because the calcined LDHs preferably uptake the hydroxyl anions during rehydration (Crepaldi et al. 2002). The rehydration of calcined LDHs is more useful in cases where the ion-exchange procedure is not favorable or prevented. For example, materials with intercalated carbonate ions have no exchange properties unless being calcined. The calcination temperature is crucial and must be high enough to expell the interlayer anions but low enough in order to prevent irrevocable oxide formation (Cavani et al., 1991). The surface area which is an important parameter in anion removing, increases after the thermal treatment of LDHs (Kovanda et al., 2006).

The removal of several anionic pollutants from water by HT-like materials *via* reconstruction or anion-exchange methods have been reported in the literature (Ulibarri et al., 2001). LDHs containing particularly interlayer nitrate, chloride and sulfate ions have been utilized for the adsorption of different anions such as F^-, Br^-, $B(OH)_4^-$, HPO_4^{2-} (Parker L.M. *et al*., 1995). Adsorption of chromate, SO_4^{2-} and organic anions are also reported (Kovanda et al., 2006).

2.1.5. Catalytic Applications of LDHs

LDHs, as such or mainly after calcination, find many industrial applications and probably will be found in future in totally unexpected areas.

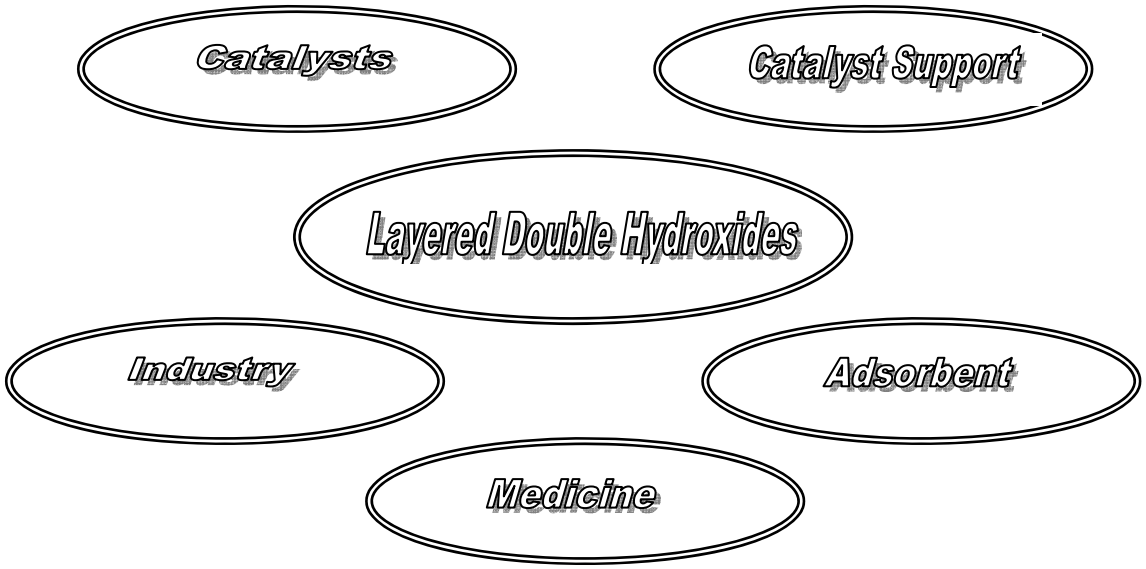

Scheme 2.1. Main industrial applications of LDHs (as such or after thermal decomposition).

Anionic clays are promising precursors of multicomponent catalysts for many applications (Cavani et al., 1991, Vaccari, 1999, Kovanda et al., 2006). Control of the acid-base properties of LDHs is very promising in preparing active catalysts for various applications. The catalysts prepared by the decomposition of the LDHs have higher activity, stability and lifetime than the individual oxides. Catalytic applications of the mixed oxides obtained by the controlled calcination of the LDHs include:

- aldol condensation of aldehydes and ketones,
- methane or hydrocarbon steam reforming,
- polymerization of alkene oxides,
- alkylation, steam reforming, hydrogenation, oxidative and non-oxidative dehydrogenation,
- gas phase oxidation, liquid phase oxidation,
- hydrocarbon (Fischer-Tropsch) synthesis,

- synthesis of aromatic compounds from alkanes,
- selective hydrogenation of maleic anhydrate to γ-butyrolactone (to produce new chlorine-free solvents),
- selective catalytic reduction (SCR) of NO by ammonia (as possible inexpensive alternative to Cu-zeolites),
- decomposition of N_2O.

2.2. Synthesis of LDHs

LDHs can be synthesised *via* different methods. Laboratory syntheses are generally simple and easy to produce. For a required composition, different methods can be applied: co-precipitation method at constant or variable pH, deposition/precipitation reactions, hydrothermal synthesis, anion exchange, structure reconstruction, delamination, salt-oxide method, two powder synthesis, electrochemical methods and hydrolysis reactions (O'Leary et al., 2002, Vaccari, 1999). Among these, co-precipitation and anion exchange methods are the most preferred methods.

2.2.1. Co-precipitation Method

Co-precipitation is the most useful method to prepare large amounts of LDHs (Cavani et al., 1991). The method consists of precipitation at increasing, decreasing or constant pH by titrating a solution containing the M^{II} and M^{III} salts with an alkali hydroxide (NaOH, KOH, etc.) or carbonate. Sequental precipitation of ions occurs and it is not possible to precipitate a pure LDH directly in every process. Aging, washing and drying processes are applied after precipitation. It is necessary to optimize the experimental conditions for each desired product in order to obtain a highly crystalline material.

At constant pH and at low supersaturations, co-precipitation technique is the most frequently applied in the preparation of LDHs. Generally pH is adjusted between 7-10 and the reflux temperature of the supersaturated solution is kept around the boiling point of water. Precipitation at low supersaturation is preferable since the slow crystal growth produces a crystalline material while at high supersaturations

less crystalline LDHs are formed due to the presence of high number of nucleation sites.

2.2.2. Anion Exchange Method

Anion exchange treatment is widely used in producing different types of LDHs because they have high anion-exchange capacities toward inorganic (Cheng and Lin, 1992; Del Arco et al., 2000) and organic anions (Meyn et al., 1990; Khan and O'Hare, 2202).

NO_3^- intercalated LDHs are widely used in anion exchange reactions because the NO_3^- ion selectivity of the LDHs is not high. The order of monovalent ion selectivities of the LDHs is $OH^- > F^- > Cl^- > Br^- > NO_3^- > I^-$. Divalent anions have higher ion selectivities and CO_3^{2-} is the most selective of the divalent ions (Miyata, 1983). A schematic representation of the anion-exchange treatment is shown in Figure 2.6.

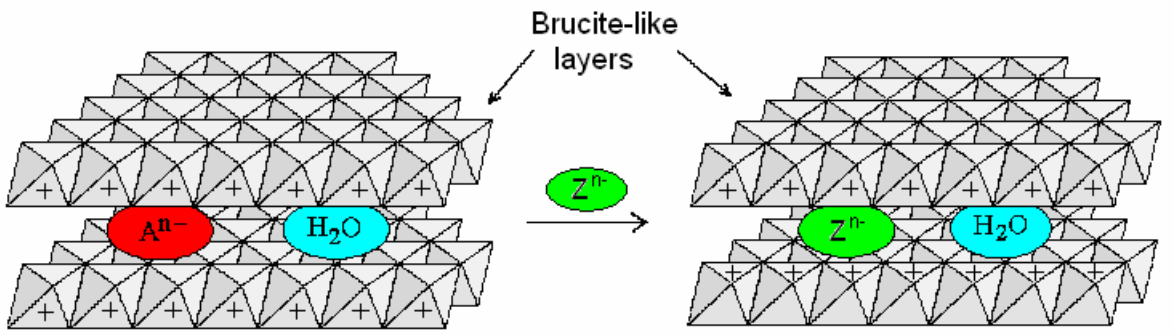

Figure 2.6. Schematic representation of anion-exchange treatment of LDHs.

2.2.3. Hydrothermal Method

Hydrothermal synthesis is also known as wet crystallization concerning the treatment of freshly precipitated mixed hydroxides or a mixture of M^{II} and M^{III} oxides and/or hydroxides in aqueous suspension especially in the presence of other anions under hydrothermal conditions (Cavani et al., 1991, Kovanda et al., 2006). With this method, amorphous precipitates transform into crystalline forms and small crystals transform into larger and well crystalline forms (Cavani et al., 1991). Hydrothermal treatment at higher temperatures and pressures in

combination with microwave heating have been reported to yield high crystallinity products with no impurities in terms of amorphous aluminum hydroxide (Möhmel et al., 2002).

2.2.4. Sol-Gel Method

The sol-gel method has become an important technique in the production of LDHs. While the Mg/Al ratio in the synthesized LDHs by conventional methods is limited in the range 1.5-3.0, this ratio can be increased with the sol-gel technique (Lopez et al., 1996). The sol-gel term comes from the distinctive increase in viscosity which occurs at a particular point in the sequence of the experimental steps. The synthesis of LDHs by the sol-gel process is started with a mixture of metal alkoxide and water in a solvent, usually alcohol. A hydrolysis occurs, H_2O and ROH are eliminated by the condensation of adjacent molecules and metal oxide linkages are formed in a three-dimensional network throughout the liquid. The system shows the characteristics of a gel, the solvent as well as water and alcohol remain inside the pores of the gel. Finally, the gel is dried at moderate temperatures less than 200°C (Rao, 1993).

2.2.5. Delamination

Delamination is the separation of the laminated structure of LDHs into layers. It is one of the most effective methods to solve the accessibility problem to the inner surfaces of the host layers. Delamination of the LDHs modified with long-chain organic anions in nonaqueous solvents was first reported by Adachi-Pagano et al. (2000) who delaminated the Zn-Al LDH containing dodecyl sulfate in butanol under refluxing conditions. They obtained a new Zn_2Al-dodecyl sulfate phase with larger size and well-oriented platelets on removing the solvent (butanol) from the colloidal solution by evaporation and by lyophilization. Similarly, Liu et al. (2006) achieved the delamination of large-sized particles of Mg-Al-NO_3-LDH into well defined nanosheets using formamide, as shown schematically in Figure 2.7. They found that the LDH delamination in formamide is instant and spontaneous, the process does not need any heat and refluxing.

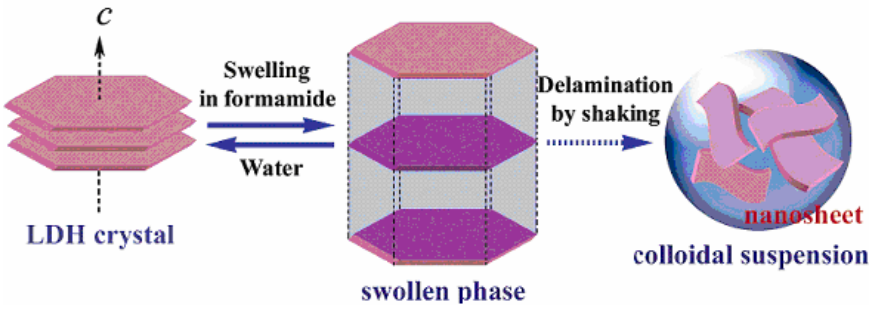

Figure 2.7. Schematic representation of a possible delamination mechanism in formamide (Liu et al., 2006).

2.3. LDHs Intercalated with Borate Ions

2.3.1. Boron and Its Applications in Industry and Material Science

Boron (B) is a light, nonmetallic trace element widely distributed in the environment combined with other substances to form inorganic borates (Coughlin, 1996). It is one of the few elements known to be essential in plants and is yet to be proven as essential in animals and humans (Woods, 1996). Elemental boron has properties that place it on the borderline between metals and nonmetals. It is a semiconductor, not a metallic conductor, and chemically it must be classified as a nonmetal (Cotton and Wilkinson, 1980).

The element B does not exist by itself in nature. Rather, it combines with oxygen and other elements to form boric acid, or inorganic salts called borates. Natural boron consists of two isotopes, ^{10}B (19.6%) and ^{11}B (80.4%). It is exceedingly difficult to prepare elemental B in a state of high purity because of its high melting point and the corrosiveness of the liquid. It can be prepared in quantity but low purity (95-98%) in an amorphous form by reduction of B_2O_3 with magnesium, followed by vigorous washing of the material with alkali, hydrochloric, and hydrofluoric acid.

$$\underset{\text{borax}}{Na_2B_4O_7.10H_2O} \xrightarrow{\text{acid}} \underset{\text{orthoboric acid}}{H_3BO_3} \xrightarrow{\text{heat}} B_2O_3 \xrightarrow{\text{Mg or Na}} 2B + 3MgO$$

This amorphous boron is a dark powder that may contain some microcrystalline B but also contains oxides and borides. Pure boron in crystalline form is a matter of

considerable complexity and difficulty even when only small research scale quantities are required. Small amounts of crystalline boron may be obtained by:

1. reducing BCl_3 with H_2. This is done on the kilogram scale.
2. pyrolysis of BI_3 (Van Arkel Method)
3. thermal decomposition of diborane or other boron hydrides.

$$2BCl_3 + 3H_2 \xrightarrow{\text{red hot W or Ta filament}} 2B + 6HCl$$

$$2BI_3 \xrightarrow[\text{Van Arkel}]{\text{red hot W or Ta filament}} 2B + 3I_2$$

$$B_2H_6 \xrightarrow{\text{heat}} 2B + 3H_2$$

Crystalline B is extremely inert chemically and only slowly oxidized by concentrated, hot nitric acid when finely powdered (Cotton and Wilkinson, 1980; Lee, 1991).

Boron is the only electron deficient, nonmetallic element in the Group 13 of Periodic Table. Normally it forms three covalent bonds using sp^2 at 120° hybrid orbitals (Lee, 1991). B is always trivalent and never monovalent although the electronic structure is $2s^2 2p$ because the total energy released in formation of three bonds in a BX_3 compound exceeds the energy of formation of one bond in a BX compound by more than enough to provide for promotion to a hybridized valence state of the sp^2 type. All monomeric, three-covalent boron compounds (trihalides, trialkyls, etc.) are planar with X–B–X bond angles 120°. Boron compounds act as electron pair acceptors (Lewis acid behavior) because of its incomplete electron octet.

Boric acid is usually obtained from borax and it forms white, needlelike crystals in which $B(OH)_3$ units are linked together by hydrogen bonds to form infinite layers of nearly hexagonal symmetry. Some reactions of boric acid are given in Scheme 2.2.

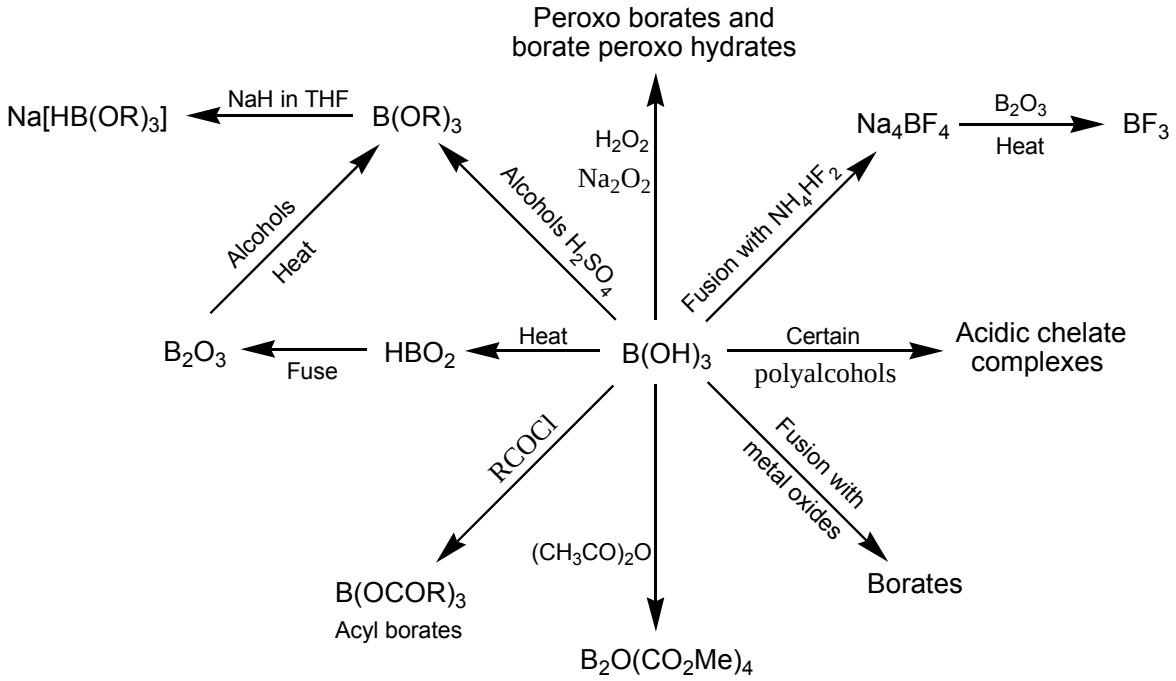

Scheme 2.2. Some reactions of boric acid.

The inorganic borates have many industrial applications, but they are primarily used in;

- the manufacture of textile and insulation fiberglass
- heat-resistant borosilicate glass
- ceramic enamels and glazes
- detergents bleaches
- fire retardants
- alloys and metals
- adhesives
- neutron capture cancer therapy
- moderators in nuclear reactors
- soldering and welding fluxes

and in other aspects of the textile, soap, leather and cosmetic industries (Coughlin, 1996).

Many of the boron compounds have been used as high performance materials with their chemical and temperature resistance, conductivity and hardness properties. B has a very high cross-section for capturing neutrons. Control rods

made of boron steel or boron carbide (B_4C) may be lowered into a reactor to absorb neutrons and thus slow the reactor down. Borides, compounds of boron and metals with varying composition, have high temperature resistance and hardness and often good thermal conductivity. Their electrical conductivity makes them usable from semi-conductors to super-conductors. Cubic boron nitride (BN) is a diamond substitute used to cut steel (Lee, 1991).

In addition to inorganic borates, organoboron compounds (borane and borohydride reagents) have become increasingly important for catalytic reactions (Burkhardt and Matos, 2006). Most recently, Boris Yakobson and colleagues from Rice University, reported the *ab initio* prediction of the existence of the boron-fullerene (B80), an unusually stable boron cage made of 80 boron atoms, which will be a significant breakthrough in materials science in the future (Szwacki et.al., 2007).

2.3.2. Aqueous Chemistry of Borate Ions

Many borates occur naturally, usually in hydrated form. Fusion of boric acid and metal oxides gives anhydrous borate anions. Hydrated borate anions can be obtained by crystallization. The stoichiometry of the borates give little idea of the structures of the anions. Cyclic or linear polymers are formed by linking together of BO_3 and/or BO_4 units *via* shared oxygen atoms. Examples to anhydrous complex borate anions are the ring anion in $K_3B_3O_6$ (Figure 2.8a) and the infinite chain anion in CaB_2O_4 (Figure 2.8b) (Cotton and Wilkinson, 1980).

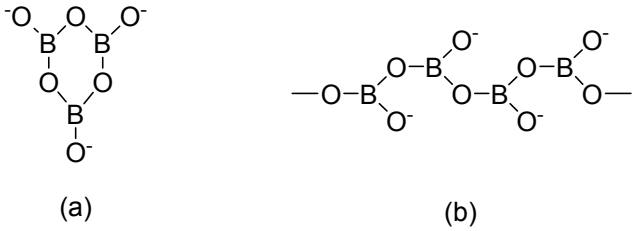

Figure 2.8. Ring borate anion (a) and the infinite chain borate anion (b).

The hydrated borate anions contain both trigonal BO_3 and tetrahedral BO_4 groups, the ratio of BO_4 to total B being equivalent to the ratio of the charge on the anion to total boron atoms. For example $KB_5O_8.4H_2O$ has one BO_4 and four BO_3,

whereas $Ca_2B_6O_{11}.7H_2O$ has four BO_4 and two BO_3 groups (Cotton and Wilkinson, 1980).

Boric acid is moderately soluble in water and is a very weak and exclusively monobasic acid that is believed to act, not as a proton donor, but as a Lewis acid, accepting OH^- to form its maximum coordination with approximately sp^3 hybridized, tetrahedral, tetrahydroxy borate anion.

$$B(OH)_3 + H_2O \leftrightarrow B(OH)_4^- + H^+ \qquad pK = 9.2 \qquad (2.1)$$

The $B(OH)_4^-$ ion occurs in several minerals. At concentrations ≤0.025 M, essentially only mononuclear species $B(OH)_3$ and $B(OH)_4^-$ are present. In concentrated solutions polymeric ions are also present (Salentine, 1983; Simon and Smith, 2000):

$$8B(OH)_3 + 4B(OH)_4^- \leftrightarrow B_3O_3(OH)_4^- + B_4O_5(OH)_4^{2-} + B_5O_6(OH)_4^- + 14H_2O \qquad (2.2)$$

As can be seen on the Scheme 2.3, polyborate anions, $B_5O_6(OH)_4^-$, $B_3O_3(OH)_4^-$ and $B_4O_5(OH)_4^{2-}$ are formed with increasing pH. With increasing pH, attack on the neutral trigonal boron is favored, but there is a discontinuity when the number of BO_4 groups exceeds 50% so that tetraborate goes directly to $B(OH)_4^-$ (Cotton and Wilkinson, 1980).

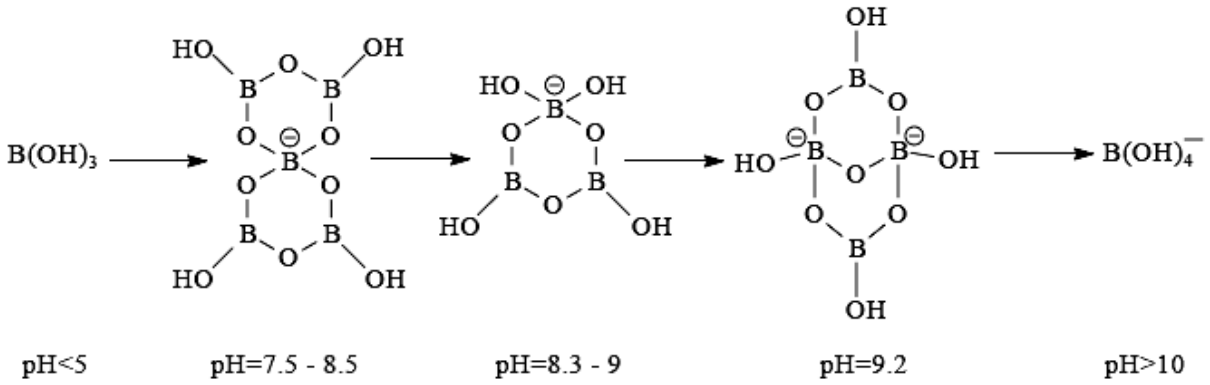

Scheme 2.3. Borate anions in aqueous solutions.

All polyborate anions hydrolyze and produce the monoborate anion, $B(OH)_4^-$, when the pH is higher than 11. In natural aqueous systems and in detergents, boric acid-borate buffer mixtures serve as pH standards.

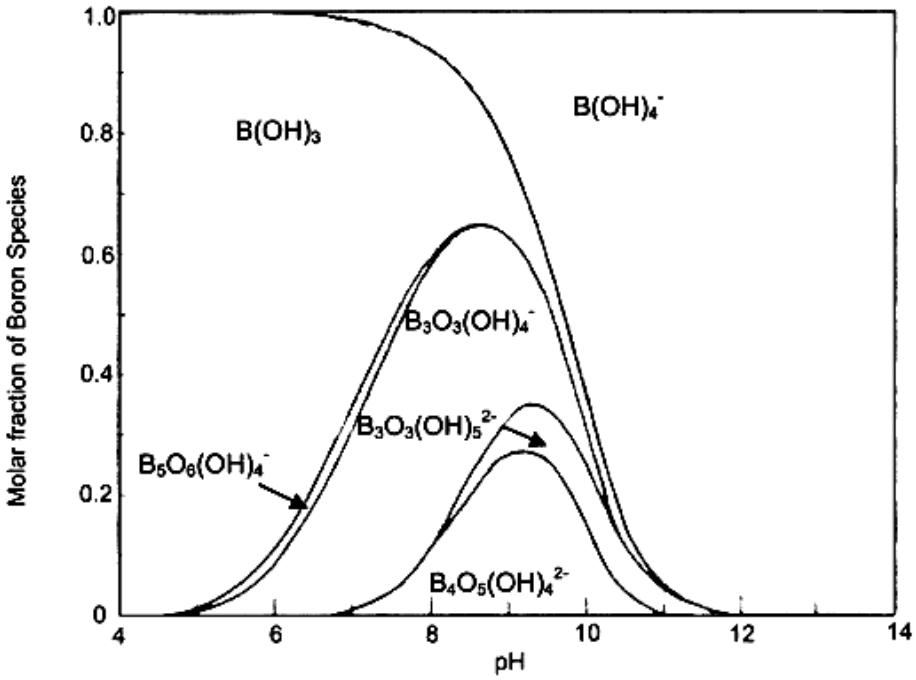

Figure 2.9. Distribution of borate anions as a function of solution pH (Bechara et al., 2002).

2.3.3. Boron Incorporation into LDHs

Although considerable interest has been devoted to the synthesis of LDHs with metal-containing anions (Rives and Ulibarri, 1999), very little work has been carried out with inorganic nonmetal ions. The synthesis of boron-intercalated LDHs appears very interesting due to the miscellanous uses of LDHs and boron materials outlined in Sections 2.1.3., 2.1.5, 2.3.1 and yet undiscovered potential applications in pharmacology and materials science. Boron intercalated LDHs have both acidic functionalities of intermediate Brønsted strength and also basic sites to promote catalytic reactions like aldol condensation and Beckmann Rearrangement (Dahlhoff et.al., 2001; Bechara et al., 2002).

Boron incorporation into LDHs has been first studied by Chen and Lin (Cheng and Lin, 1992). The authors did not succeed in obtaining a crystalline LDH-borate by direct synthesis nor by nitrate exchange. Bhattacharyya and Hall (1992) have

reported the preparation of a LDH-triborate by direct synthesis with boric acid but presented a limited information to the literature. In 1996, Li et al. investigated the structures of tetraborate pillared HTs prepared via hydrothermal synthesis however observed a partial exchange with nitrate ions only after severe hydrothermal treatment. Parker et al. (1995) and Shi et al. (2005) studied borate exchange with CO_3-HT compounds. Due to the robust nature of CO_3-HTs toward anion exchange reactions, Del Arco et al. (2000) studied borate intercalation with NO_3-HT precursors under N_2 atmosphere and characterized the product before and after calcination at different temperatures. The authors stated that synthesis under precise pH values is necessary to avoid depolymerization of tetraborate anions which enhances the thermal stability of the material. In order to introduce much boron as possible in the structure, preparation conditions should be carefully set to avoid formation of different phases and surfaces with different acid properties.

2.4. The Goal of This Work

This study focuses on the preparation and complete characterization of borate intercalated layered double hydroxides by adapting mild mechanochemical and solvothermal methods. The effects of:

- method of preparation,
- pH of preparation,
- type of borate anion,
- nature of the interlayer region,

will be analyzed with the aim of obtaining well-structured borate-LDHs. The study also aims to investigate the boron uptake behavior of Mg-Al-NO_3-LDH for the remediation of boron present in waters.

3. EXPERIMENTAL

3.1. Materials

The reagents $Mg(NO_3)_2.6H_2O$ (Sigma), $Al(NO_3)_3.9H_2O$ (Carlo-Erba), NaOH (Merck), $(NH_4)_2B_4O_7.4H_2O$ (Aldrich), H_3BO_3 (Sigma), Adipic Acid (Aldrich), Terephtalic Acid (BDH), Carminic Acid (Aldrich), Sulphuric Acid (Analar) and Hydrochloric Acid (Merck) were used as received.

3.2. Synthesis of LDH's

The experiments, except the synthesis by mechanochemical activation, were conducted under nitrogen atmosphere and in deionized water in order to avoid carbonate contamination in the interlayer region.

3.3. Direct Synthesis of Borate Intercalated LDH's

Direct synthesis is a one-step procedure. Mixing the solutions containing Mg and Al nitrates in a molar ratio of 2:1, and a solution containing excess boron species (either boric acid or ammonium tetraborate) leads to the precipitation of borate ion intercalated HT-like materials. pH is initially set to basic, but allowed to vary throughout the precipitation process. This is one of the preferred ways but the alternative route, precipitation at constant pH, is also applied.

3.3.1. Co-precipitation Method

3.3.1.1. Co-precipitation with Ammonium Tetraborate Tetrahydrate

6.05 g $Al(NO_3)_3.9H_2O$ (16.1 mmol) and 8.26 g $Mg(NO_3)_2.6H_20$ (32.2 mmol) were dissolved in 100 mL degassed, deionized water. To this solution, 1.8 M 60 mL NaOH and 100 mL 0.30 M $(NH_4)_2B_4O_7.4H_2O$ (TB) solutions were added simultaneously, dropwise. The final solution was refluxed for 5 hours and aged for 4 days at room temperature. The resulting precipitate was washed five times with 90 mL deionized water in order to remove the free ions. The product (**A1.1**) was dried under vacuum at 40°C. 4.74 g product was obtained.

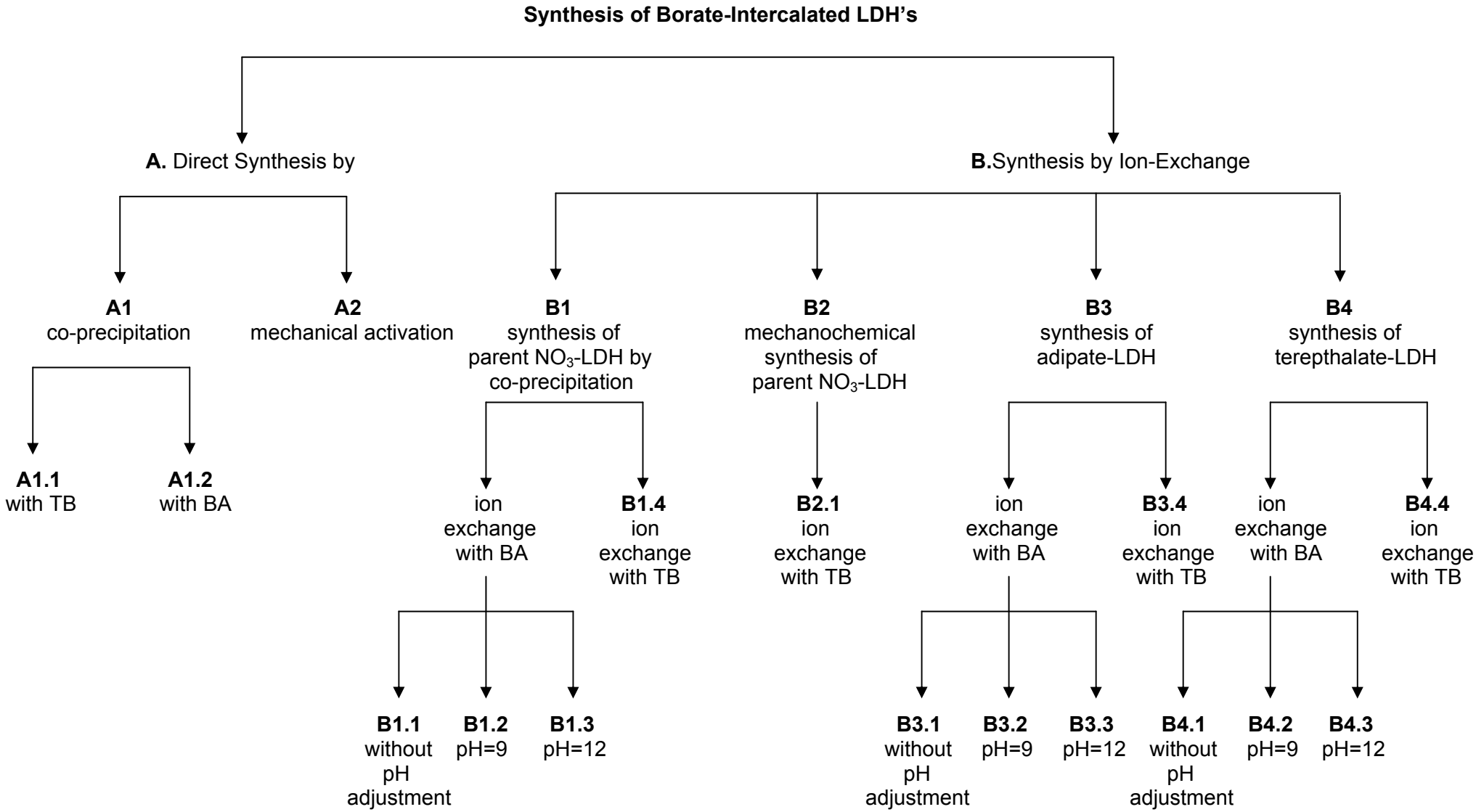

Scheme 3.1. Flow chart of synthetic studies.

3.3.1.2. Co-precipitation with H_3BO_3

6.56 g $Al(NO_3)_3.9H_2O$ (17.5 mmol) and 8.97 g $Mg(NO_3)_2.6H_20$ (35.0 mmol) were dissolved in 50 mL degassed, deionized water. To this solution, 6.6 M 38 mL NaOH and 250 mL 0.6 M H_3BO_3 (BA) solutions were added dropwise. The system was refluxed under nitrogen atmosphere for 5 hours and then aged for 4 days. The resulting precipitate was washed five times with 90 mL deionized water in order to remove the free ions. The product (**A1.1**) was dried under vacuum at 40°C. 4.83 g product was obtained.

3.3.2. Mechanochemical Synthesis

3.3.2.1. Mechanochemical Synthesis with Boric Acid

4.00 g $Mg(NO_3)_2.6H_2O$ (15.6 mmol) , 2.92 g $Al(NO_3)_3.9H_2O$ (7.78 mmol) and 0.48 g BA (7.81 mmol) were powdered and manually ground with 1.94 g NaOH pellets in a mortar. The product (**A2**) was washed four times with 20 mL water, dried under vacuum at 40°C, powdered and analyzed. 1.70 g product was obtained.

3.4. Synthesis by Ion Exchange

Anion exchange is a two- or sometimes three-step procedure involving the preparation of the precursor nitrate- or expanded-LDH first, than exchanging the interlayer ions with borate ions.

Two different methods were applied:

Method 1: Borate-exchange with nitrate-LDH,

Method 2: Borate-exchange with LDH's expanded with polyoxo organic anions (like aliphatic (adipate, AD) and aromatic (terephtalate, TP) dicarboxylates)

3.4.1. Synthesis of Nitrate-LDH by Co-precipitation Method

300 mL 0.74 M NaOH solution was added dropwise from a separation funnel to a 200 mL solution containing 22.0 g $Mg(NO_3)_2.6H_2O$ (86.0 mmol) and 16.1 g $Al(NO_3)_2.9H_2O$ (43.0 mmol) (Mg/Al=2) at room temperature. After adding the base solution, the system was stirred under nitrogen atmosphere at 90°C for 4 hours. The slurry was aged for 3 weeks before filtration. The product was washed 5 times

with 500 mL deionized water and dried at 40°C under vacuum. 8.82 g product **(B1)** was obtained.

3.4.1.1. Boric Acid-Exchange with Nitrate-LDH without pH adjustment

0.366 g nitrate-LDH (**B1**) was added to 170 mL solution (pH ~5) containing 0.550 g (8.90 mmol) BA. The system was refluxed at 90°C under nitrogen atmosphere for 9 hours. The slurry was stirred 24 hours before aging for 24 hours. When the ion-exchange procedure was stopped, the pH of the slurry increased to 7.5. 0.3 g product (**B1.1**) was obtained.

3.4.1.2 Boric Acid-Exchange with Nitrate-LDH at pH 9.0

0.368 g nitrate-LDH (**B1**) was added to 170 mL solution containing 0.550 g (8.90 mmol) BA. The initial pH of the mixture was adjusted to 9.0 with 25 mL 1.0M NaOH solution. The system was refluxed at 90°C under nitrogen atmosphere for 9 hours. The slurry was stirred for 24 hours before aging for 24 hours. When the ion-exchange procedure was stopped the pH of the slurry decreased to 8.8. 0.400 g product (**B1.2**) was obtained.

3.4.1.3. Boric Acid-Exchange with Nitrate-LDH at pH 12

0.550 g nitrate-LDH (**B1**) was added to a 120 mL solution containing 0.551 g (8.90 mmol) BA. The pH was adjusted to 12.0 by 1.7 M NaOH solution and ion-exchange was proceeded at this pH. The system was refluxed under nitrogen atmosphere at 90°C for 9 hours. The slurry was stirred 24 hours before aging for 24 hours. 0.274 g product (**B1.3**) was obtained.

3.4.1.4. Tetraborate Anion-Exchange with Nitrate-LDH

0.551 g nitrate-LDH (**B1**) was added to a 110 mL borate solution containing 5.36 g (20.4 mmol) TB. The system was refluxed at 90°C under nitrogen atmosphere for 6 hours and then continuously stirred for 80 hours before aging for 24 hours. The precipitate was washed several times with 200 mL deionized water and dried under vacuum at 40°C. 0.558 g product (**B1.4**) was obtained.

3.5. Synthesis of Nitrate-LDH by Mechanochemical Method

A simple and more productive method was developed to prepare LDHs. Manual grinding the hydrated solid precursors in a mortar and washing the paste several times to remove the free ions, yielded a product with similar characteristics to that obtained by co-precipitation.

The synthesis was conducted as: 1.940 g (50.0 mmol) NaOH pellets were added to a powder mixture of 4.00 g (15.6 mmol) Mg- and 2.93 g (7.80 mmol) Al- nitrates and manually ground to a paste. The paste was washed and 1.65 g product (**B2**) was obtained after drying under vacuum at 40°C.

3.5.1. Tetraborate Anion-Exchange with Mechanochemically Prepared Nitrate-LDH

0.497 g nitrate-LDH (**B2**) was added to 100 mL TB solution containing 3.01 g (11.4 mmol) $(NH_4)_2B_4O_7.4H_2O$. The system was refluxed at 90°C under nitrogen atmosphere for 6 hours and then continuously stirred for 80 hours. The precipitate was washed several times with 200 mL deionized water and dried under vacuum at 40°C. 0.5 g product (**B2.1**) was obtained.

3.6. Synthesis of Expanded LDH's

3.6.1. Synthesis of Adipate-LDH

200 mL solution containing 19.9 g (77.6 mmol) $Mg(NO_3)_2.6H_2O$ and 14.6 g (38.9 mmol) $Al(NO_3)_2.9H_2O$ was added dropwise from a separation funnel to a solution containing 11.0 g (75.3 mmol) adipic acid and 14.6 g (365 mmol) NaOH. The mixture was stirred at 90°C for 5 hours and aged for 5 days under nitrogen atmosphere. The precipitate was filtered, washed 5 times with 500 ml deionized water and dried under vacuum at 40°C. 0.1 g product (**B3**) was obtained.

3.6.1.1. Boric Acid-Exchange with Adipate-LDH without pH Adjustment

0.371 g adipate-LDH (**B3**) was added to 170 mL solution (pH ~5) containing 0.551 g (8.9 mmol) BA. The system was refluxed at 90°C under nitrogen atmosphere for 9 hours. The slurry was stirred 24 hours before aging for 24 hours. When the ion-

exchange procedure was stopped, the pH of the slurry increased from the natural pH of BA to 7.5. The product was filtered and washed with 180 mL deionized water. 0.400 g product (**B3.1**) was obtained.

3.6.1.2. Boric Acid-Exchange with Adipate-LDH at pH 9.0

0.371g adipate-LDH (**B3**) was added to 170 mL solution containing 0.550 g (8.9 mmol) BA. The initial pH of the mixture was adjusted to 9.0 with 1 M NaOH solution. The system was refluxed at 90°C under nitrogen atmosphere for 9 hours. The slurry was stirred 24 hours before aging for 24 hours. When the ion-exchange procedure was stopped, the pH of the slurry decreased to 8.5. The product was filtered and washed with 180 mL deionized water. 0.430 g product (**B3.2**) was obtained.

3.6.1.3 Boric Acid-Exchange with Adipate-LDH at pH 12

0.550 g adipate-LDH (**B3**) was added to 120 mL solution containing 0.551 g (8.9 mmol) BA. The pH was adjusted to 12 by 1.68 M NaOH solution and ion-exchange was proceeded at this pH. The system was refluxed at 90°C under nitrogen atmosphere for 9 hours. The slurry was stirred 24 hours before aging for 24 hours. The product was filtered and washed with 180 mL deionized water. 0.281 g product (**B3.3**) was obtained.

3.6.1.4. Tetraborate Anion-Exchange with Adipate-LDH

0.551 g adipate-LDH was added to a 115 mL borate solution containing 5.36 g (20.4 mmol) $(NH_4)_2B_4O_7.4H_2O$. The system was refluxed at 90°C under nitrogen atmosphere for 6 hours. After refluxing, the system was continuously stirred for 80 hours and aged for 60 hours before washing with 200 ml deionized water and dried under vacuum at 40°C. 0.466 g product (**B3.4**) was obtained.

3.6.2. Synthesis of Terepthalate-LDH

10.0 g (39.0 mmol) $Mg(NO_3)_2.6H_2O$ and 7.32 g (19.5 mol) $Al(NO_3)_2.9H_2O$ were dissolved in 200 mL deionized water and this solution was added to 120 mL solution containing 7.23 g (180 mmol) NaOH and 6.28 g (37.8 mmol) terepthalic

acid. The mixture was stirred and heated for 90°C under nitrogen atmosphere at pH 9.0 for 5 hours. The precipitate was filtered, washed with 500 mL deionized water and dried under vacuum at 40°C. 5.71 g product (**B4**) was obtained.

3.6.2.1. Boric Acid-Exchange with Terephthalate-LDH without pH adjustment

0.369 g terephthalate-LDH (**B4**) was added to 170 mL solution (pH ~5) containing 0.551 g (8.90 mmol) BA. The system was refluxed under nitrogen atmosphere at 90°C for 9 hours. The slurry was stirred 24 hours before aging for 24 hours. When the ion-exchange procedure was stopped the pH of the slurry increased from the natural pH of boric acid to 7.5. The product was filtered and washed with 180 mL deionized water. 0.400 g product (**B4.1**) was obtained.

3.6.2.2. Boric Acid-Exchange with Terephthalate-LDH at pH 9

0.377 g terephthalate-LDH (**B4**) was added to 170 mL solution containing 0.550 g (8.9 mmol) BA. The initial pH of the mixture was adjusted to 9 with 1 M NaOH solution. The system was refluxed at 90°C under nitrogen atmosphere for 9 hours. The slurry was stirred 24 hours before aging for 24 hours. When the ion-exchange procedure was stopped, the pH of the slurry decreased to 8.5. The product was filtered and washed with 180 mL deionized water. 0.450 g product (**B4.2**) was obtained.

3.6.2.3. Boric Acid-Exchange with Terephthalate at pH 12.0

0.551 g terephthalate-LDH (**B4**) was added to 120 mL solution containing 0.551 g (8.9 mmol) BA. The pH was adjusted to 12.0 by 1.7 M NaOH solution and ion-exchange was proceeded at this pH. The system was refluxed under nitrogen atmosphere at 90°C for 9 hours. The slurry was stirred 24 hours before aging for 24 hours. The product was filtered and washed with 180 mL deionized water. 0.260 g product (**B4.3**) was obtained.

3.6.2.4. Tetraborate Anion-Exchange with Terephthalate-LDH

0.550 g terepthalate-LDH (**B4**) was added to 115 mL borate solution containing 5.50 g (20.9 mmol) $(NH_4)_2B_4O_7.4H_2O$. The system was refluxed at 90°C under nitrogen atmosphere for 6 hours. After refluxing, the system was continuously

stirred for 80 hours and aged for 60 hours before washing several times with 200 mL deionized water and dried under vacuum at 40°C. 0.388 g product (**B4.4**) was obtained.

3.7. Boron Removal From Aqueous Solutions by Nitrate-LDH

Boron adsorption experiments were conducted at 30°C, at the same pH of the stock solutions prepared from H_3BO_3 and $(NH_4)_2B_4O_7.4H_2O$.

The effect of the adsorbent dose was investigated by varying the amount of LDH and calcined-LDH (CA-LDH) from 0.05 g to 1.6 g in 50 mL 250 ppm stock boron solutions. The mixtures were stirred for 96 h in capped flasks, centrifuged and the supernatants were collected for the residual boron determination.

The effect of the contact time was investigated by using 300 mg LDH and CA-LDH samples in 25 mL 250 ppm boron solutions. The mixtures were stirred for different time intervals in capped flasks, centrifuged and the supernatants were collected for the residual boron determination.

3.8. Characterization

3.8.1. Chemical Analyses

3.8.1.1. C, H, N Contents

C, H, N contents were determined by a LECO CHNS-932 elemental analyzer with 0.01% accuracy.

3.8.1.2. Mg and Al Contents

Mg and Al contents were determined by a Horiba Jovin Yvon Ultima-2 ICP-OES Atomic Emission Spectrometer.

3.8.1.3. B Contents

B contents in the LDH samples were determined by a Horiba Jovin Yvon Ultima-2 ICP-OES Atomic Emission Spectrometer after dissolving the samples in 100 mL, 60% HNO_3. The residual boron in supernatants were analyzed according to the well-known Carmine method (Weicher, 1963):

0.1 mL HCl solution (1 mL concentrated HCl + 11 mL deionized water) was added to 2 mL boron solution. 10 mL concentrated H_2SO_4 was added and the resulting solution was cooled to room temperature. To this solution, 10 mL carmine solution (0.23 g carmine, dissolved in 250 mL concentrated H_2SO_4) was added. After one hour, the absorbance of this solution at 585 nm was measured in a Unicam2 UV-Vis spectrophotometer, with reference to a blank solution obtained by the same procedure using 2 mL deionized water. The boron contents were calculated using the calibration curves obtained with the standard H_3BO_3 and $(NH_4)_2B_4O_7.4H_2O$ solutions.

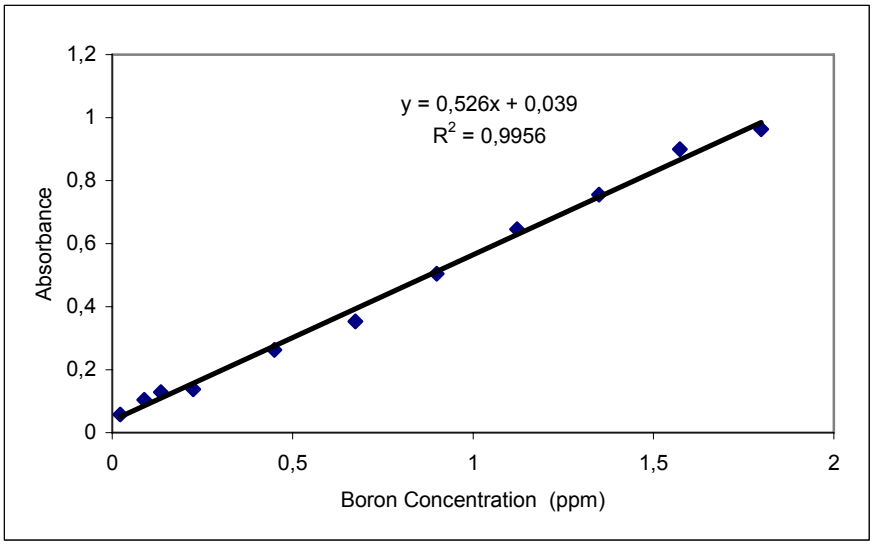

Figure 3.1. Calibration curve obtained with H_3BO_3 standard solution.

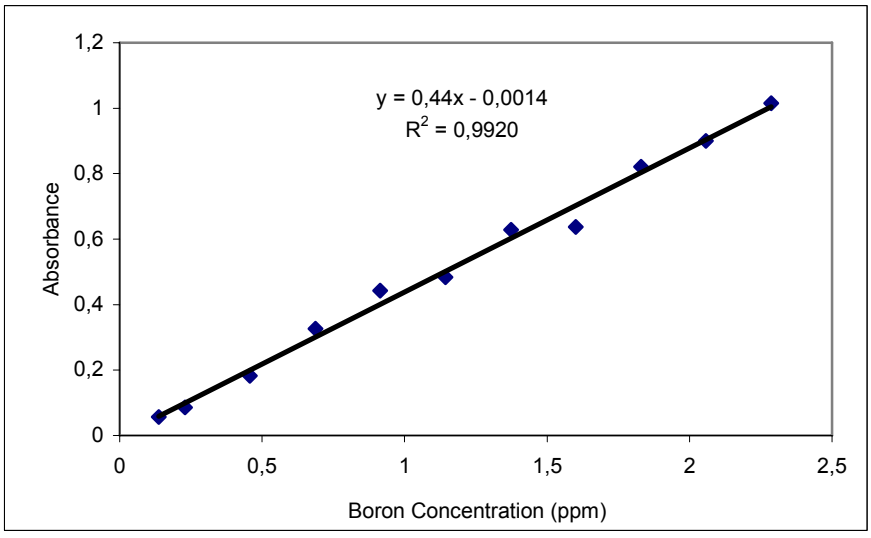

Figure 3.2. Calibration curve obtained with $(NH_4)_2B_4O_7.4H_2O$ standard solution.

3.8.2. XRD Analyses

The powder X-ray diffraction (PXRD) patterns were obtained by reflection from the powder samples packed in a sample holder with,

i. Philips PW 1140 diffractometer using Cu Kα radiation (λ=1.5418 Å). The diagrams were recorded in the 3-70° (2theta) range at a scan speed of 2°/min and a time constant of 1 s.

ii. Siemens D-500 diffractometer using Cu Kα radiation (λ=1.54050 Å). The diagrams were recorded in the 2-70° (2theta) range at a scan speed of 3°/min and a time constant of 1.5 s.

iii. Rigaku D/MAX-2200 diffractometer using Cu Kα radiation (λ=1.54056 Å). The diagrams were recorded in the 2-70° (2theta) range at a scan speed of 2°/min and a time constant of 1 s.

3.8.3. Thermal Analyses

Thermal analyses (TGA, DTA) were performed by the Shimadzu DTG-60H system, in dynamic nitrogen atmosphere (30 mL/min) at a heating rate of 10° C/min.

3.8.4. FTIR Analyses

FTIR spectra were measured in 400-4000 cm^{-1}, by using the KBR pellet technique with Mattson 1000, Perkin-Elmer 1730 and Perkin-Elmer Spectrum One instruments.

3.8.5. NMR Analyses

^{11}B MAS NMR spectra were recorded at 128.4 MHz on a Bruker Avance 400 spectrometer using short, 0.6-μs (equivalent to 15°) radio-frequency (rf) pulses, 2-s recycle delay, and fast (14 kHz) spinning rate. Chemical shifts are quoted in ppm from $BF_3.O(C_2H_5)_2$. ^{27}Al MAS NMR spectra were recorded at 104.3 MHz using short, 0.6-μs (equivalent to 10°) radio-frequency pulses, 1-s recycle delay, and 14 kHz spinning rates. For ^{13}C analysis, a Ramped-Amplitude Cross-Polarization (RAMP-CP) was used in the 1H channel to transfer magnetization from 1H to 13C. The 1H rf field was ramped from 100% to 50%, while the X rf field was set to

60kHz. Chemical shifts are quoted in ppm from $Al(NO_3)_2$ and TMS for ^{27}Al and ^{13}C, respectively.

2D Experiment:

The triple quantum (3Q) ^{11}B NMR was recorded using a three-pulse sequence. In this experiment the excitation of the 3Q coherences and its conversion into 0Q coherences, was achieved by applying two strong *rf* pulses, followed by a SPAM $\pi/2$ pulse (Ferreira et. al., 2003) for the conversion step ($\pm 3Q \rightarrow -1Q$), to further enhance the sensitivity. The symmetrization of pathways ($0Q \rightarrow \pm 3Q \rightarrow 0Q$) allows the simultaneous acquisition of the echo and anti-echo signals with equal intensity, leading to pure absorption spectra. A multiplex phase cycling (Malicka et.al., 2005) procedure was used for the selection of $\pm 3Q$ coherences. The lenghts of the first and second hard pulses (radio frequency magnetic field amplitude, υ_1 = 219 kHz) were 2.5 and 1.0 ms, respectively. The length of the third soft pulse ($\upsilon_1 \approx 9$ kHz) was 9 ms. The MAS rate was υ_R =14 kHz. 60 points were acquired in the t1 domain in increments of ($1/\upsilon_R$) = 35.71 ms. The recycle delay was 1 s, and 84 scans were recorded for each t1 value. The ppm scale was referenced with respect to $K_5BW_{12}O_{40}$ [$\delta(^{11}B)$=2.25 ppm] (Ferreira et. al., 2003).

3.8.6. Morphological Analyses

SEM images were recorded by Cameca SU-30 Semprobe and Zeiss Evo 50 EP SEM with 12 kV accelerating voltage and 130-150 pA beam current.

3.8.7. Surface Area Measurements

The specific surface areas (BET) were determined with Micrometrics, Flowsorb II 2300 and Monosorp Model/Quantochrome instruments.

3.8.8. Zeta Potential Measurements

Zeta potential measurements were carried out using a Malvern Nano ZS90.

4. RESULTS AND DISCUSSION

4.1. Chemical Compositions of the LDH samples

The approximate chemical compositions and some properties of the prepared LDH samples are given in the following tables. The samples were analyzed for their Mg and Al contents for the composition of the HT layers and for their boron, nitrogen and carbon contents for the composition of the interlayer region. The approximate charge balance in the formulas was established by assuming the neutralization of aluminum atoms by the interlayer nitrate, borate, carboxylate or carbonate anions. Nature of the intercalated borate species was deduced from ^{11}B MAS NMR data. Although the sample preparation was strictly conducted under nitrogen atmosphere, a minor amount of carbonate contamination was inevitable in some cases.

For most of the samples, the experimental Mg:Al molar ratios are different, which is generally the case for LDHs (Weir et al., 1997), than the ratios that charged in the preparations as Mg:Al=2. This may be due to

i. the partial removal of Mg^{2+} from the layers or

ii. formation of a separate but X-ray inert $Al(OH)_3$ phase.

$Mg(OH)_2$ is fairly soluble at pH 8 and below, therefore a large amount of Mg^{2+} may be removed from the layers to the solution phase particularly in the long co-precipitation processes and lost during washing.

4.2. Structural Characterization of LDH's

PXRD is the main analytical technique for the characterization of LDH's. Interpretation of PXRD and other physical data for the structural characterization of the LDH's have been **representatively** given below, for the nitrate-LDHs.

4.2.1. Structural Characterization of Nitrate-LDHs

4.2.1.1. Structural Characterization of Nitrate-LDH Prepared by Conventional Precipitation (B1)

The PXRD pattern of the nitrate-LDH (**B1**), prepared by co-precipitation from the precursor salt solutions, is shown in Figure 4.1. The pattern shows broad asymmetric peaks at higher angles, which are characteristics of clay minerals possessing a layered structure and similar to the pattern of natural HT. At low 2θ angles, a sharp symmetric 003 reflection is observed.

Positions of the first two intense peaks, corresponding to (003) and (006) planes are dependent on the size of the interlayer anions (Cavani et al., 1991). The *d* spacing (8.55 Å), was calculated from the first sharp basal reflection (003) by using the Bragg equation (2θ=10.34 Å). The gallery height was found to be 3.75 Å by subtracting the layer thickness (8.55Å-4.8Å=3.75Å) from the *d* value. This distance allows the orientation of interlayer NO_3^- anions in tilted position as shown in Scheme 4.1 (Del Arco et al., 2000). The first component of the doublet peak at ca. 2θ=60° is related with the plane (110) and corresponds to the average metal-metal distance (1.5 Å) in the layers.

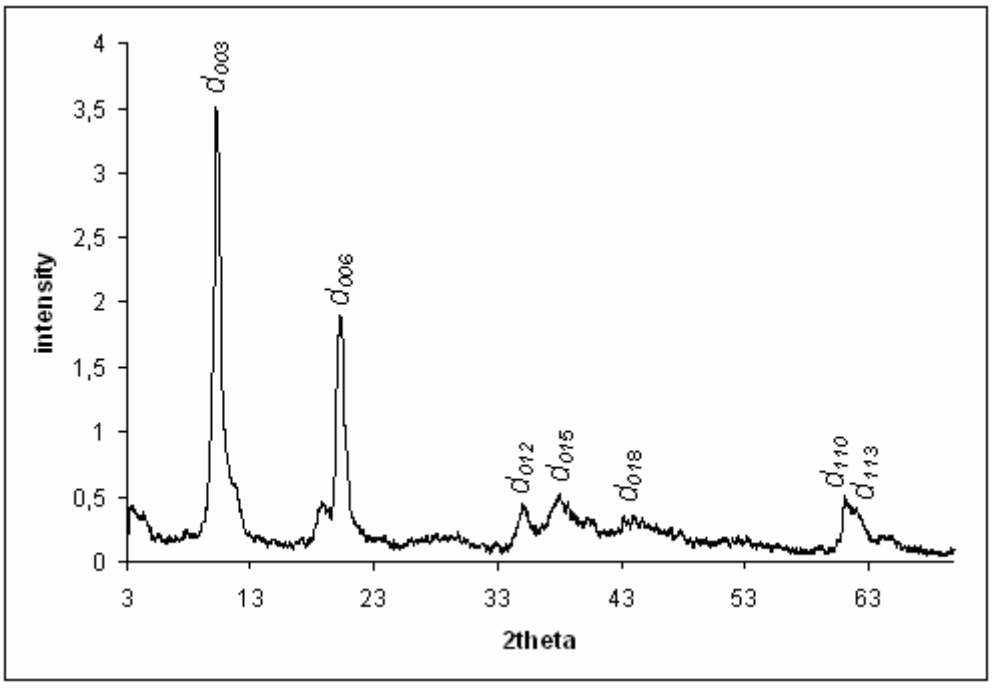

Figure 4.1. PXRD pattern of nitrate-LDH (**B1**).

Although FTIR spectroscopy is not exactly a diagnostic technique for LDHs, it is useful to characterize the interlayer anions between the basal sheets (Cavani et al., 1991). Figure 4.2 shows the FTIR spectrum of **B1**. The layer O-H vibrations can be identified around 3400-3600 cm^{-1} (stretching) and 950-1000 cm^{-1} (bending) (Hernandez-Moreno M., 1985). The peak at 3453 cm^{-1} is mainly due to the Al-OH bond (Kloprogge and Frost, 1999). The 3525 cm^{-1} peak belongs to both Mg-OH and Al-OH stretchings. The peak at 1377 cm^{-1} indicates the ν_3 anti-symmetric stretching of nitrate anion. Bending mode of the interlayer and/or adsorbed water appears at 1633 cm^{-1}. 827 cm^{-1} peak is attributed to the out of plane deformation (ν_2 mode) of nitrate anions. Finally, the peaks at 668 and 550 cm^{-1} belong to the Mg–O and Al–O stretching modes (Kloprogge, 1999; Del Arco et al., 2000; Kustrowski, 2005).

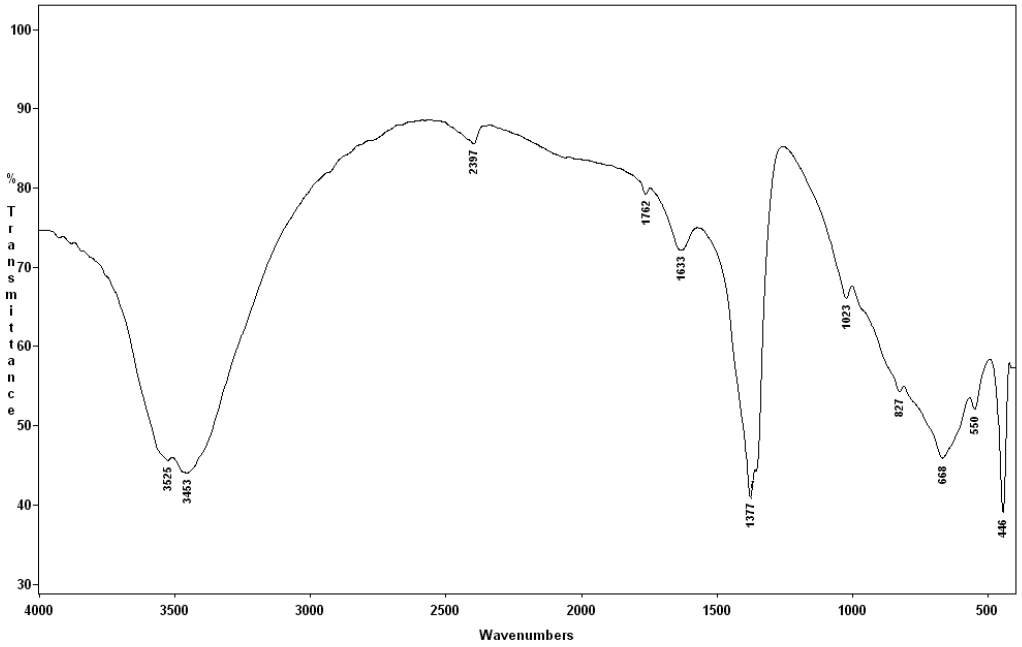

Figure 4.2. FTIR spectrum of **B1**.

The TGA and DrTGA curves of the **B1** are shown in Figure 4.3. Surface (free) water evaporates below 140°C. The loss of interlayer water molecules follows afterwards and continues up to 375 °C. Dehydroxylation, removal of the hydroxyl groups from the layers as water vapour, and decomposition of the interlayer anions occur at higher temperatures up to 600°C. The total mass loss at 900°C is 53.1 %. The calculated mass loss for the formation of Mg- and Al- oxides (0.58

mol MgO + 0.21 mol Al_2O_3) from the formula of **B1** is 51.7 %. The agreement between the two values confirms the reliability of the derived formula.

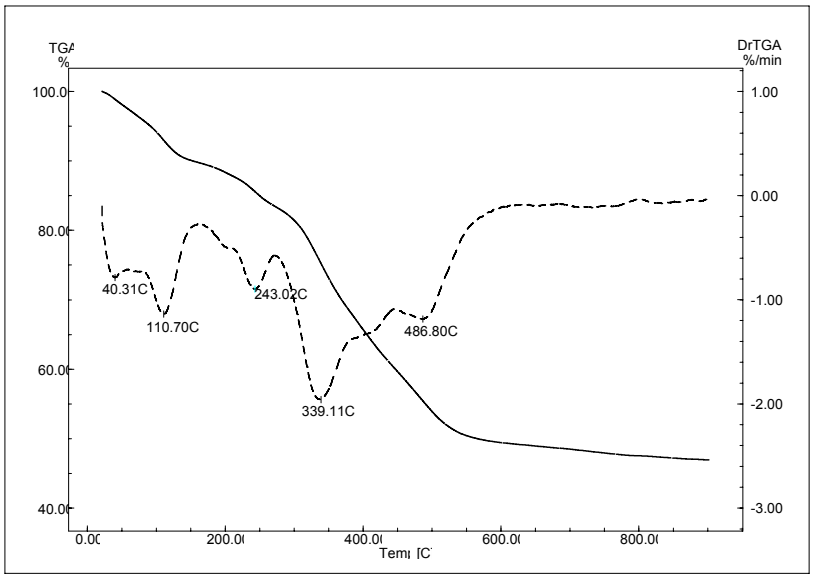

Figure 4.3. TGA (—) and derivative TGA (DrTGA) (---) curves of **B1**.

Figure 4.4 shows the ^{27}Al MAS NMR spectrum of **B1**. Substitution of some of the Mg^{+2} ions with Al^{+3} ions creates a net positive charge on the layers wherein Al^{+3} cations locate themselves in the octahedral sites. The spectrum displays a single peak at 10.4 ppm indicating the presence of the six-coordinated aluminium atoms with equal chemical surroundings (Del Arco et al., 2000).

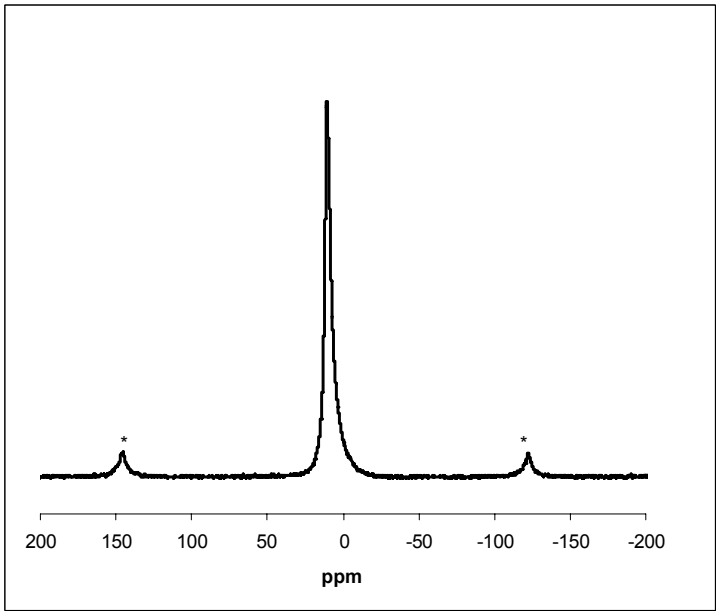

Figure 4.4. ^{27}Al MAS NMR spectrum of **B1** (*Spinning side bands).

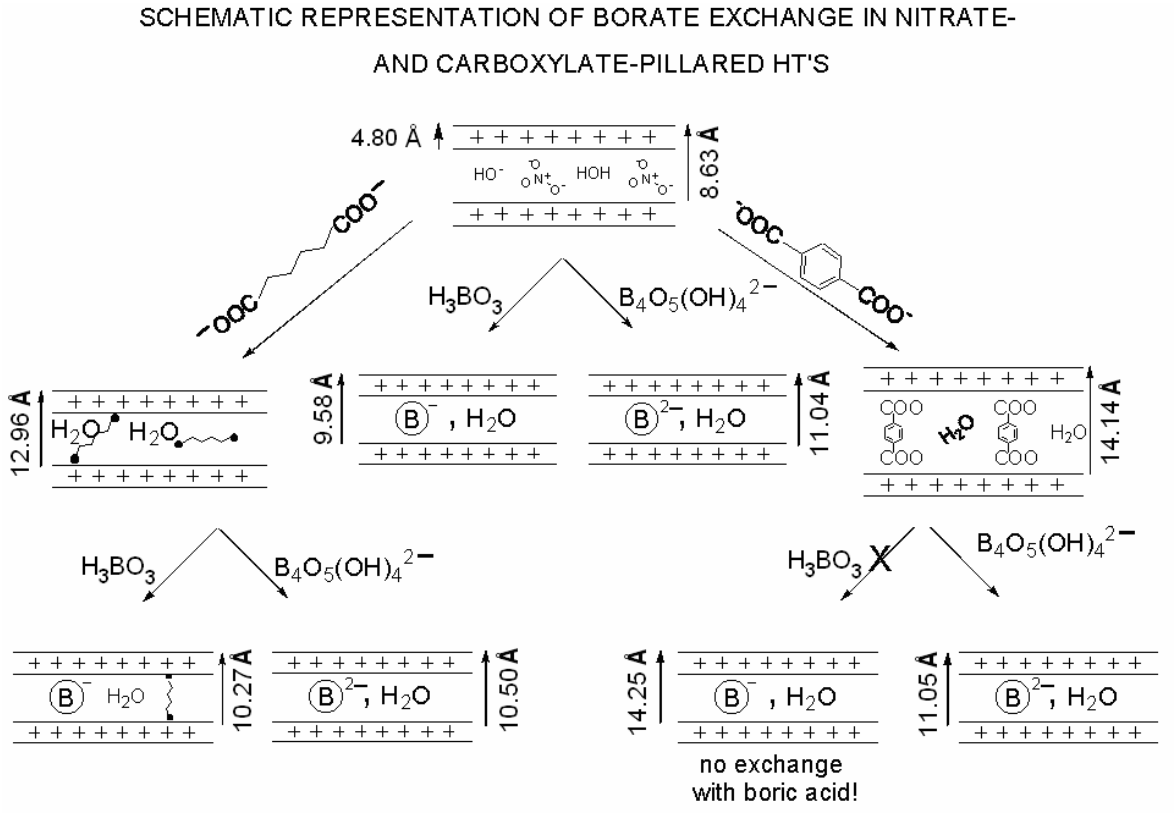

Scheme 4.1. Schematic representation of borate exchange in nitrate– and carboxylate- ion intercalated LDHs.

The formula of **B1** derived from the analytical results is: $[Mg_{0.58}Al_{0.42}(OH)_2](NO_3)_{0.36}(CO_3)_{0.028}.0.6H_2O]$. According to this formula, the experimental Mg:Al molar ratio (1.4) of the LDH sample is smaller than that charged in the preparation (2.0). It is possible to obtain LDH's with x [x=Al/(Al+Mg)] values of up to 0.44 (Cavani et al., 1991) and this can be an advantage for anion adsorption since solids with lower Mg:Al ratios have increased number of positive sites (Al^{+3} ions) in the layers and therefore allow easier exchange of interlayer anions with foreign ions (Del Arco et al., 2000).

The structure and the surface morphology of the **B1** was analysed by scanning electron microscopy. The layered structure of the sample can be easily visualized from the SEM images shown in Figure 4.5.a and b. Stacking of layers in rose-like morphology (Figure 4.5.b) is typical for such materials.

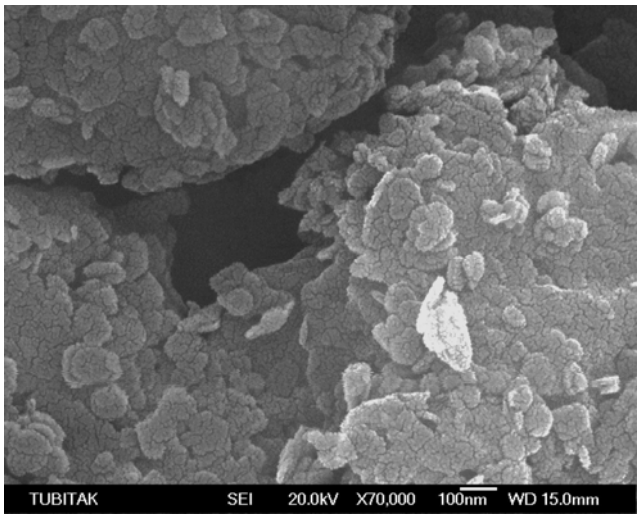

a

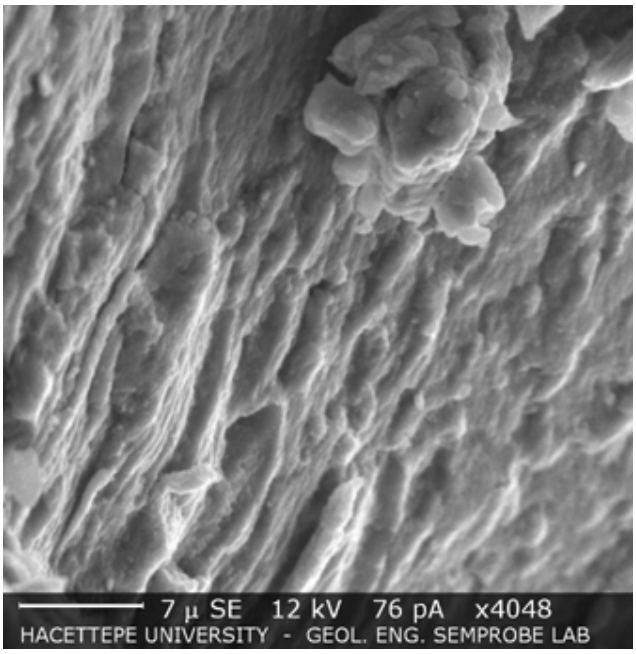

b

Figure 4.5. SEM images of **B1**.

4.2.1.2. Structural Characterization of Nitrate-LDH Prepared by Mechanochemical Activation (B2)

Mechanochemical reactions have been known for a long time where the transformation can be induced by milling or manual grinding. Such reactions between solid reactants without a solvent are important from both the environmental and topochemical viewpoints. Using mechanochemical synthesis, one can avoid manipulations with large amounts of solutions, the emission of noxious gases and the release of wastewater. These solvent-free, less

conventional procedures are beginning to be used as viable routes for the preparation of LDHs. There is only one report in the literature regarding the formation of Mg-Al-LDH by mixing magnesium hydroxide with aluminum chloride, nitrate and sulfate in a high-energy planetary-type activator (Isupov et al., 2000). In this work, a simpler mechanochemical method has been developed. Manual grinding the hydrated magnesium and aluminum nitrate salts in a mortar and washing the paste several times, yielded a product with similar characteristics to that obtained by co-precipitation. Figure 4.6 shows the PXRD pattern of the NO_3-LDH (**B2**) prepared by this simple and more productive method comparatively with the sample prepared by conventional technique (**B1**). The patterns show a close structural similarity. Even though the crystallinity of **B2** is not so high, all characteristic peaks of layered double hydroxides can be easily recognized. The *d* spacings, 8.63Å for **B1** and 8.59Å for **B2** were calculated from the first sharp basal reflection (003) by using the Bragg equation. The interlayer distances were calculated by subtracting the sheet thickness (4.8 Å) from the *d* values. The gallery heights thus obtained, 3.83 Å (**B1**) and 3.79 Å (**B2**), may allow the accommodation of NO_3^- anions between the layers in tilted position (Scheme 4.1).

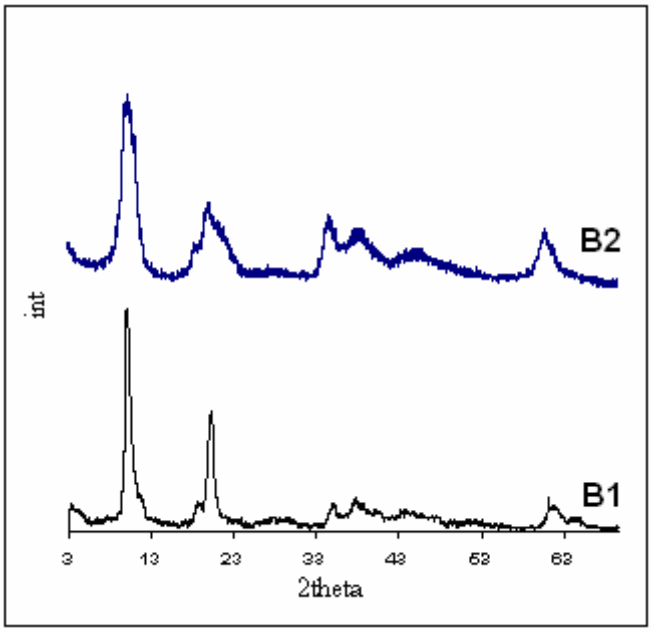

Figure 4.6. PXRD patterns of **B1** and **B2**.

The FTIR spectrum of the mechanochemically prepared LDH (**B2**) is shown in Figure 4.7. The spectrum is very similar to that prepared by the co-precipitation method, as described in Section 4.2.1.1.

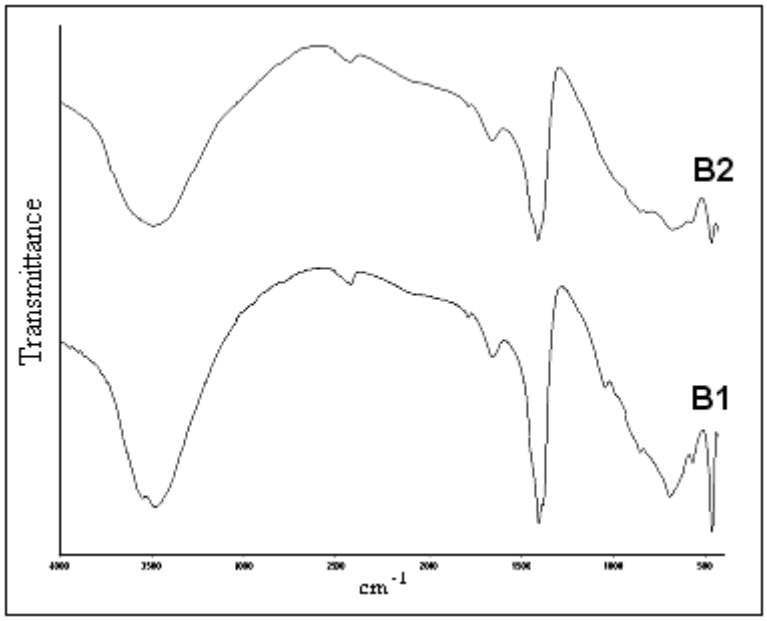

Figure 4.7. FTIR spectra of **B1** and **B2**.

To better analyze the Al sites in the layers, ^{27}Al MAS NMR analyses were employed. As shown in Figure 4.8, both samples displayed a single, sharp resonance centered at 9-10 ppm (10.4 ppm for **B1** and 9.76 ppm for **B2**) indicating the presence of the six-coordinated aluminium atoms with equal chemical surroundings rather than perturbed aluminum atoms (Del Arco et al., 2000).

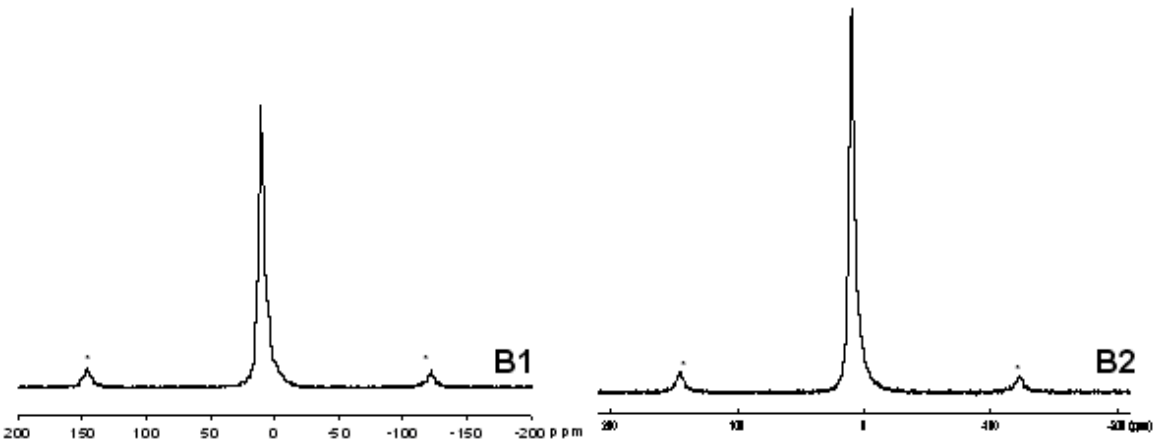

Figure 4.8. ^{27}Al MAS NMR spectra of **B1**and **B2** (*Spinning side bands).

Thermal decomposition behavior of **B1** and **B2** are also similar as shown in Figure 4.9. Surface (free) water evaporates below 140°C. The loss of interlayer water molecules follows afterwards and continues up to 375°C. Dehydroxylation, removal of the hydroxyl groups from the layers as water vapour, and decomposition of the interlayer anions occur at higher temperatures up to 600°C. For the sample **B2**, the total mass loss at 900°C is 50.3 %. The calculated mass loss for the formation of Mg- and Al- oxides (0.64 mol MgO + 0.18 mol Al_2O_3) from the formula of **B2** is 52.4 %. The agreement between the two values confirms the reliability of the derived formula.

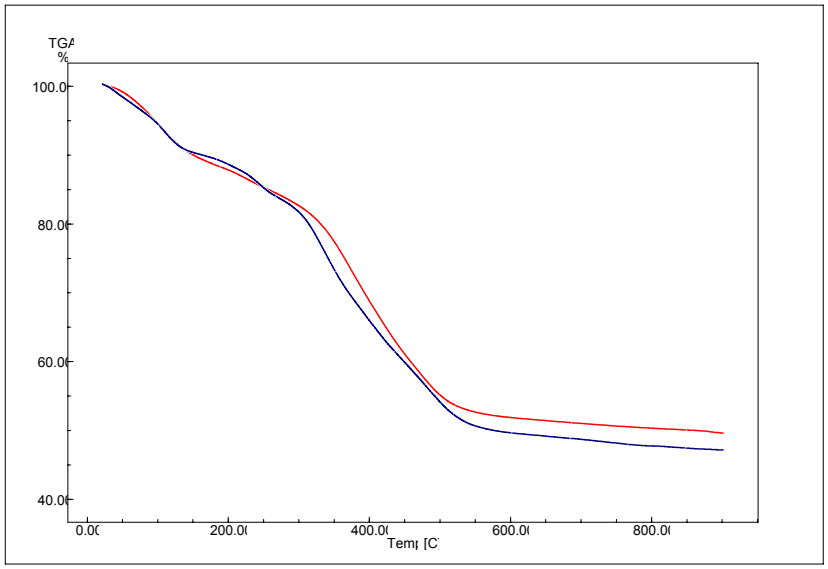

Figure 4.9. TGA curves of **B1** (—) and **B2** (—).

An examination of some properties of the samples **B1** and **B2** was comparatively undertaken (Table 4.1). The zeta potential value of **B1** at neutral pH is nearly zero which means that the surface possesses no residual positive charge and the layer charge is completely balanced. BET surface area of **B1** is correlated with the presence of interlayer pores and intercrystalline pores related with the better crystallinity of the sample (Bravo-Suarez, 2004). On the other hand, due to the rapid nucleation in the mechanochemical process, some Al^{3+} ions might have become crowded on the surface sites in **B2**, resulting in a higher surface charge and hence giving a positive ζ value. The correlation of the surface charge density and the Mg:Al ratio with the microporous structure of LDH's has been analyzed by

Weir and Kydd (1998). It is likely that the materials with higher surface charge densities contain smaller pores and slight changes in the layer composition may result in different BET surface areas.

Table 4.1. Chemical compositions and some properties of **B1** and **B2**.

Sample	Formula	Mg/Al	d_{003}(Å)	S_{BET} (m^2g^{-1})	ζpot. (mV)
B1	$[Mg_{0.58}Al_{0.42}(OH)_2](NO_3)_{0.42}\cdot 0.6H_2O$	1.4	8.63	23	+0.85
B2	$[Mg_{0.64}Al_{0.36}(OH)_2](NO_3)_{0.36}\cdot 0.6H_2O$	1.8	8.59	6	+9.86

Regardless of the experimental Mg:Al ratios given in Table 4.1, PXRD patterns of **B1** and **B2** indicated well formed LDHs which means that the true composition in the layers is different than the bulk composition.

The products have similar morphologies where layering within **B2** is evident from its SEM image shown in Figure 4.10.

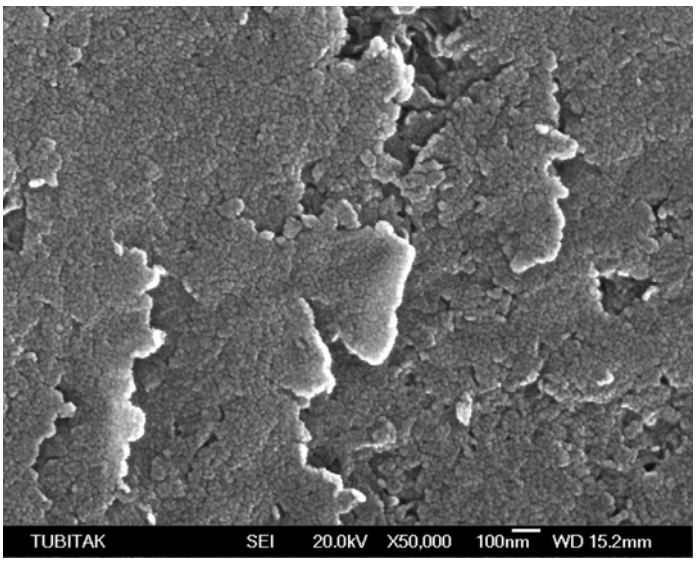

Figure 4.10. SEM image of **B2**.

4.2.2. Structural Characterization of Borate Intercalated LDH's Prepared by Direct Methods

4.2.2.1. Borate Intercalation by Co-Precipitation

PXRD patterns of the borate intercalated LDH's prepared *via* co-precipitation method with BA (**A1.1**) and TB (**A1.2**) solutions are shown in Figure 4.11. **A1.1** displayed a higher crystallinity. The first three sharp peaks correspond to the (003), (006) and (009) diffractions and the first peak at 9.77° corresponds to a *d* spacing of 9.05 Å. The interlayer space was calculated as 4.25 Å by subtracting the layer thickness of the LDH from the *d* value.

The broad PXRD pattern obtained for **A1.2** indicated that a poorly crystalline LDH was formed with TB ions. Apparently, self-organization with the larger TB anions led to a less-ordered structure in the co-precipitation method. Apart from their crystallinities, samples **A1.1** and **A1.2** have similar chemical compositions and properties (Table 4.2).

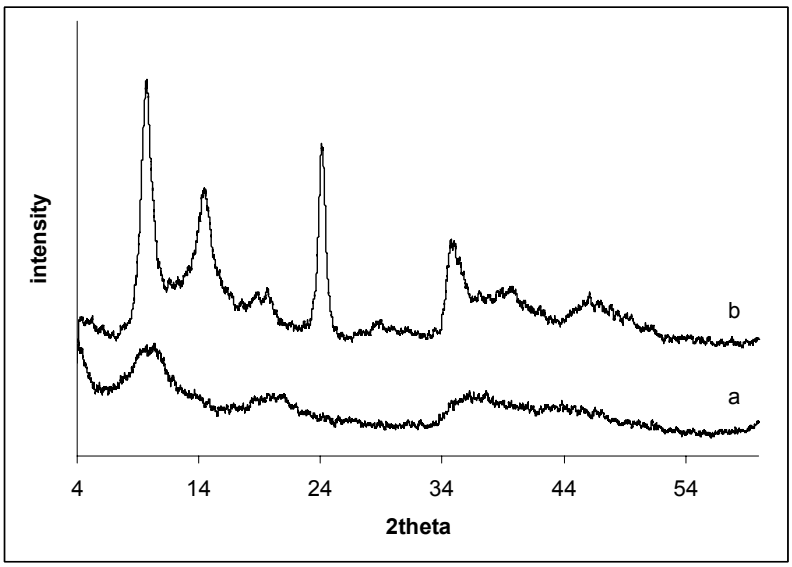

Figure 4.11. Powder XRD patterns of boron intercalated LDH's prepared by co-precipitation with a- tetraborate (**A1.2**) and b- boric acid (**A1.1**) solutions.

Table 4.2. Chemical compositions and some properties of borate-LDH samples prepared by co-precipitation.*

Sample	Formula	d_{003}(Å)	Mg/Al	B%	BET (m^2/g)
A1.1	$[Mg_{0.59}Al_{0.26}(OH)_2](NO_3)_{0.96}[BO_x]_{0.328}.\ 0.5H_2O$	9.05	2.25	3.5	39
A1.2	$[Mg_{0.56}Al_{0.28}(OH)_2](NO_3)_{0.04}[BO_x]_{0.36}.0.5H_2O$	8.48	2	3.7	52

*The nature of the borate species in the interlayer region is uncertain.

The FTIR spectrum of the well-crystalline product (**A1.1)** is seen in Figure 4.12. The peaks at 1367 cm^{-1}, 1492 cm^{-1}, 939 cm^{-1} and 801 cm^{-1} are assigned to ν_3 BO_3 stretchings; those at 1144 cm^{-1} and 1001 cm^{-1} are assigned to ν_3 BO_4 stretchings and those at 674 cm^{-1}, 553 cm^{-1} and 447 cm^{-1} are the LDH lattice modes (Li et al., 1996).

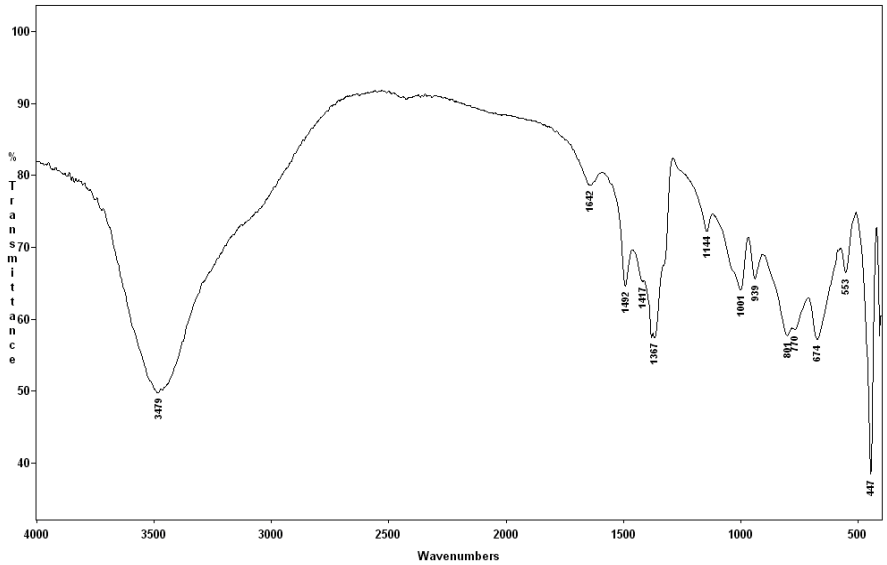

Figure 4.12. FTIR spectrum of **A1.1**.

The TGA and DrTGA curves of **A1.1** are shown in Figure 4.13. The weight loss up to 146°C is due to the evaporation of the surface (free) water followed by the loss of interlayer water molecules up to 235°C. Dehydroxylation, removal of the hydroxyl groups from the layers as water vapour, and the decomposition of the interlayer nitrate and borate anions occur at higher temperatures and continue up

to 720°C. The boron-intercalated sample is thermally more stable than the NO_3-LDH sample.

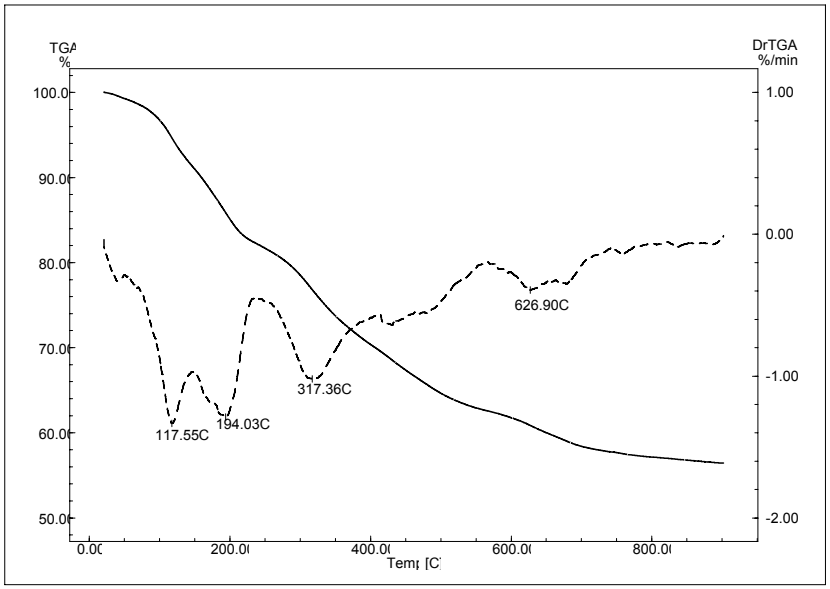

Figure 4.13. TGA (—) and DrTGA (---) curves of **A1.1**.

4.2.2.2. Borate Intercalation by Mechanical Activation

Figure 4.14 shows the PXRD pattern of the LDH sample (**A2**) synthesized mechanochemically with BA. The crystallinity of the product is low. In this case, the fast organization of the layers and the interlayer ions in the mortar, with the presence of boric acid molecules, led to the formation of a poorly crystalline material. Nevertheless, a layered structure could be obtained to some extent since the observed *d* spacing (ca 8.74 Å) is close to that of the nitrate-LDH prepared by co-precipitation (8.63 Å).

The characteristic vibrations of interlayer nitrate ions are recognized in the FTIR spectrum of this product, as described in Section 4.2.1.1, while no peak could have been assigned to the presence of interlayer borate anions. PXRD pattern and the FTIR spectrum revealed that the synthesized product is indeed NO_3-LDH and direct borate intercalation did not occur. It appears that the soft mechanical activation by manual grinding is sufficiently effective in the organization of small ions like Mg^{2+} and Al^{3+} into a layered structure with nitrate ions but ineffective in the simultaneous intercalation of boric acid molecules.

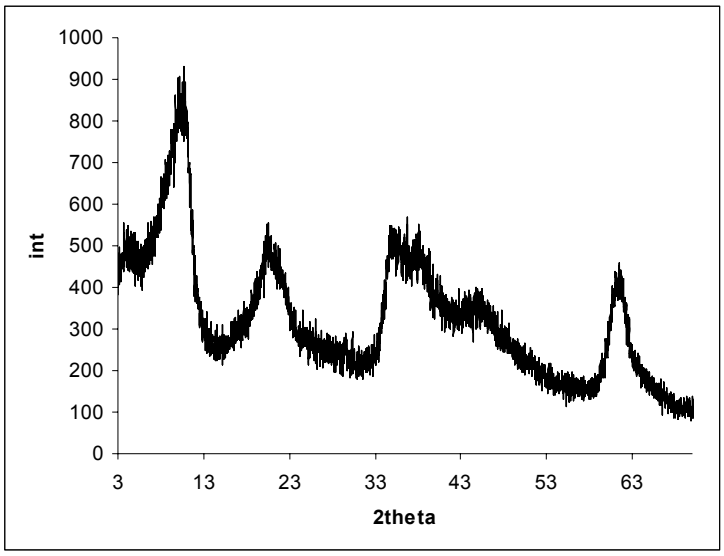

Figure 4.14. PXRD pattern of **A2.**

4.2.3. Borate Intercalation by Ion-Exchange with Nitrate-LDH

Ion-exchange studies were performed with the NO_3-LDH sample (**B2**) described in **4.2.1.1**. Exchange experiments were conducted with boric acid solution at different pH values and with ammonium tetraborate solution. It is well known that in aqueous solutions, a distribution of borate species is established between mono- and polyborate species based on concentration, temperature and pH considerations (Figure 4.16). The nature and the amount of borate species intercalated not only depends on the initial pH of the borate solutions but also to the local pH changes in the layers during the ion exchange process since HT-like compounds are known to have buffering properties (Ferreira et al., 2006).

4.2.3.1. Boric Acid-Exchange with Nitrate-LDH without pH adjustment (B1.1)

Figure 4.16 shows the PXRD pattern of the LDH sample after exchanging the nitrate ions with boric acid solution, without making any pH adjustment. During the ion-exchange process, pH increased from the natural pH of boric acid solution (4.5-5) to 7.6. The increase in the pH may be due to the removal of some $Mg(OH)_2$ from the layers at the initial low pH of the medium. This results in the decomposition of the layers as can be realized from the low Mg/Al ratio obtained for this sample (Table 4.3). Consequently, a low crystalline material was obtained. The basal spacing calculated from the Bragg equation is 9.46 Å. The galleries expanded from 8.63 Å to 9.46 Å by exchanging the nitrate ions with the larger

borate anions. The pattern showed the presence of impurity phases with peaks at 2θ=18.26° and 20.26°.

Table 4.3. Chemical compositions and some properties of borate-LDHs prepared by exchange with boric acid solution.

Sample	Formula	d_{003} (Å)	Mg/Al	B%	DrTGA* peak (°C)
B1.1	$[Mg_{0.49}Al_{0.51}(OH)_2][BO_x]_{0.33}(CO_3)_{0.14}\cdot 0.5H_2O$	9.58	0.94	3.4	694
B1.2	$[Mg_{0.57}Al_{0.43}(OH)_2][B_4O_5(OH)_4]_{0.094}(NO_3)_{0.0085}(CO_3)_{0.125}\cdot 0.5H_2O$	9.46	1.31	3.8	699
B1.3	$[Mg_{0.68}Al_{0.32}(OH)_2][B_3O_3(OH)_4]_{0.036}(NO_3)_{0.017}(CO_3)_{0.11}\cdot 0.6H_2O$	7.69	2.13	1.2	676

*DrTGA peak temperature corresponding to the collapse of the lattice

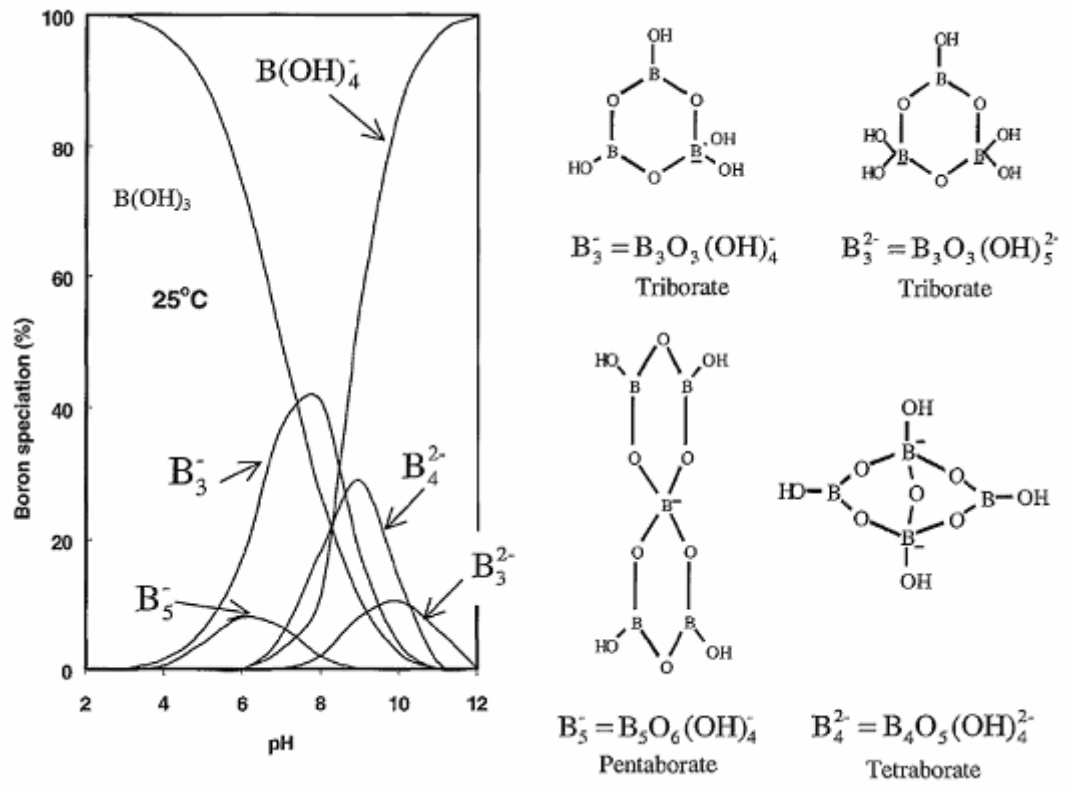

Figure 4.15. Distribution of boron species in aqueous solutions (Simon and Smith, 2000).

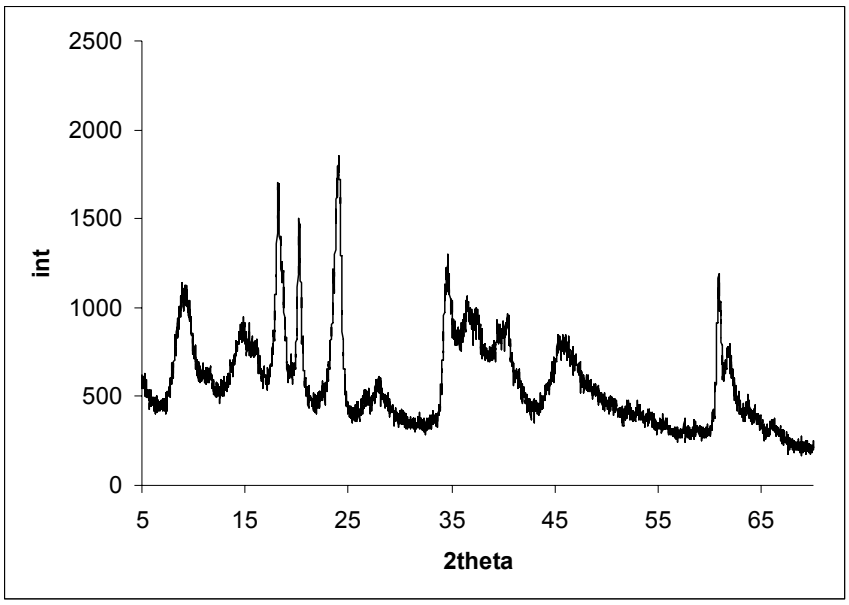

Figure 4.16. PXRD pattern of **B1.1**.

FTIR spectrum of **B1.1** shown Figure 4.17, is similar to the borate-intercalated sample prepared by co-precipitation, as described in **4.2.2.1**.

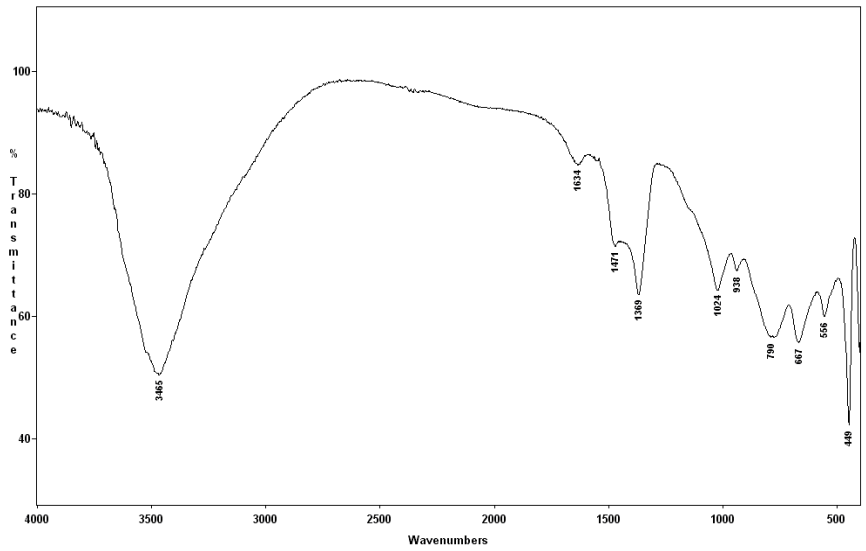

Figure 4.17. FTIR spectrum of **B1.1**.

Analytical results and the FTIR spectrum confirmed the presence of boron in **B1.1**. The increase in the *d* spacing provided evidence that the incorporated boron are intercalated (Table 4.3).

The exact nature of the borate species in the interlayer region was investigated by the solid state ^{11}B-NMR technique. The trigonally coordinated boron has a higher second-order quadrupolar interaction and exhibits doublet patterns, while the tetrahedrally coordinated boron exhibits relatively narrow lines (Li et al., 1996). The proportion of tri-B/tetra-B in the borate species is determined by computing the related peak areas.

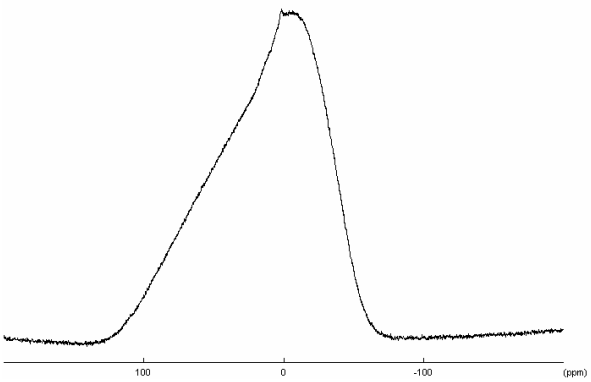

Figure 4.18. ^{11}B MAS NMR spectrum of **B1.1** (ppm from $K_5BW_{12}O_{40}$).

The ^{11}B MAS NMR spectrum in Figure 4.18 shows small, unresolved ^{11}B peaks corresponding nearly to the background rotor boron. Therefore the exact nature of the borate species could not be obtained from the ^{11}B NMR data. This is reflected in the approximate formula given in Table 4.3.

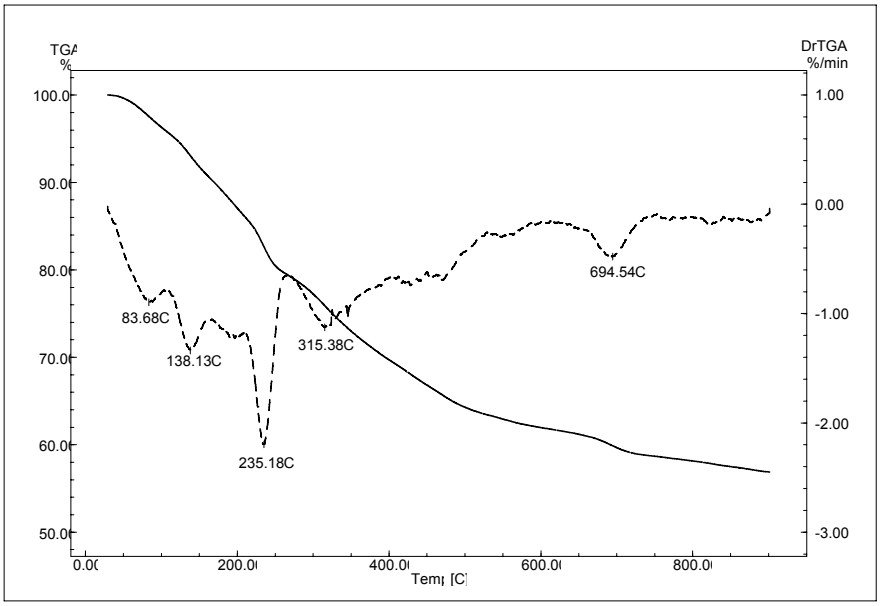

Figure 4.19. TGA (—) and DrTGA (---) curves of **B.1.1**.

The TGA and DrTGA curves of **B1.1** are shown in Figure 4.19. The sample is thermally stable and decomposition continues up to ca. 700°C.

4.2.3.2. Boric Acid-Exchange with Nitrate-LDH at pH 9 (B1.2)

Figure 4.20 shows the PXRD pattern of the LDH sample after exchanging the nitrate ions with boric acid solution at pH 9. The basal spacing of the sample was calculated as 9.46Å which is almost equal to that of the sample synthesized without pH adjustment (**B1.1**). The displayed PXRD pattern of **B1.2** also looks very similar to that of **B1.1**, but with a better crystallinity.

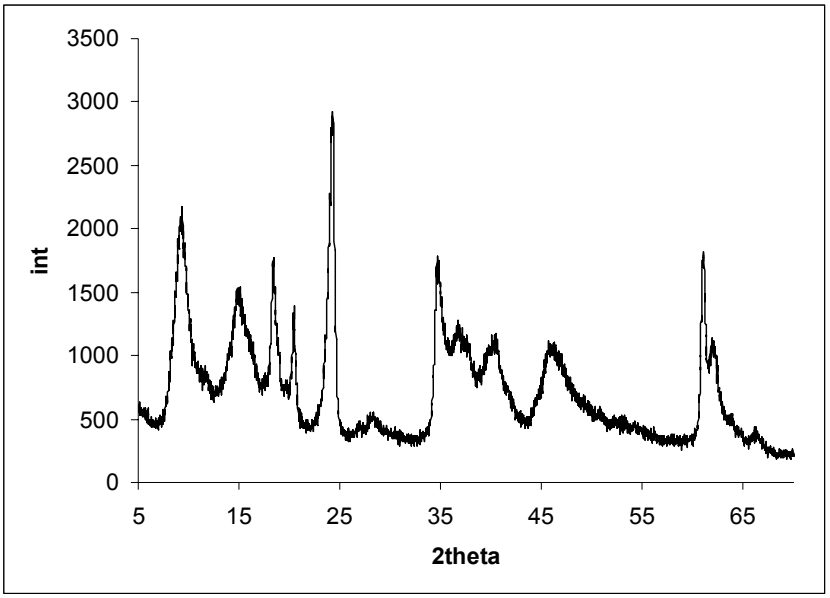

Figure 4.20. PXRD pattern of **B1.2**.

The FTIR spectrum of **B1.2** is shown in Figure 4.21. Like their PXRD patterns, FTIR spectra of **B1.1** and **B1.2** are similar as well.

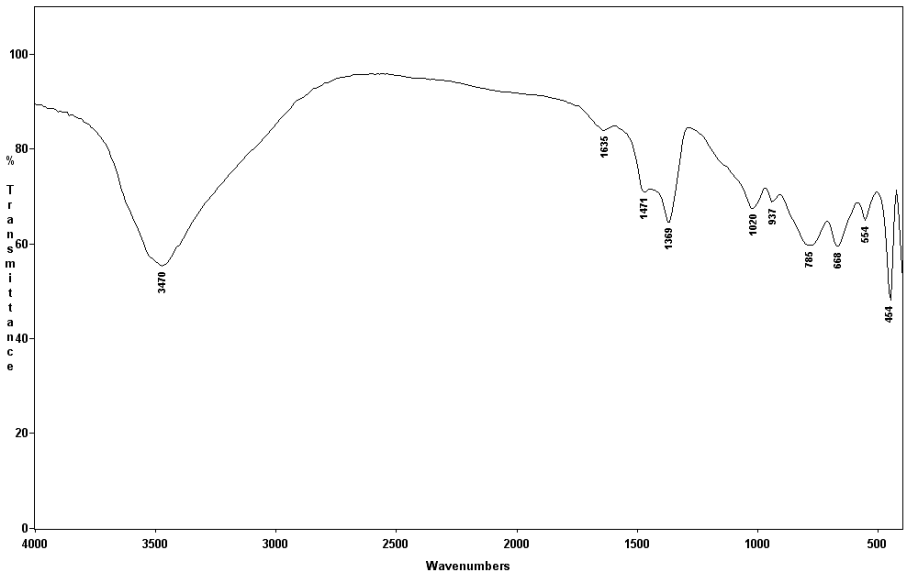

Figure 4.21. FTIR spectrum of **B1.2**.

Although the PXRD diffraction patterns and the FTIR spectra of **B1.1** and **B1.2** are very similar, the ^{11}B MAS NMR spectra of the samples are different. The 2D ^{11}B MQ MAS spectrum of **B1.2** clearly shows the presence of two different types of boron atoms (Figure 4.22). The singlet signal at 2.25 ppm is assigned to the tetrahedrally coordinated boron (tetra-B) and the doublet signal at 15.08 ppm is assigned to the trigonally coordinated boron (tri-B) (Li et al., 1996). The proportion of tri-B/tetra-B in the borate species is determined by computing the related peak areas. The computed ratio from the spectral data is 1 and corresponds to the B_4^{2-} species where two tri- and two tetra-coordinated boron atoms are present. In the 1D^{11}B MAS NMR spectrum shown in Figure 4.23, the second component of the doublet is overlapped by the singlet peak. Thus the formula of **B1.2** was approximately derived as: $[Mg_{0.57}Al_{0.43}(OH)_2][B_4O_5(OH)_4]_{0.094}(NO_3)_{0.0085}(CO_3)_{0.091}.0.5H_2O$.

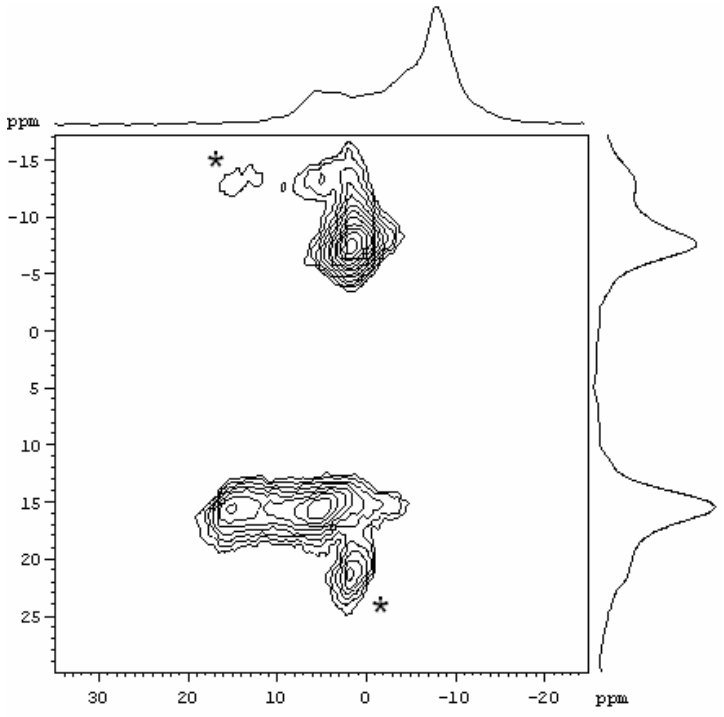

Figure 4.22. 2D ^{11}B MQMAS spectrum of **B1.2** (*spinning side bands).

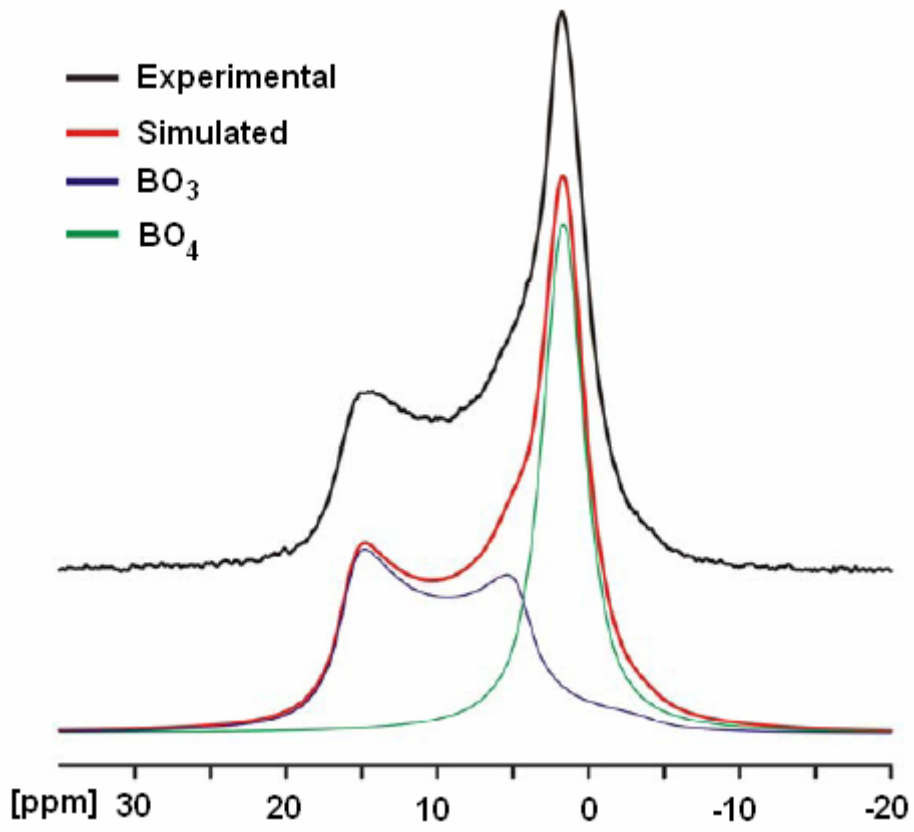

Figure 4.23. Experimental and simulated ^{11}B MAS NMR spectrum of **B1.2** (ppm from $K_5BW_{12}O_{40}$).

According to the observed *d* spacing value; the gallery height in **B1.2** is 9.46Å-4.8Å=4.66Å. This distance can allow the accommodation of $[B_4O_5(OH)_4]^{2-}$ ions, for which the dimension is 3.6 Å, only in horizontal or slightly tilted orientation (Figure 4.24).

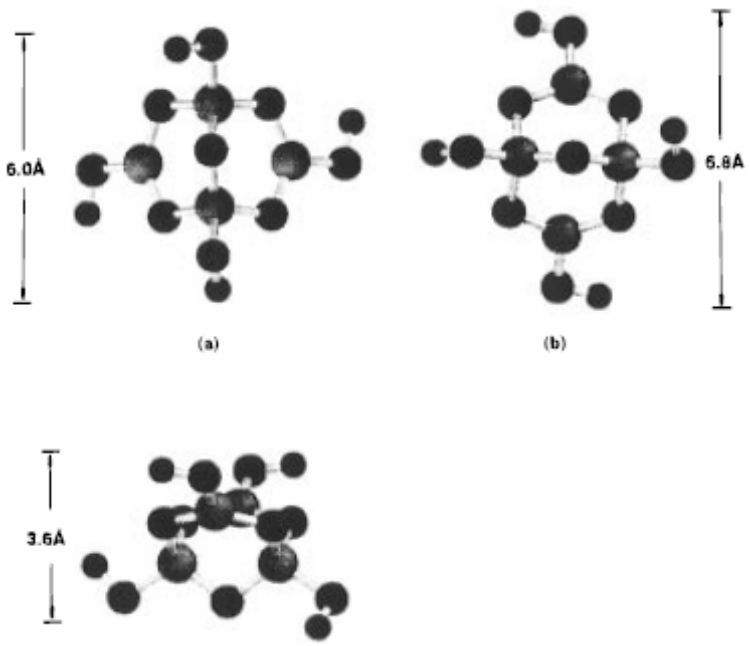

Figure 4.24. Schematic drawing of the tetraborate anion along different projections obtained after energy minimization and geometry optimization using the Spartan calculations. (large balls: boron, medium balls: oxygen, small balls: hydrogen) (Li et al., 1996)

Figure 4.25 shows the TGA, DrTGA and DTA curves of **B1.2**. The endothermic peaks seen on the DTA curve at 78 and 130°C correspond to the loss of surface and interlayer water. The peaks at 187, 233, 308 and 508°C correspond to the dehydroxylation of the LDH sheets and of the interlayer anion, $[B_4O_5(OH)_4]^{2-}$. The exothermic peak at 717°C can be assigned to the complete lattice collapse and phase transition to a mixed oxide system (Li et al., 1996; Cheng and Lin, 1992).

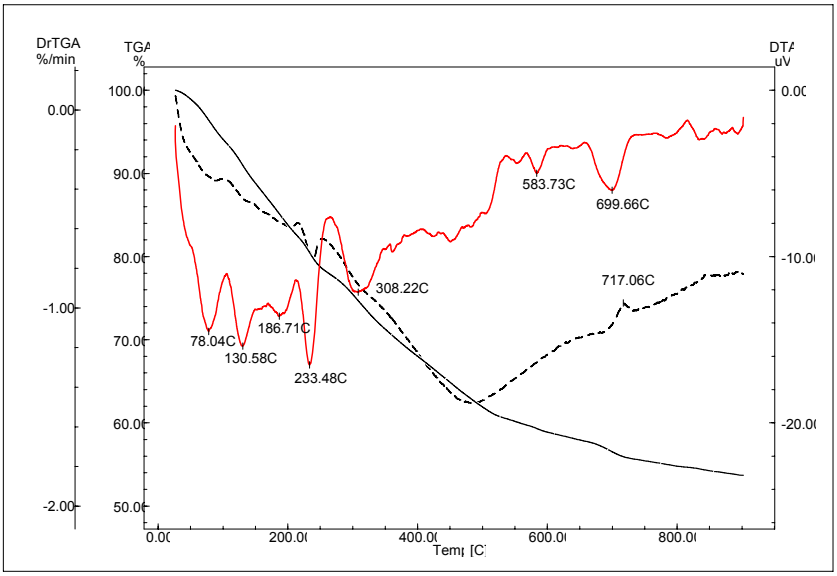

Figure 4.25. TGA (—), DrTGA (—) and DTA (---) curves of **B1.2**.

4.2.3.3. Boric Acid-Exchange with Nitrate-LDH at pH 12 (B1.3)

A highly crystalline sample was obtained at pH 12. The basal spacing of the layered material was calculated as 7.65 Å from the PXRD pattern shown in Figure 4.26.

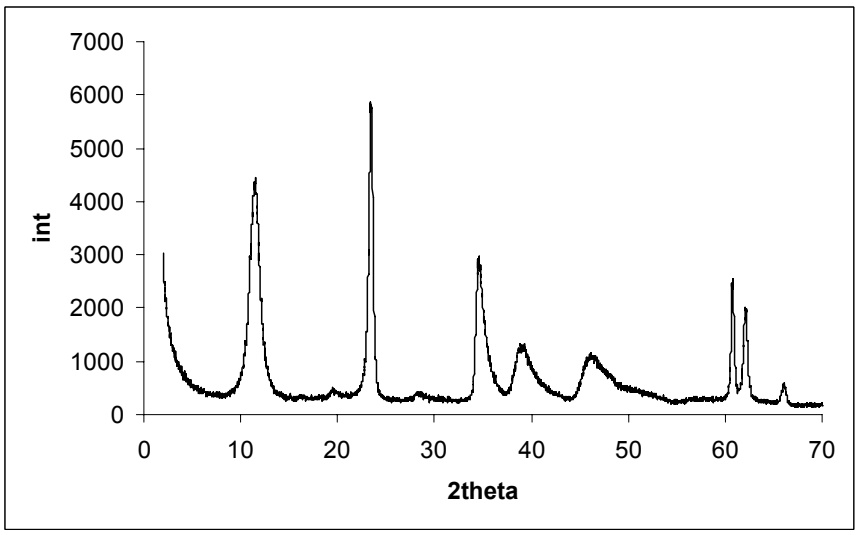

Figure 4.26. PXRD diffraction pattern of **B1.3**.

Figure 4.27 shows the ^{11}B MAS NMR spectrum of **B1.3**. Two types of boron peaks can be clearly seen. The tri-B/tetra-B peak area ratio was calculated as

63:37(~2:1) indicating the intercalating B_3^- ion which has two trigonal and one tetrahedral boron atoms.

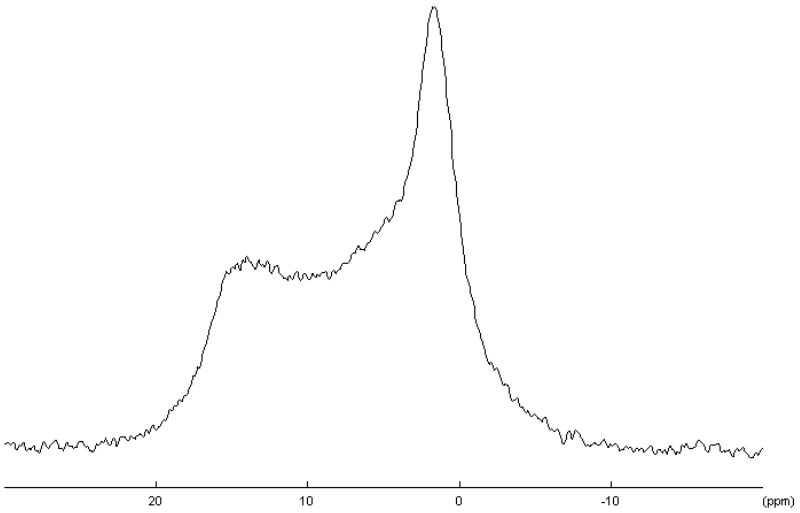

Figure 4.27. ^{11}B MAS NMR spectrum of the sample **B1.3** (ppm from $K_5BW_{12}O_{40}$).

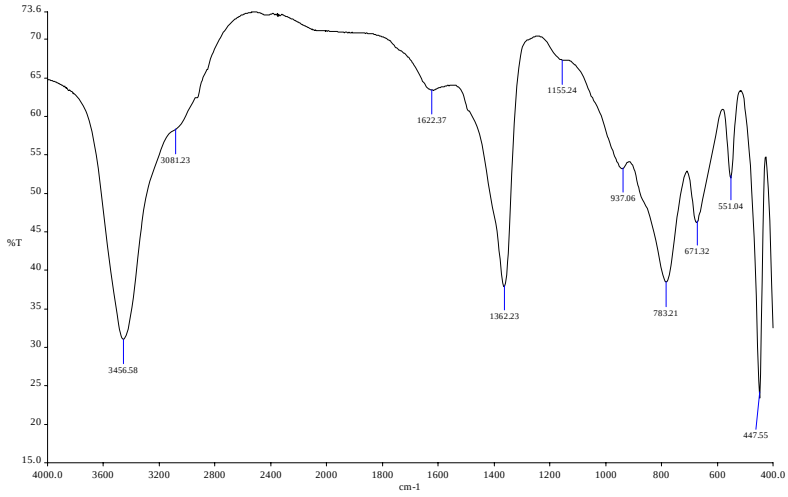

Figure 4.28. FTIR spectrum of the sample **B1.3**.

The FTIR spectrum of the sample **B1.3** is shown in Figure 4.28 which shows carbonate peaks besides the characteristic borate peaks. The peaks at 1155 cm^{-1} and at 937 cm^{-1} correspond to the ν_3 BO_4 stretching and B–OH in plane bending vibrations and to ν_1 BO_3 stretchings. The 3450 cm^{-1} peak is due to the OH stretching and is broadened by the hydrogen bonding between the interlayer water molecules and anions (Del Arco et al., 2000). The shoulder around 3081 cm^{-1} is

due to the interaction between water and the contaminating interlayer carbonate anions (Kloprogge, 2005). The interlayer carbonate peaks at 1362 cm^{-1} and 671 cm^{-1} are due to the ν_3 and ν_4 modes of the carbonate anion. The peaks at 551 cm^{-1} 447 cm^{-1} are assigned to the LDH lattice vibrations.

From the analytical results and the ^{11}B-NMR data, the formula of sample **B1.3** is: $[Mg_{0.68}Al_{0.32}(OH)_2][B_3O_3(OH)_4]_{0.036}(NO_3)_{0.017}(CO_3)_{0.11}\cdot 0.6H_2O$. The small interlayer separation (7.69Å-4.8Å=2.89 Å) may allow the triborate anions and also the other anions in horizontal orientation.

A careful analysis of Table 4.3 reveals that, as the pH of the exchange process increases, the Mg/Al ratio approaches to the experimentally applied ratio. At low pH values, due to the low Mg/Al ratios (increasing Al^{3+} substitution in the layers), LDHs showed a higher affinity towards exchange with borate anions while the LDH sample prepared via borate-exchange at pH 12, contained the lowest amount of boron. pH 9 may be regarded as the most preferable pH in terms of incorporating maximum boron in the LDH structure from boric acid solution.

Although the exchange processes were conducted with the boric acid solution, the intercalated borate species determined by ^{11}B NMR analyses are different than the species expected from those shown in Figure 4.15. Normally, all polyborate anions hydrolyze and dominantly produce the monoborate anions, $B(OH)_4^-$, at pH 12. However, NMR data clearly revealed that the intercalated species in sample **B1.3** is the triborate anions rather than monoborate anions. It appears that a transformation of the borate species occurs between the layers due to the local pH's at the inner surfaces of the layers which may change the structure and the orientation of the borate anions.

Thermal stability of boron containing LDHs are greater than the NO_3-LDHs. Among the three samples prepared by exchange with boric acid solution, **B1.2** with the highest boron content displayed the highest DrDTG peak temperature corresponding to the total collapse of the lattice. Sample **B1.3**, with the lowest boron content, collapsed at a lower temperature by approximately 20°C (Table 4.3, Figure 4.29).

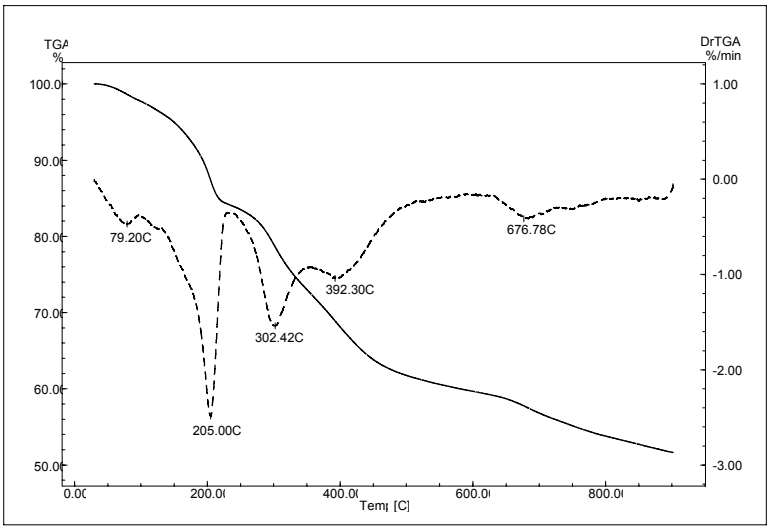

Figure 4.29. TGA (—) and DrTGA (---) curves of **B1.3**.

4.2.3.4. Tetraborate Anion-Exchange with Nitrate-LDH (B1.4)

The chemical formula of the tetraborate pillared LDH derived from analytical results is: $[Mg_{0.53}Al_{0.47}(OH)_2][B_4O_5(OH)_4]_{0.14}(NO_3)_{0.009}(CO_3)_{0.035}\cdot 0.6H_2O$. ^{11}B MAS NMR spectrum of **B1.4** in Figure 4.30 shows characteristic tetrahedral and trigonal boron peaks. The peak area ratio is 1, corresponding to the intercalation of B_4^{2-} ions between the basal layers.

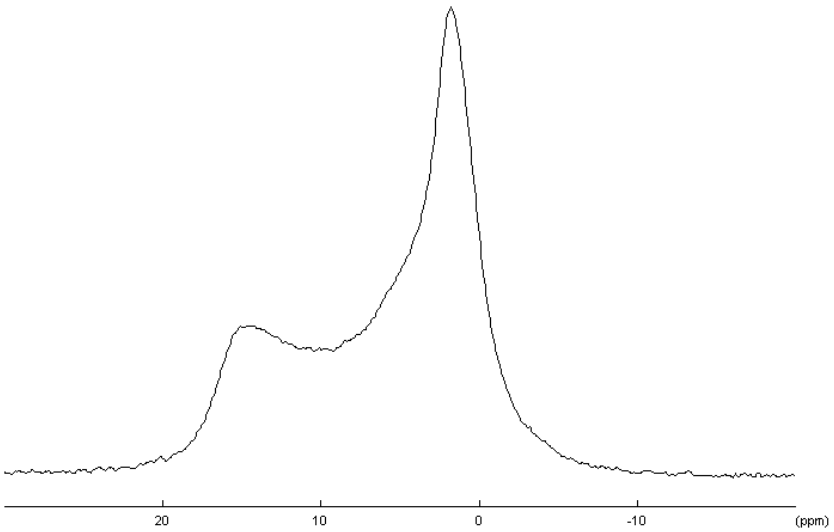

Figure 4.30. ^{11}B MAS NMR spectrum of **B1.4**.

Figure 4.31 shows the PXRD pattern of the sample (**B1.4**) prepared by ion-exchange with tetraborate solution. The basal spacing expanded from 8.55 Å to 11.04 Å. The interlayer distance was calculated as 6.24 Å by subtracting the layer thickness 4.8 Å from the *d* spacing. A large amount of boron was incorporated into the structure (Table 4.6) and the voluminous tetraborate anions probably adopted a perpendicular orientation to overcome the steric restrictions resulting in a pillared structure with a large interlayer separation.

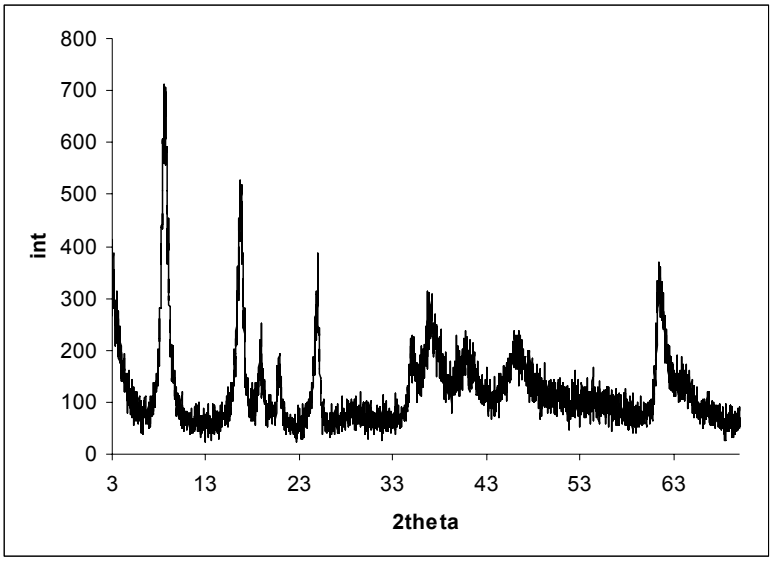

Figure 4.31. PXRD pattern of **B1.4**.

The FTIR spectrum of the sample shows tetraborate vibrations (Figure 4.32). The broad band observed around 3467 cm^{-1} is due to the OH stretching mode and is broadened by extensive hydrogen bonding between the interlayer anions and interlayer water molecules (Del Arco et al., 2000). The bands at 1471 cm^{-1}, 1420 cm^{-1} and 1353 cm^{-1} are assigned to ν_3 BO_3 stretching and B–OH plane bending vibrations, those at 933 cm^{-1} and 808 cm^{-1} are the ν_1 and ν_2 of trigonal boron and those at 1150 cm^{-1} and 1024 cm^{-1} band can be assigned to ν_3 BO_4 stretching and B–OH plane bending vibrations, respectively.

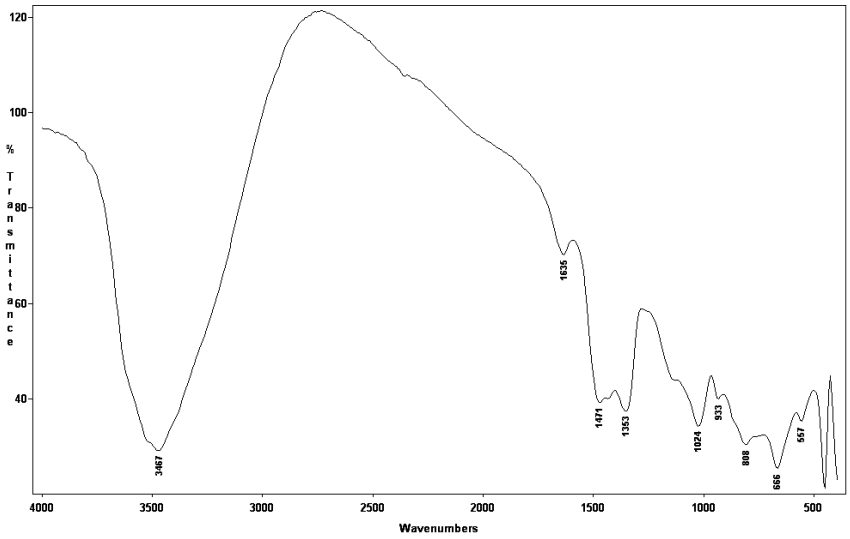

Figure 4.32. FTIR spectrum of **B1.4**.

Figure 4.33 shows the TGA, DrTGA and DTA curves of sample **B1.4.** Pillaring the LDH structure by perpendicular intercalation of TB ions stabilized the structure and prevented gallery collapse upon dehydration. **B1.4** decomposed at higher temperatures than the previous **B1.1**, **B1.2** and **B1.3** samples. The exothermic peak seen on the DTA curve at 734°C can be assigned to the complete lattice collapse and transition to a mixed oxide phase (Cheng and Lin, 1992; Li et al., 1996).

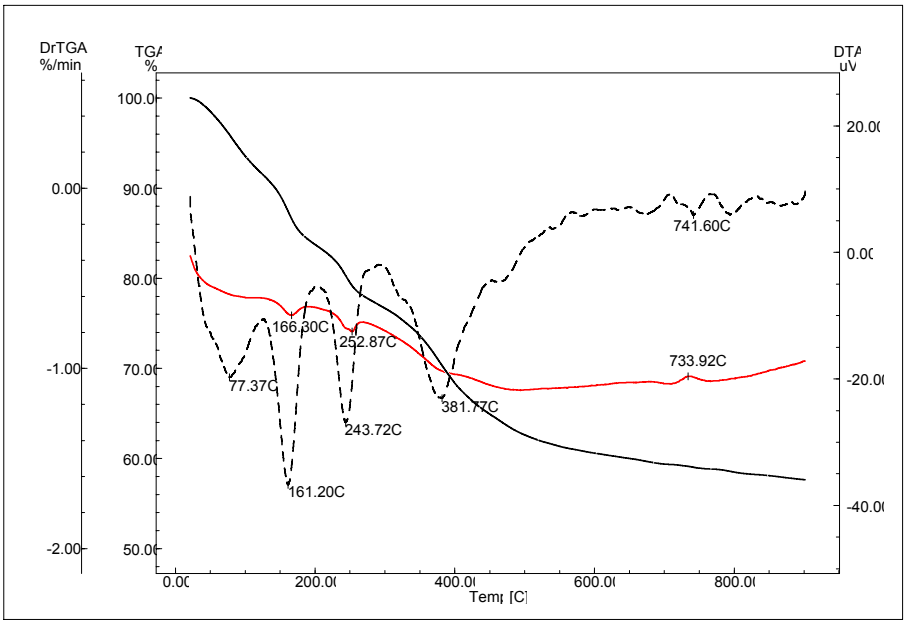

Figure 4.33. TGA (—), DrTGA (---) and DTA(—) curves of **B1.4**.

Only one peak has been noticed at 9.49 ppm on the ^{27}Al MAS NMR spectra of sample **B1.4** (Figure 4.34). This single peak is assigned to octahedrally coordinated aluminum atoms in the basal sheets.

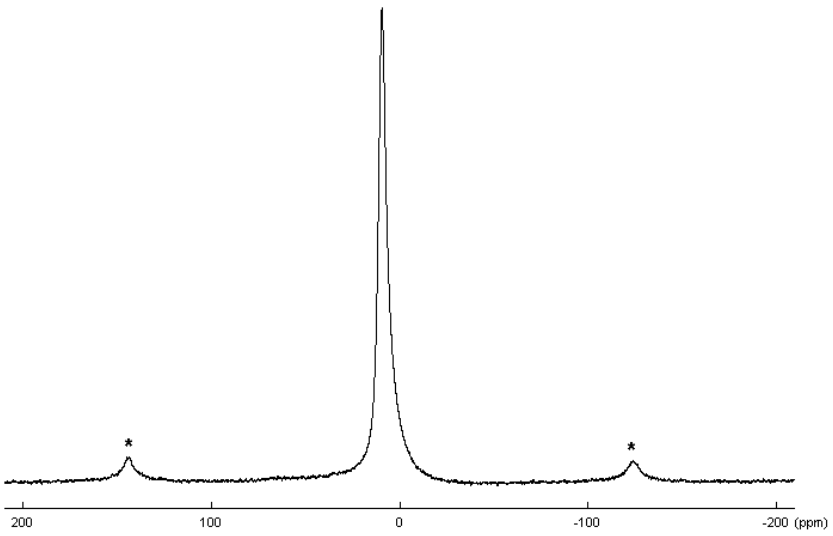

Figure 4.34. ^{27}Al MAS NMR spectrum of **B1.4** (*Spinning side bands).

Figure 4.35 shows the SEM picture of the tetraborate-pillared LDH sample. The layers can be clearly seen.

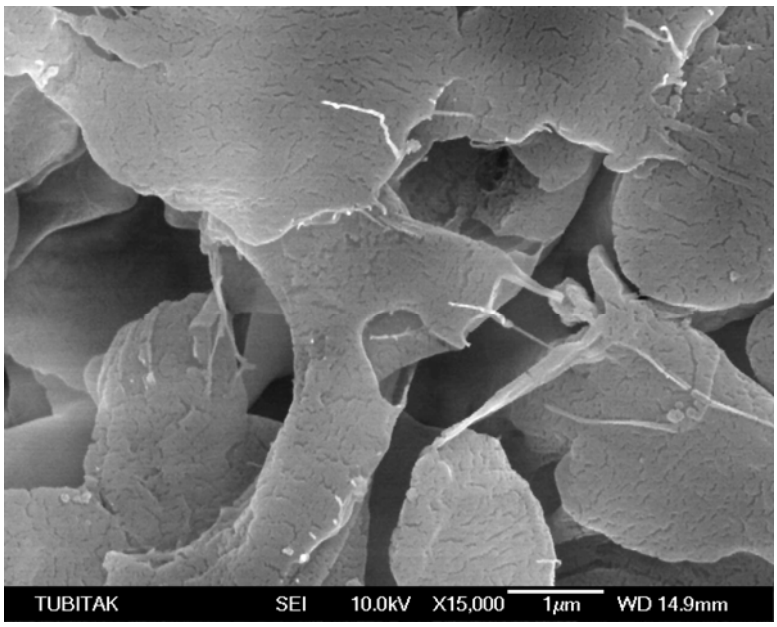

Figure 4.35. SEM image of **B1.4**.

4.2.3.5. Tetraborate Anion-Exchange with Mechanochemically Prepared Nitrate-LDH

Sample **B2** was tested for its anion exchange property with borate ions and the obtained boron intercalated derivative (**B2.1**) was structurally analyzed in comparison with the analogous **B1.4**.

Fig 4.36 shows the PXRD diagrams of **B2.1** and. **B1.4.** The close proximity in the d_{003} values of boron intercalated samples (Table 4.4.) further emphasizes the structural relationship between the parent LDH samples prepared mechanochemically and by co-precipitation. Intercalation of boron was confirmed by the expansion in the basal spacings. In parallel to the increase in the interlayer pores by exchanging the smaller nitrate anions with the larger borate anions, the surface areas increased from 5.9m^2/g (**B2**) to 25 m^2/g (**B2.1**) and from 22 m^2/g (**B1**) to 83.3m^2/g (**B1.4**). The four-fold increase in the BET values on borate intercalation is noteworthy.

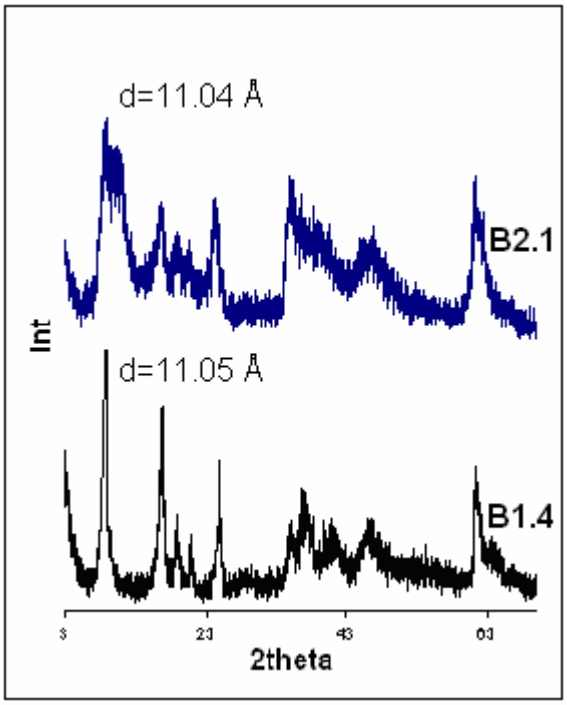

Figure 4.36. PXRD patterns of the samples **B2.1** and. **B1.4**.

Table 4.4. Chemical compositions and some properties of tetraborate-LDHs obtained from conventionally and mechanochemically prepared nitrate-LDHs.

Sample	Formula	Mg/Al	d_{003} (Å)	S_{BET} (m^2g^{-1})
B2.1	$[Mg_{0.62}Al_{0.38}(OH)_2](NO_3)_{0.18}[B_4O_5(OH)_2]_{0.10} \cdot 0.6H_2O$	1.6	10.9	25
B1.4	$[Mg_{0.53}Al_{0.47}(OH)_2][B_4O_5(OH)_4]_{0.14}(NO_3)_{0.009}(CO_3)_{0.035} \cdot 0.6H_2O$	1.1	11.0	83

The FTIR, ^{27}Al MAS NMR, ^{11}B MAS NMR spectra and thermograms of **B2.1** and **B1.4** also displayed very similar features verifying the usability of mechanochemically prepared LDH in borate exchange reactions as well as the conventional LDHs.

4.2.4. Structural Characterization of LDHs Expanded with Adipate Ions

LDHs with interlayer spaces widely expanded by organic species have been used in order to facilitate the access to the exchangeable anions. Exchange of interlayer anions by dicarboxylic acid anions was first reported by Miyata and Kumura (Miyata and Kumura, 1973). In the following sections, borate ion intercalation with LDH samples expanded with an aliphatic dicarboxylate (adipate-) and an aromatic dicarboxylate (terephthalate-) will be described.

Figure 4.37 shows the PXRD pattern of the adipate-LDH sample (**B3**) expanded with a basal spacing *d* (003) of 12.66 Å. The exchange of the larger adipate anions with the nitrate ions is clear from the increase in the interlayer distance. The length of the adipate anion is 10.2 Å (Drezdzon, 1988) while the distance between the layers is 12.66Å-4.8Å =7.9Å. The perpendicular orientation of the adipate anions was therefore not possible. As shown in Scheme 4.1, AD ions were randomly intercalated, tilted and horizontally, yielding a material with low crystallinity.

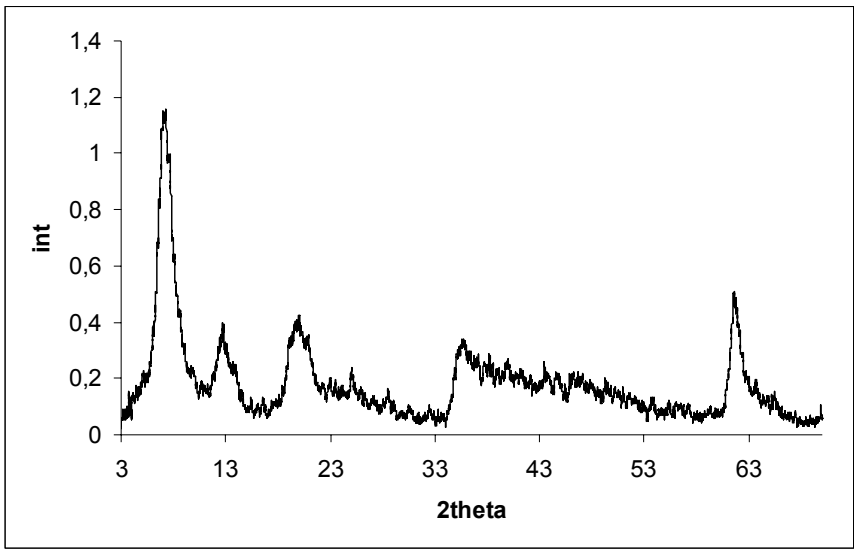

Figure 4.37. PXRD pattern of **B3**.

The FTIR spectrum of **B3** is shown in Figure 4.38. Antisymmetric, symmetric stretching and deformation vibrations of alkyl C–H groups are seen respectively at, 2943 cm^{-1}, 2868 cm^{-1} and 1410 cm^{-1}. The strong peak observed at 1558 cm^{-1} is due to the antisymmetric COO^- vibration. C–O stretching vibration is seen at 1212 cm^{-1}. The broad bands around 3400 cm^{-1} and 1560 cm^{-1} are assigned to the hydroxyl stretching and deformation vibrations of the basal layers and interlayer water molecules (Yıldız and Genç, 1993; Aisawa et.al., 2002; Kloprogge et.al., 2004).

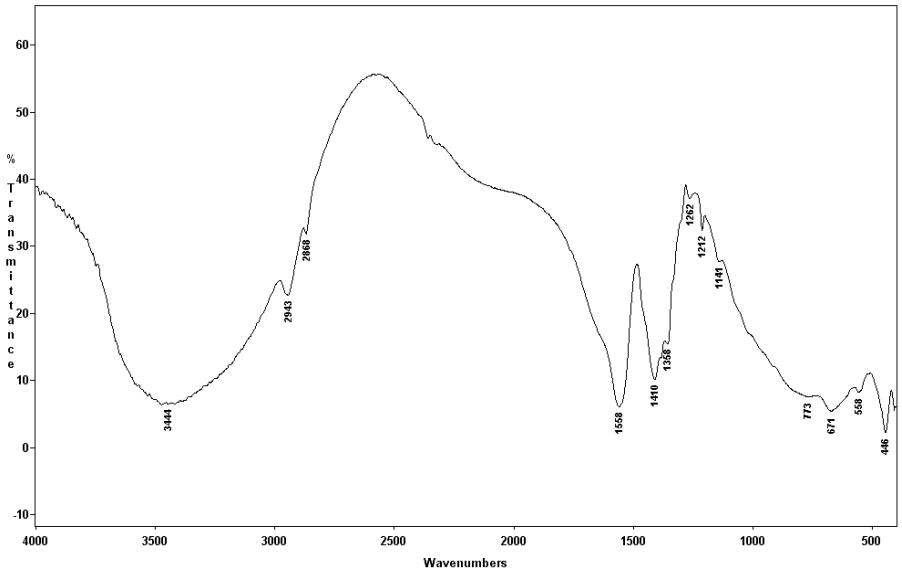

Figure 4.38. FTIR spectrum of **B3**.

Figure 4.39 shows the ^{13}C CP MAS NMR spectrum of the adipate-LDH. The peak at 183.20 ppm corresponds to the carboxyl carbons and the peaks at 38.07 ppm and 26.81 ppm correspond to C_α and C_β atoms. The lower intensity peak at 170.45 ppm can be assigned to the carbon atom of the contaminating carbonate anion.

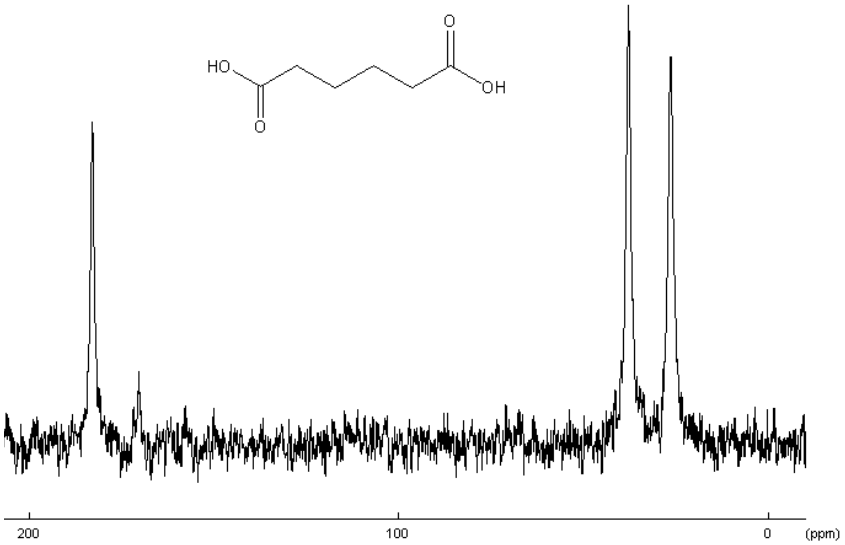

Figure 4.39. ^{13}C CP MAS NMR spectrum of **B3**.

Thermal decomposition behaviour of **B3** is seen in Figure 4.40. Following the dehydration and dehydroxylation steps up to 310°C, exothermic decomposition of the interlayer adipate anions took place at 372°C and 422°C (Aisava et.al., 2002). The exothermic peak at 524°C on the DTA curve corresponds to the transformation of the layered structure to mixed oxide phases (Cheng and Lin, 1992). Figure 4.41 shows the SEM image of **B3**. Efforts for measuring the BET surface area of this sample failed. Easy elimination of water molecules from the large galleries created a humid atmosphere at the surface while heating the sample for BET analysis and therefore the measurement could not be performed.

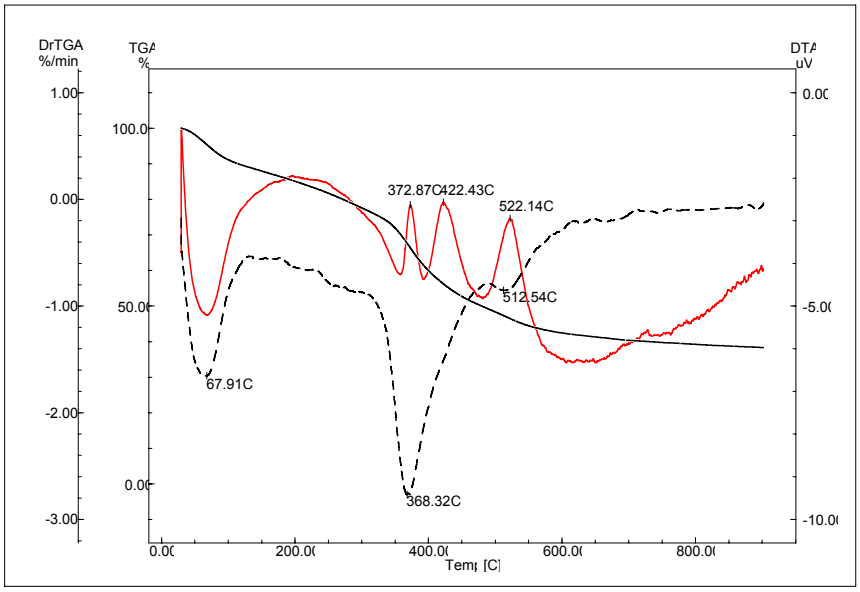

Figure 4.40. TGA (—), DrTGA (---) and DTA (—) curves of adipate-LDH (**B3**).

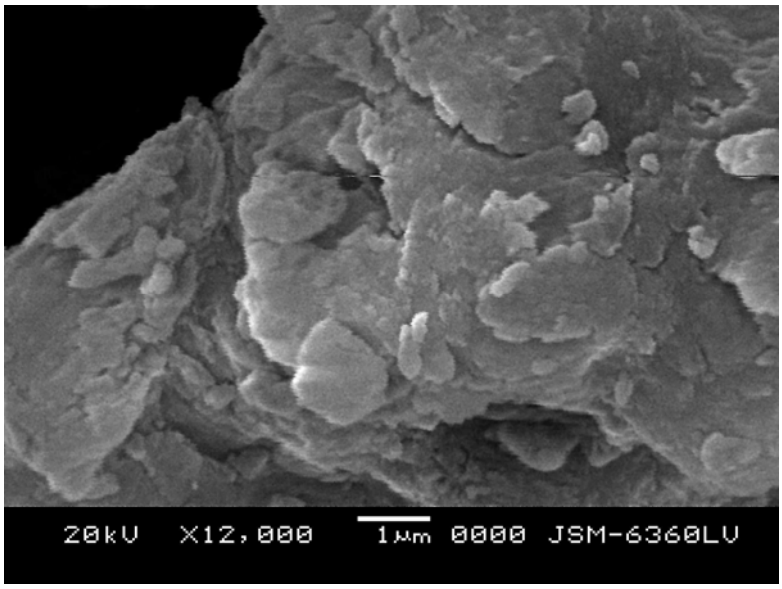

Figure 4.41. SEM image of adipate-LDH (**B3**).

The chemical composition of the sample was found as: $[Mg_{0.62}Al_{0.38}(OH)_2](NO_3)_{0.056}(AD)_{0.157}.0.5H_2O$. Exchanging most of the interlayer nitrate ions with AD ions did not cause any perturbation in the Al^{3+} sites. The single peak at 10.11 ppm in the ^{27}Al MAS NMR spectrum indicated the presence of six-coordinated Al^{3+} (Figure 4.42).

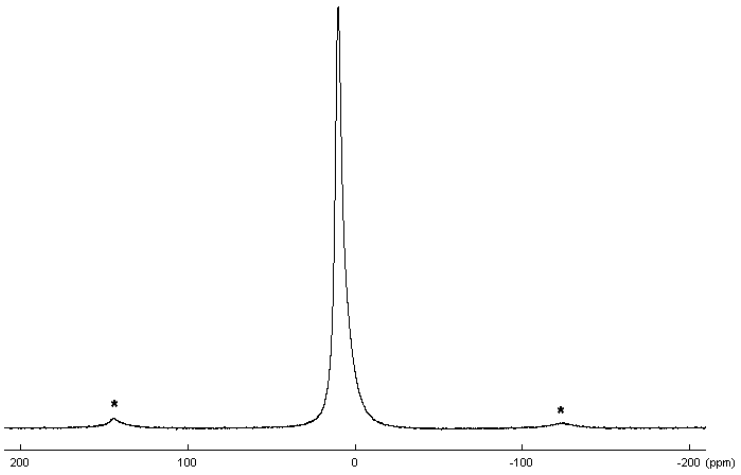

Figure 4.42. ^{27}Al MAS NMR spectrum of **B3** (*Spinning side bands).

4.2.4.1. Boric Acid-Exchange with Adipate-LDH without pH Adjustment

Figure 4.43 shows the PXRD pattern of the LDH sample (**B3.1**) after exchanging the AD ions with boric acid solution, without making any pH adjustment. The basal spacing of the sample was reduced to 10.27 Å. The randomly oriented interlayer AD ions are protonated with the boric acid solution and readily exchanged with the smaller borate anions. The galleries were shrunk from 12.66 Å to 10.27 Å after the exchange process. The pattern showed the presence of impurity phases with peaks at 2θ=18.66° and 20.46°.

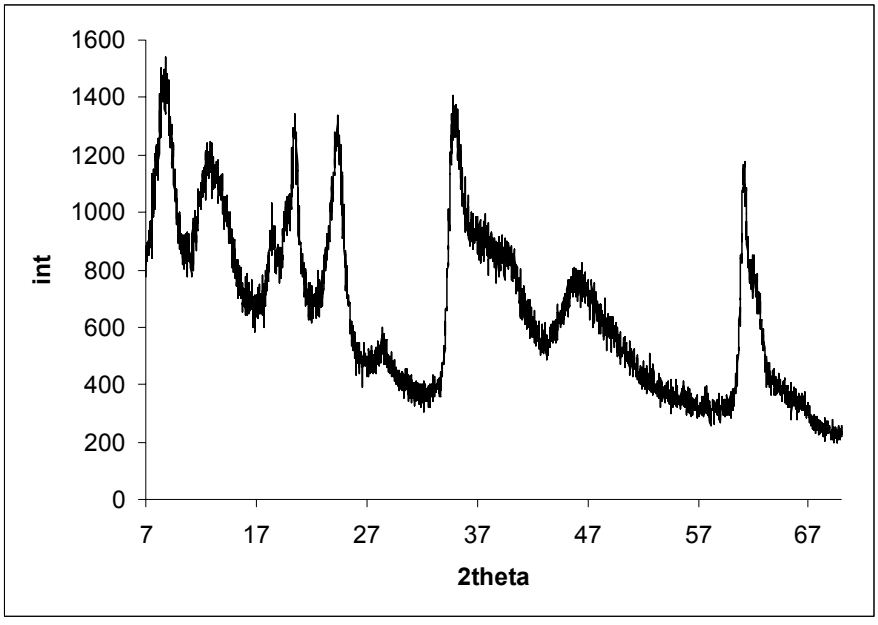

Figure 4.43. PXRD pattern of the sample **B3.1**.

Very little differences were observed between the FTIR spectra of samples **B3** and **B3.1**. The relative FTIR peak intensities of interlayer adipate anions decreased after exchange with boric acid (Figure 4.44).

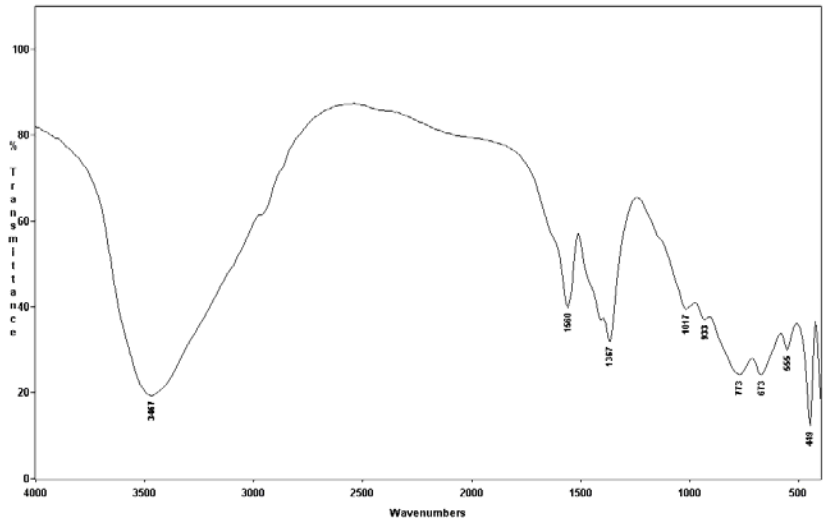

Figure 4.44. FTIR spectrum of **B3.1**.

According to the ^{11}B MAS NMR spectrum shown in Figure 4.45, boric acid was intercalated in the form of B_3^- species. The signals at 2.26 ppm and at 15.08 ppm are assigned respectively to tetrahedrally coordinated boron and the trigonally coordinated boron (Li et al., 1996). The calculated peak area ratio (tri-B/tetra-B) was 2:1 which means that the intercalated species are triborate anions.

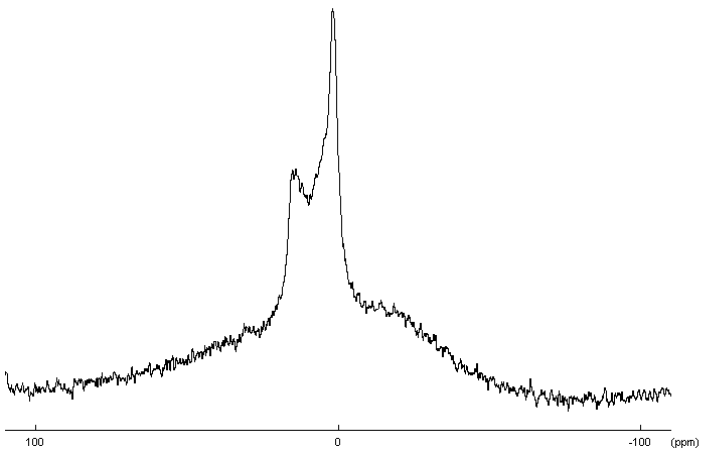

Figure 4.45. ^{11}B MAS NMR spectrum of **B3.1**.

Figure 4.46 shows the thermal decomposition of the sample **B3.1**. When compared with the TGA, Dr-TGA and DTA curves of adipate-LDH (**B3**), decomposition temperature shifted by 100°C to higher temperatures. The sample becomes thermally more stable after boron incorporation.

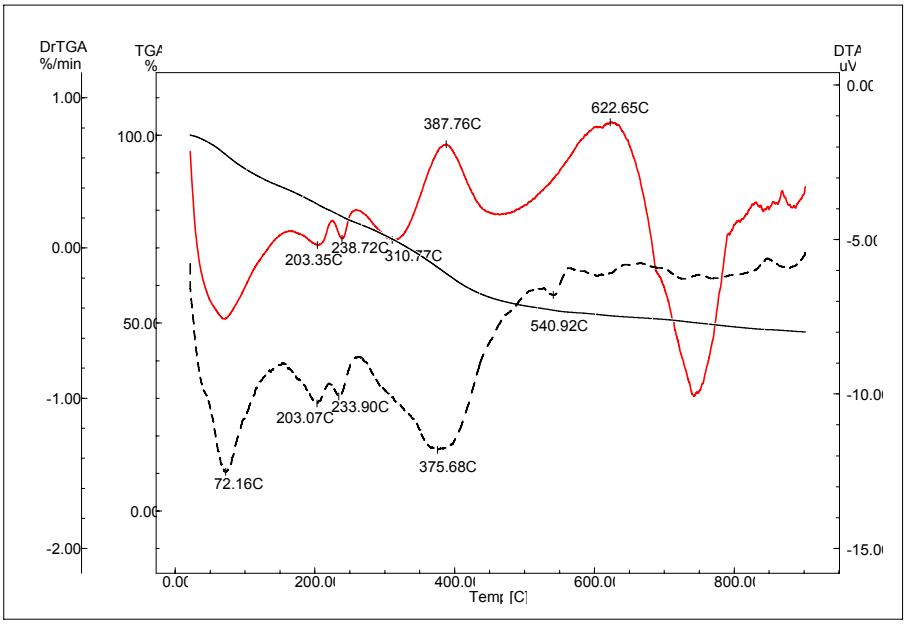

Figure 4.46. TGA(—), DrTGA (---) and DTA (—) curves of sample **B3.1**.

4.2.4.2. Boric Acid-Exchange with Adipate-LDH at pH 9.0

PXRD pattern of the sample **B3.2** is shown in Figure 4.47 and is very similar to that of **B3.1** but with a better crystallinity. The ion-exchange procedure in this step was performed at pH 9. The borate anions are found in tetraborate form (B_4^{2-}) at this pH (Simon and Smith, 2000). Because of the higher charge density of the borate species, all the adipate anions exchanged with tetraborate anions.

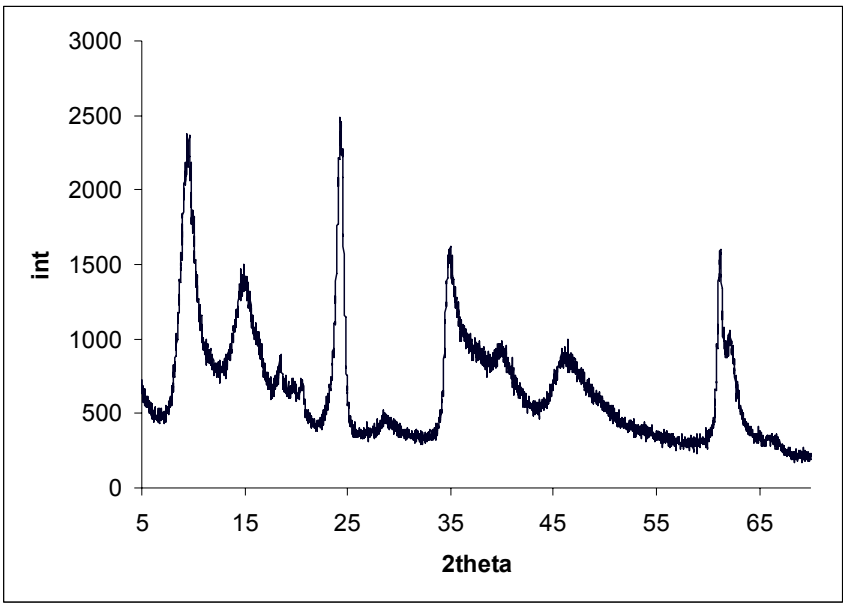

Figure 4.47. PXRD pattern of **B3.2**.

The nature of the intercalated borate was confirmed by the ^{11}B MAS NMR spectrum (Figure 4.48). The ratio of the trigonal (14.32 ppm) to tetragonal (2.25 ppm) peak areas was calculated as 1 that confirms tetraborate intercalation. FTIR spectrum of **B3.2** displayed characteristic borate vibrations as described in the previous sections. The basal spacing was measured as 9.20Å with a gallery height of 9.20Å -4.8Å =4.4Å allowing horizontal orientation of TB ions.

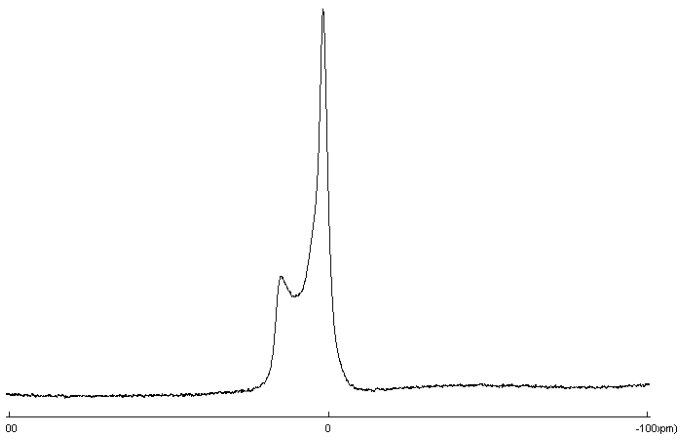

Figure 4.48. ^{11}B MAS NMR spectrum of **B3.2**.

No change was noted in the ^{27}Al MAS NMR spectrum of after exchanging the AD ions with borate ions at pH 9 (Figure 4.49).

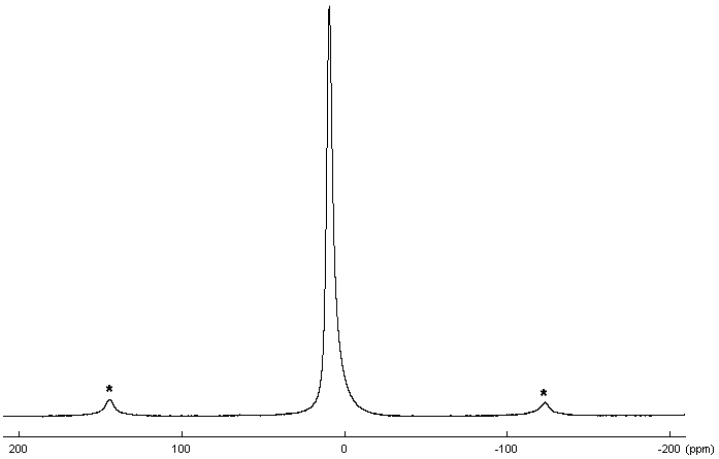

Figure 4.49. ^{27}Al MAS NMR spectrum of sample **B3.2** (*Spinning side bands).

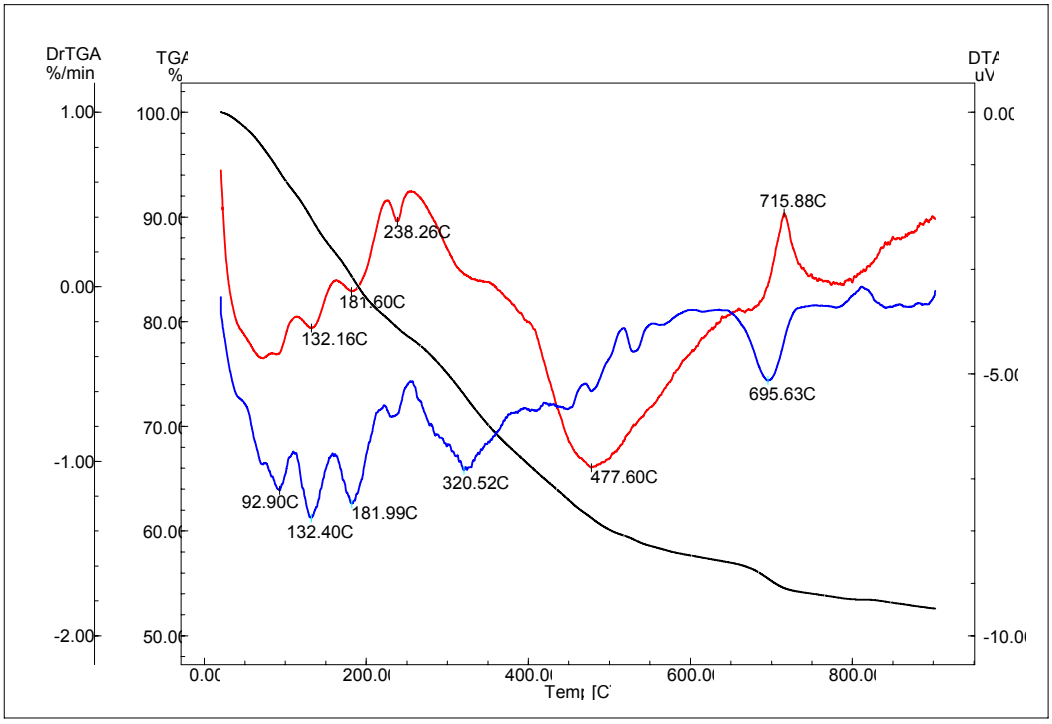

Figure 4.50. TGA (—), DrTGA (—) and DTA (—) curves of **B3.2**.

Figure 4.50 shows the TGA, DrTGA and DTA curves of the tetraborate-pillared layered double hydroxide. When compared with the TGA, Dr-TGA and DTA curves of **B3** and **B3.1**, the sample becomes even more stable by intercalating tetraborate ions. The complete lattice collapse and a phase transition was observed at 715°C .

Table 4.5. Chemical compositions and some properties of borate-LDH samples prepared by boric acid exchange with adipate-LDH.

Sample	Formula	d_{003} (Å)	Mg/Al	B%
B3.1	$[Mg_{0.55}Al_{0.45}(OH)_2]\ [B_3O_3(OH)_4]_{0.076}(NO_3)_{0.003}(AD)_{0.074}\cdot 0.6H_2O$	10.27	1.21	2.28
B3.2	$[Mg_{0.61}Al_{0.39}(OH)_2][B_4O_5(OH)_4]_{0.094}(CO_3)_{0.11}\cdot 0.6H_2O$	9.38	1.57	3.97
B3.3	$[Mg_{0.68}Al_{0.32}(OH)_2]\ [(B_4O_5(OH)_5]_{0.0967}(AD)_{0.046}(CO_3)_{0.022}\cdot 0.6H_2O$	8.61	2.11	2.06

4.2.4.3. Boric Acid-Exchange with Adipate-LDH at pH 12

A highly crystalline borate pillared LDH (**B3.3**) was obtained from adipate-LDH by exchange with boric acid at pH 12 (Figure 4.51).

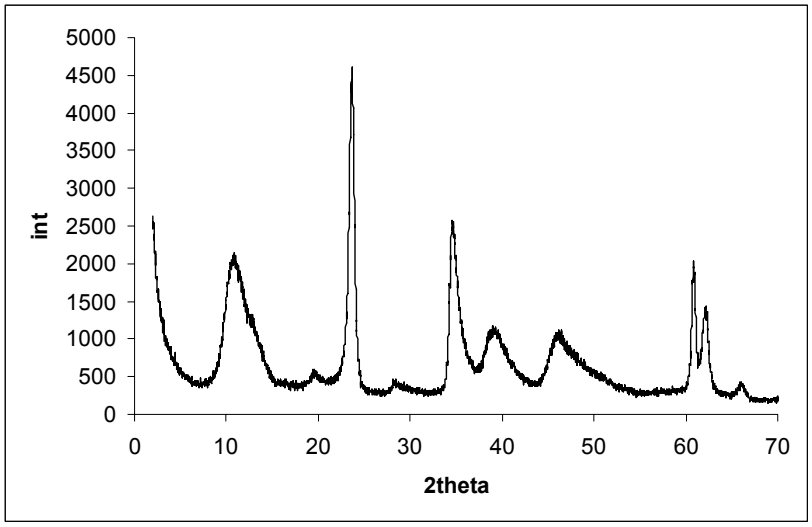

Figure 4.51. PXRD diffraction pattern of **B3.3**.

From the analytical results and the ^{11}B-NMR spectrum shown in Figure 4.52, the formula of sample **B1.3** contains tetraborate anions which must be intercalated horizontally in the small interlayer separation (8.61Å - 4.8Å = 3.8 Å). As previously mentioned in section **4.2.3.3.**, the intercalated boron was in the form of B_4^{2-} at pH 12 rather than the expected monoborate ion. It appears that a transformation occurred in the interlayer space after borate intercalation due to the local pH changes. Table 4.5. reveals that the highest boron incorporation was achieved at pH 9.

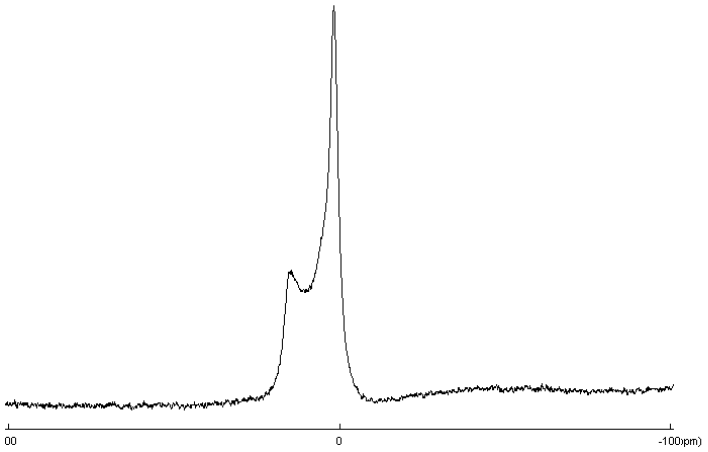

Figure 4.52. ^{11}B MAS NMR spectra of the sample **B3.3**.

FTIR spectrum of **B3.3** displayed characteristic borate vibrations as described in the previous sections. TGA, DrTGA and DTA showed similar features as with **B3.1.** (Figure 4.53).

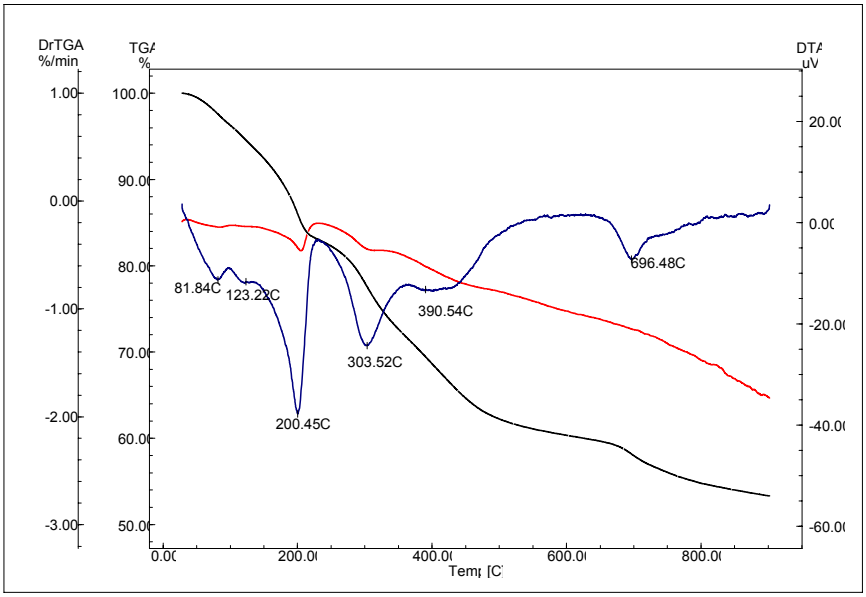

Figure 4.53. TGA (—), DrTGA (—) and DTA (—) curves of sample **B3.3**.

The results summarized in Table 4.5. reveal that AD ions exchange with the borate anions present in the boric acid solution at every pH value applied. The intercalating borate anions transform into polyborate species in the interlayer space and repel the randomly oriented AD ions.

4.2.4.4. Tetraborate Anion-Exchange with Adipate-LDH

The basal spacing in **B3** is large enough for TB ions to enter the interlayer space freely. As a result, the interlayer AD ions were exchanged nearly completely by the TB ions. Figure 4.54 shows the PXRD pattern of the adipate-LDH after exchange with TB anions. The basal spacing shrunk from 12.66 Å to 10.50 Å, giving rise to an interlayer distance of 5.7 Å. This space allows the intercalation of TB ions in tilted position (Figure 4.24).

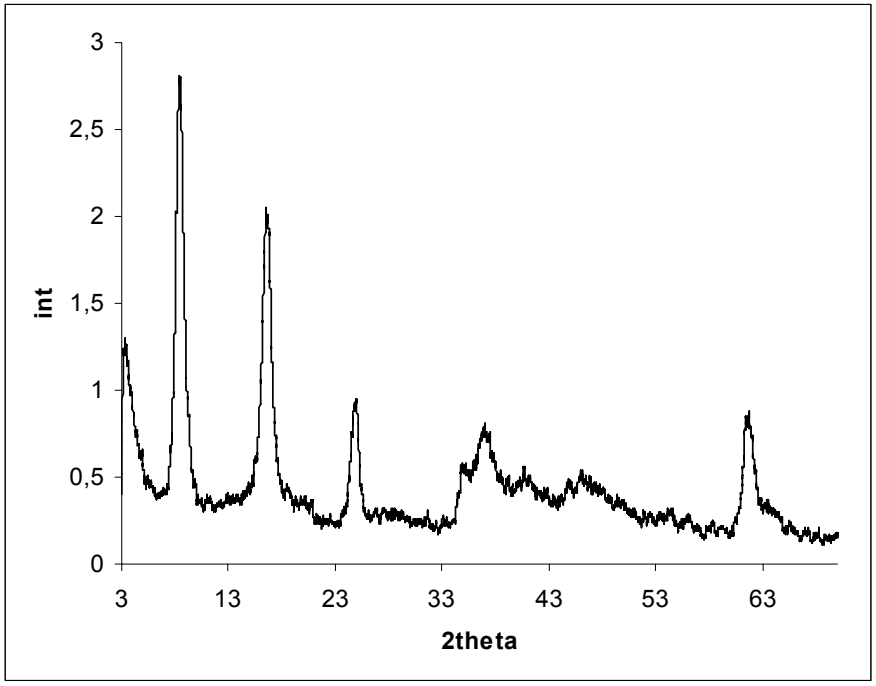

Figure 4.54. PXRD pattern of **B3.4**.

The FTIR spectrum of **B3.4** showed characteristic borate peaks (Figure 4.55) as described in previous sections. No peak could have been detected regarding the presence of AD ions in the structure.

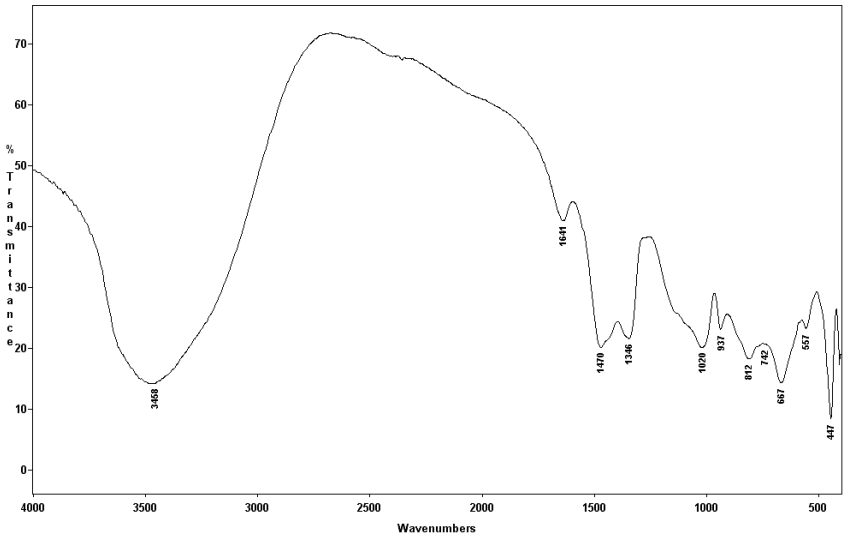

Figure 4.55. FTIR spectrum of **B3.4**.

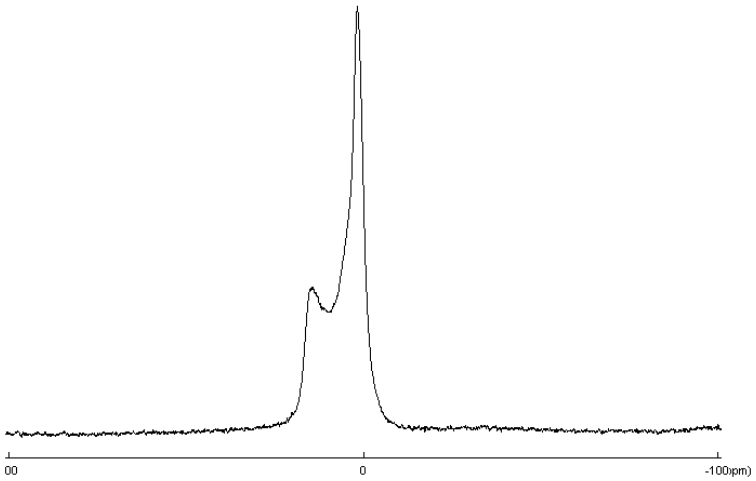

Figure 4.56. ^{11}B MAS NMR spectrum of **B3.4**.

The ^{11}B MAS NMR spectrum of **B3.4** in Figure 4.56 shows the characteristic signals of tetrahedral (2.25 ppm) and trigonal (14.22 ppm) boron atoms. The relative peak area ratio (triborate/tetraborate) is 1, and thus ^{11}B MAS NMR data indicates the presence of TB anions between the basal layers.

It is realized from the ^{27}Al MAS NMR spectrum of this sample that the ion-exchange procedure did not change the framework of the basal sheets. The single peak at 9.63 ppm is assigned to octahedrally coordinated aluminum atoms in the basal sheets (Figure 4.57).

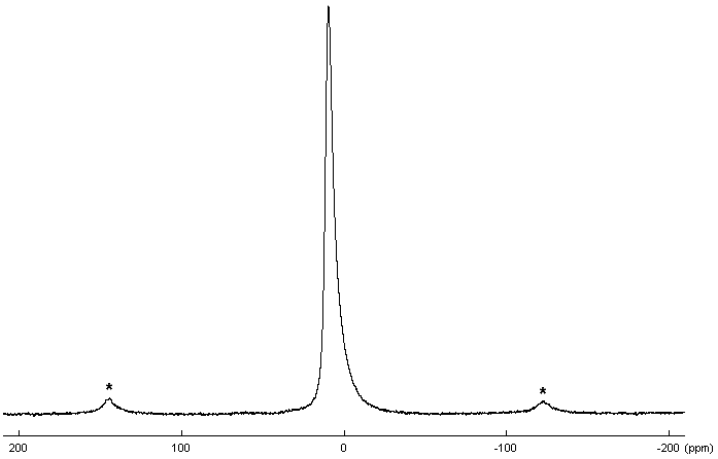

Figure 4.57. ^{27}Al MAS NMR spectrum of **B3.4** (*:Spinning side bands).

Table 4.6. reveals that LDH samples prepared by exchanging the interlayer ions with TB ions yielded materials with high boron content. Swelling the interlayer space with AD ions first and then the feasible exchange with TB ions gave a LDH with more than 6% boron.

Table 4.6. Chemical compositions and some properties of LDH samples prepared with tetraborate ion exchange.

Sample	**Formula**	d_{003}**(Å)**	**Mg/Al**	**B%**	**BET (m^2/g)**
B1.4	$[Mg_{0.53}Al_{0.47}(OH)_2][B_4O_5(OH)_4]_{0.14}(NO_3)_{0.009}(CO_3)_{0.035}\cdot 0.6H_2O$	11.04	1.14	5.3	83
B3.4	$[Mg_{0.58}Al_{0.42}(OH)_2][(B_4O_5(OH)_5]_{0.17}(AD)_{0.017}\cdot 0.6H_2O$	10.50	1.35	6.3	67
B4.4	$[Mg_{0.56}Al_{0.44}(OH)_2][B_4O_5(OH)_4]_{0.19}\ (TP)_{0.022}\cdot 0.6H_2O$	11.05	1.28	6.5	66

TB intercalated LDH samples displayed higher thermal stabilities and large surface areas. Figure 4.58 shows the TGA, DrTGA and DTA curves of sample **B3.4.** The complete lattice collapse and a phase transition were observed at 745°C.

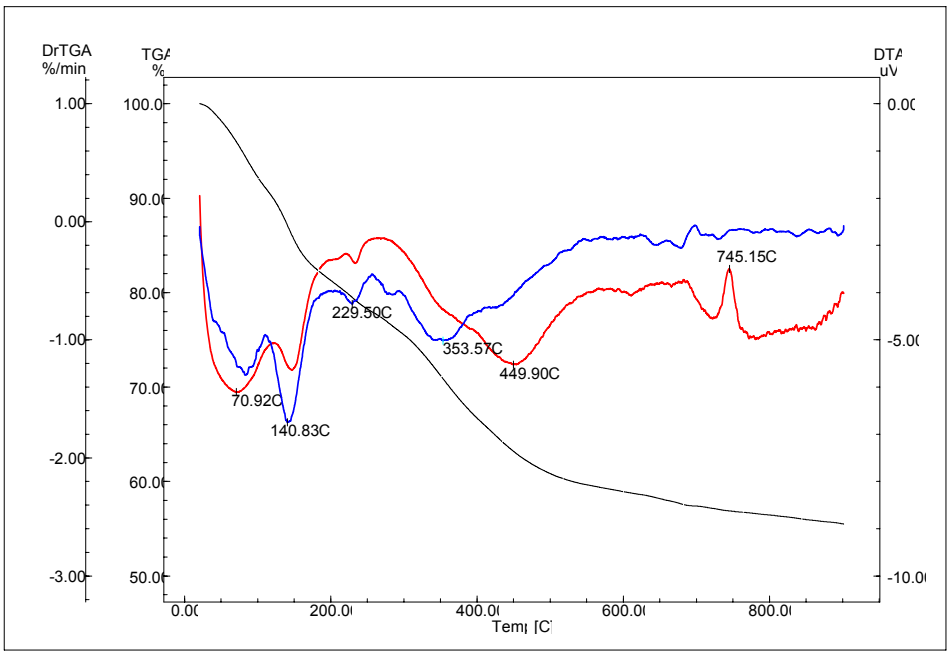

Figure 4.58. TGA (—), DrTGA (—) and the DTA (—) curves of **B3.4**.

4.2.5. Structural Characterization of LDHs Expanded with Terephthalate Ions

The selectivity of LDHs towards TP ion intercalation is higher than that of OH^- and therefore the exchange reaction was fast and a high degree of exchange was achieved (Table 4.7). Figure 4.59 shows the PXRD pattern of the terephthalate-LDH (**B4**). The basal spacing *d* (003) of the LDH is 14.14 Å. The interlayer space for terephthalate anion intercalation is 14.14Å - 4.8Å = 9.34Å. The length of the TP ion is 9.2 Å (Crepaldi et.al., 2002) and it is found in its dianionic form in the experimental pH conditions. Thus, the perpendicular orientation of the TP anions is energetically favored as represented in Scheme 4.1., owing to the greater host-guest interactions resulting in a highly crystalline, pillared LDH. Pillaring provides a route to prepare nanoporous materials with tunable chemical properties by allowing entering anions for interpillar access.

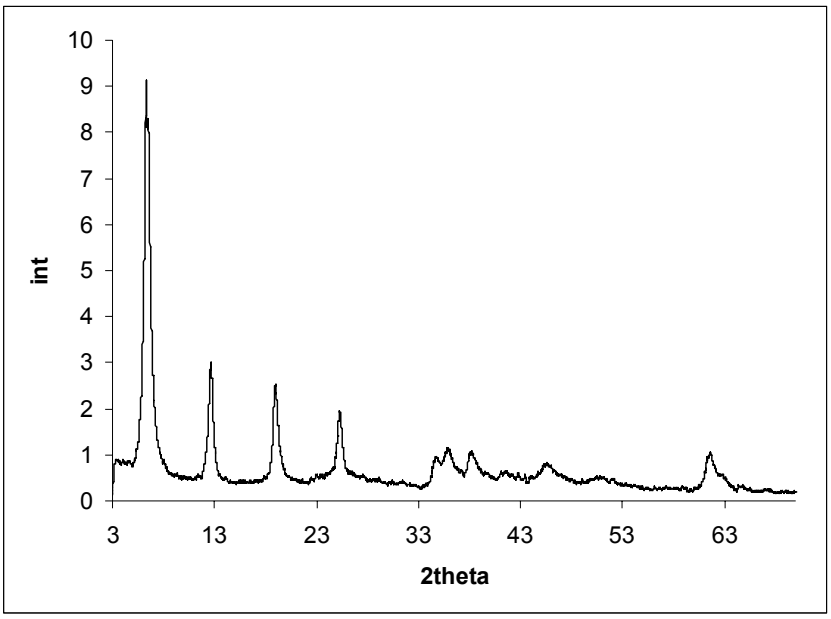

Figure 4.59. PXRD pattern of **B4**.

FTIR spectrum of **B4** is shown in the Figure 4.60. The intercalated terephthalate peaks could be easily defined. The strong peak observed at 1558 cm^{-1} is the antisymmetric stretching vibration of COO^{-}, the peaks at 1151 cm^{-1} and 1107 cm^{-1} can be assigned to C–O stretching vibrations and O–H bending vibrations. And the broad bands around 3400 cm^{-1} and 1564 cm^{-1} are assigned to the hydroxyl stretching and deformation vibrations of the basal layers and interlayer water molecules (Yıldız and Genç, 1993; Aisawa et.al., 2002; Kloprogge et.al., 2004).

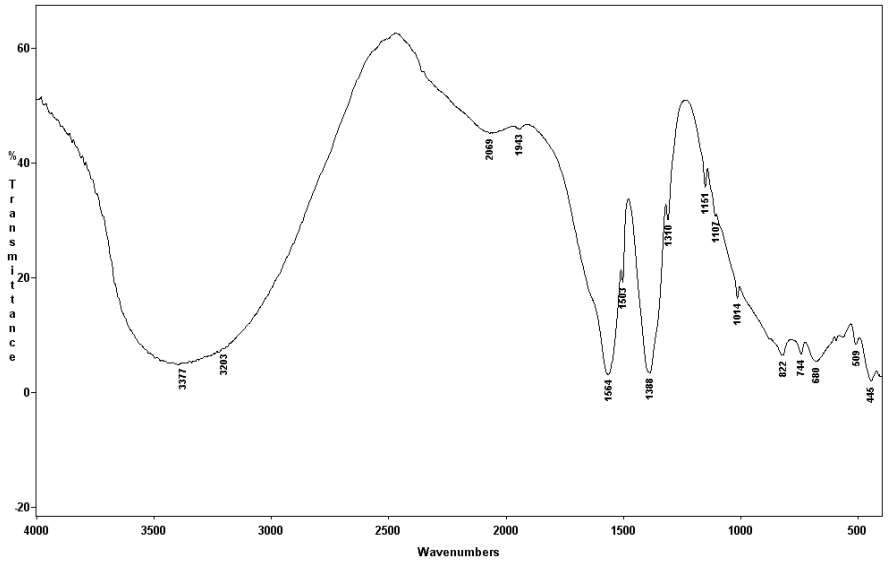

Figure 4.60. FTIR spectrum of **B4**.

Figure 4.61 shows the ^{13}C CP MAS NMR spectrum of the terephthalate-LDH. The peak at 173.84 ppm corresponds to the carboxyl carbon atoms and the peaks at 128.58 ppm and 136.62 ppm correspond to C_α and C_β atoms. No peak was detected that can be assigned to the adsorbed carbonate anion.

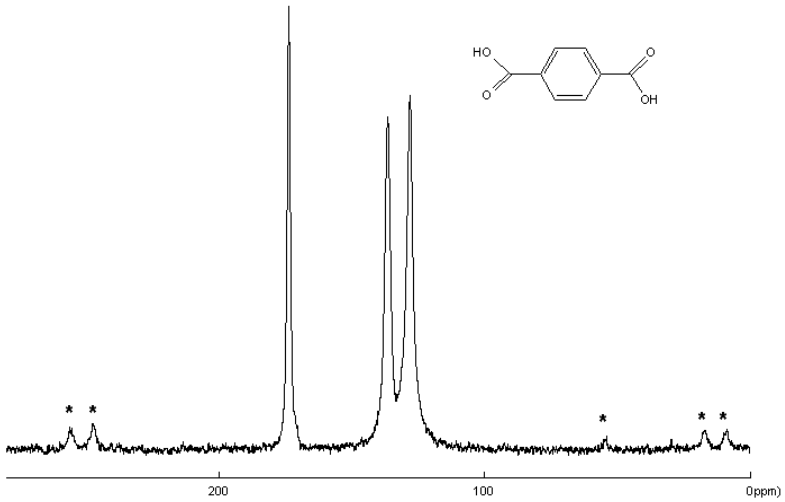

Figure 4.61. ^{13}C CP MAS NMR spectra of the sample **B4** (*: Spinning side bands).

Thermal decomposition of **B4** is seen in the Figure 4.62. Following the dehydration and dehydroxylation steps, decomposition and combustion of the interlayer terephthalate anion took place up to 600°C. The layered structure of the sample can be visualized from the SEM image shown in Figure 4.64. Like the adipate-LDH, the surface area of this sample could not be measured because of the humid atmosphere formed at the surface of the material during the BET analysis.

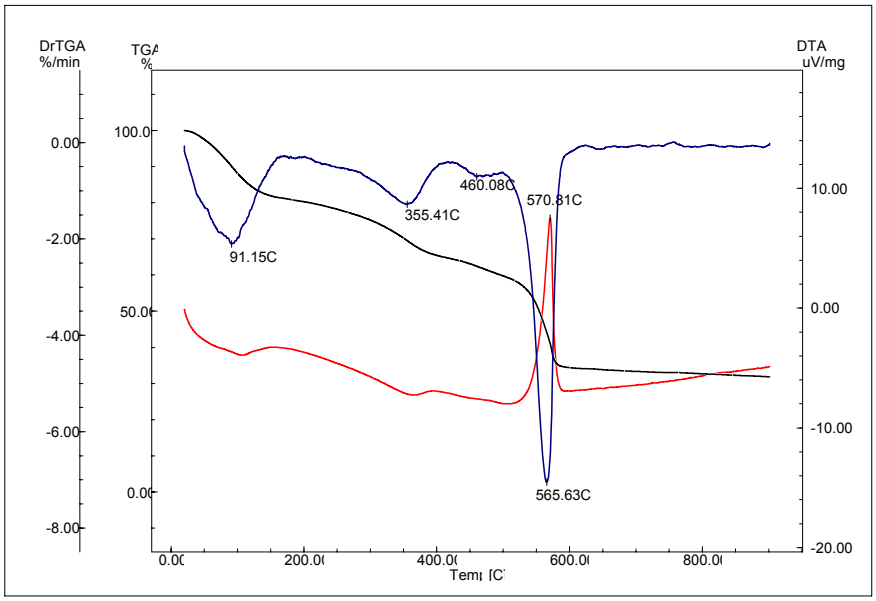

Figure 4.62. TGA (—), DrTGA (—) and DTA (—) curves of **B4**.

The layered structure of the sample B4 can be seen on the SEM image on Figure 4.63.

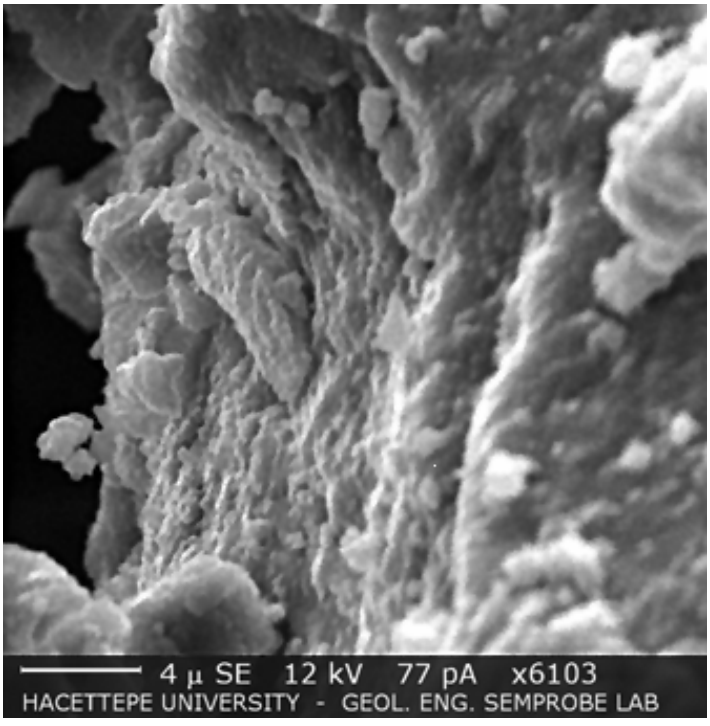

Figure 4.63. SEM image of **B4**.

4.2.5.1. Boric Acid-Exchange with Terephthalate-LDH without pH Adjustment

The chemical analysis of the sample obtained by treating the terephthalate-LDH (B4) with boric acid solution (**B4.1**) gave the formula: $Mg_{0.59}Al_{0.41}(OH)_2](TP)_{0.20}.0.7H_2O$. According to the formula, no exchange with boric acid solution occurred as confirmed by the following XRD and spectral analyses.

PXRD patterns and the FTIR spectra of samples **B4.1** and **B4** are comparatively shown in Figures 4.64 and 4.65 respectively. No evidence was observed for borate intercalation neither on the PXRD pattern nor on FTIR spectrum. The PXRD patterns are almost the same. The basal spacing of **B4.1** is 14.25 Å which is very close to the *d* value of **B4**. FTIR spectra are also similar with little changes. The LDHs exhibit OH stretching peaks in the 2700-4000 cm^{-1} range, normally broadened by the hydrogen bonding interactions between the interlayer water molecules and interlayer anions (Del Arco et al., 2000). This peak became sharper after treating **B4** with boric acid solution. During the treatment, the pH of the solution increased from ~5 to 7.5 which means that the sample released some hydroxyl groups into the solution by a disruption in the hydrogen-bonded network structure.

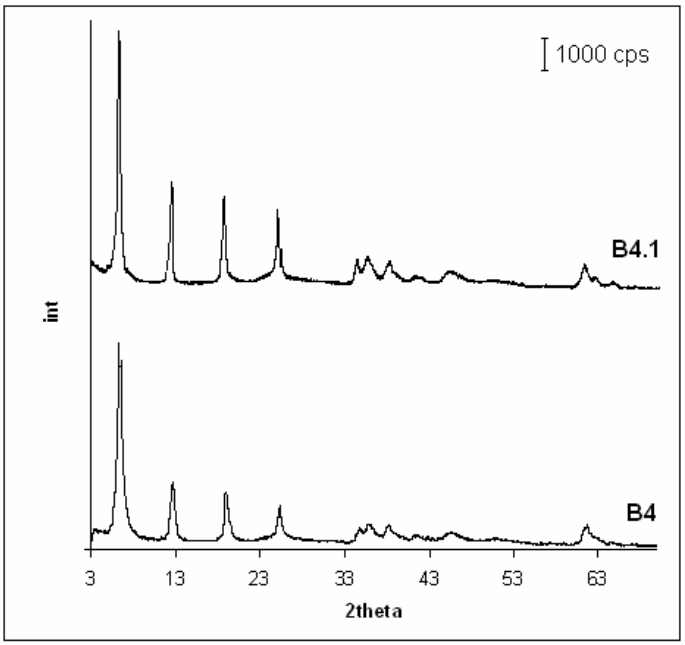

Figure 4.64. PXRD pattern of the sample **B4.1**.

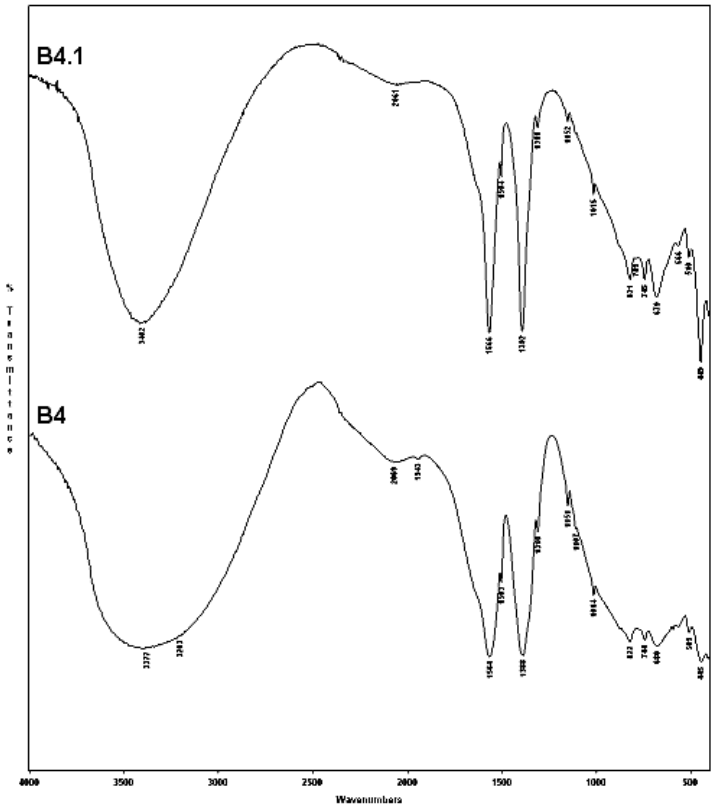

Figure 4.65. FTIR spectra of **B4** and **B4.1**.

Though not incorporated into the structure, boric acid treatment increased the thermal stability of **B4** by about 30 °C. Protonation of the interlayer OH groups possibly resulted in a disruption in the intermolecular hydrogen bonding interactions. Instead, stronger TP-layer interactions took place. This is reflected in the PXRD pattern of **B4.1** with a slight increase in crystallinity and its high BET surface area; 122.22 m^2/g, as well.

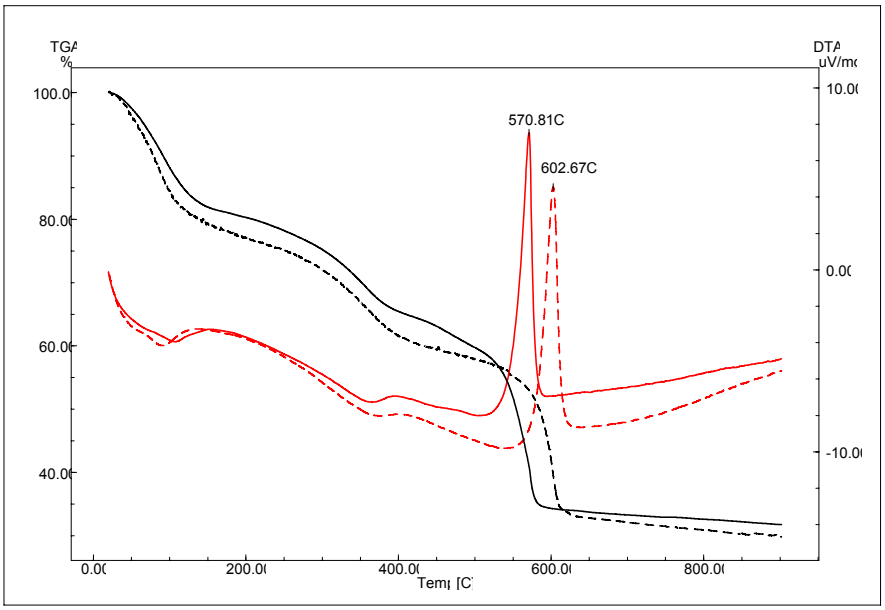

Figure 4.66. TGA (—) and DTA (—) curves of the **B4** (—,—) and **B4.1** (---,---).

4.2.5.2. Boric Acid-Exchange with Terephthalate-LDH at pH 9

When the boric acid treatment was performed at pH 9, the obtained LDH sample (**B4.2**) displayed a multi-phase PXRD pattern (Figure 4.67). The intense peaks correspond to terephthalate-LDH which has a 14.20Å basal spacing. The broad peaks correspond to smaller crystalline sized borate-intercalated LDH with a 11.30 Å basal spacing.

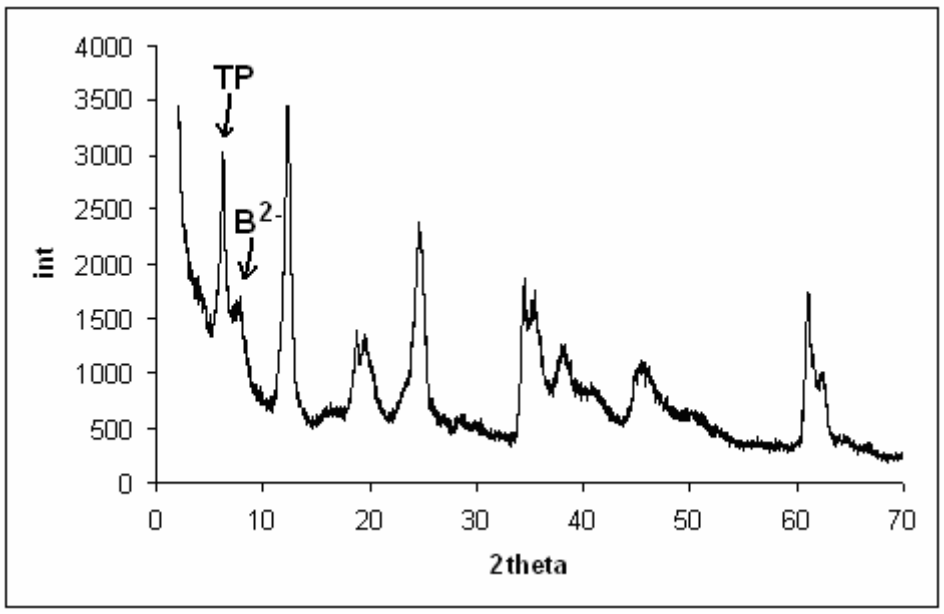

Figure 4.67. PXRD pattern of **B4.2**.

The FTIR spectrum in Figure 4.68 shows both terephthalate and borate peaks. Although the borate peaks were overlapped by the carboxylate peaks to some extent, ν_3 BO_3 stretching and B–OH plane bending vibrations (1499 cm^{-1}), ν_1 and ν_2 BO_3 (931 cm^{-1} and 816 cm^{-1}) and are recognized. 1150 cm^{-1} and 1012 cm^{-1} peaks may be assigned to ν_3 BO_4 or to C–O stretching vibrations and O–H bending and B–OH plane bending vibrations. The strong peak observed at 1558 cm^{-1} is the antisymmetric vibration of COO^-.

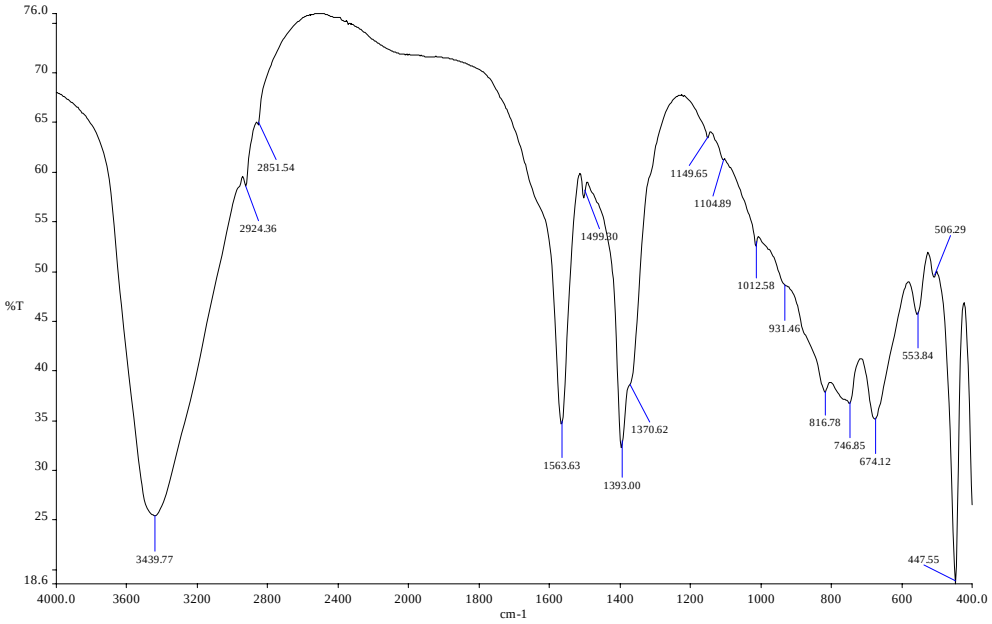

Figure 4.68. FTIR spectrum of **B4.2**.

The ^{11}B MAS NMR spectrum of sample **B4.2** confirms borate intercalation (Figure 4.69). However, the calculated triborate/tetraborate proportion is 59/41 and does not match with to a certain type of borate species. Both B_4^{2-} and B_3^- might have been intercalated.

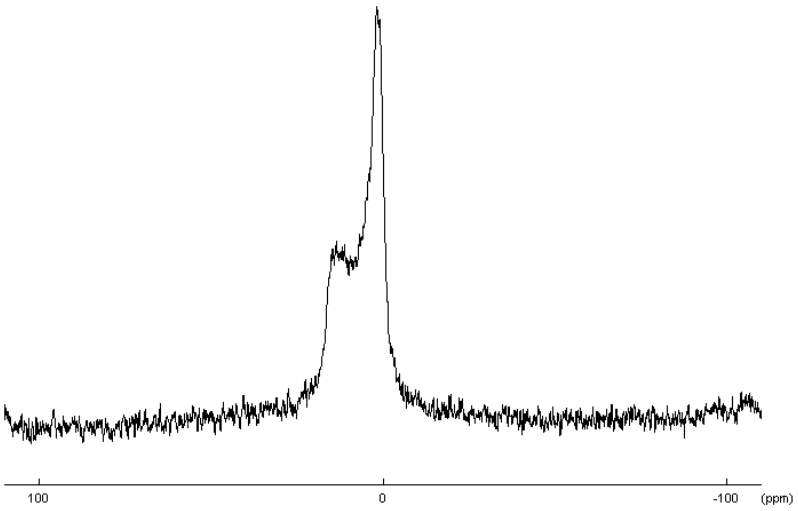

Figure 4.69. ^{11}B MAS NMR spectrum of **B4.2**.

^{13}C CP MAS NMR spectrum confirmed the presence of TP ions in **B4.2** (Figure 4.70). The three peaks at 173.3 ppm, 136.9 ppm and 128.5 ppm belong to the carboxyl, α and β carbon atoms of TP, respectively. An additional peak was observed at 170.7 ppm which can be assigned to the contaminating carbonate anions.

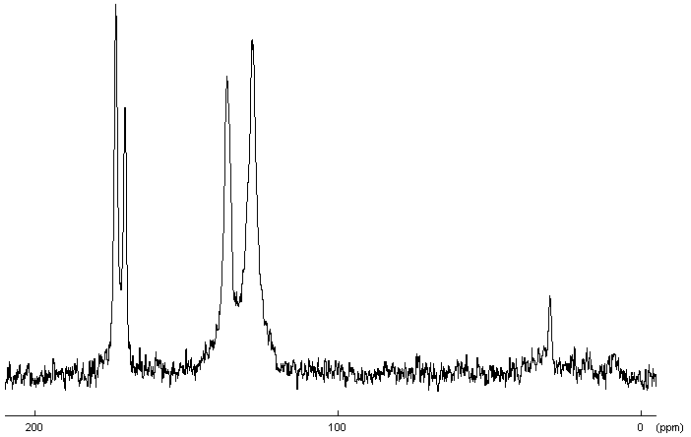

Figure 4.70. ^{13}C CP MAS NMR spectrum of **B4.2**.

The layers remained their integrity during ion-exchange at pH 9, no change was occurred in the positions of Al^{3+}ions. The single peak in the ^{27}Al MAS NMR spectrum of **B4.2** at 9.64 ppm shows octahedrally coordinated aluminum atom (Figure 4.71).

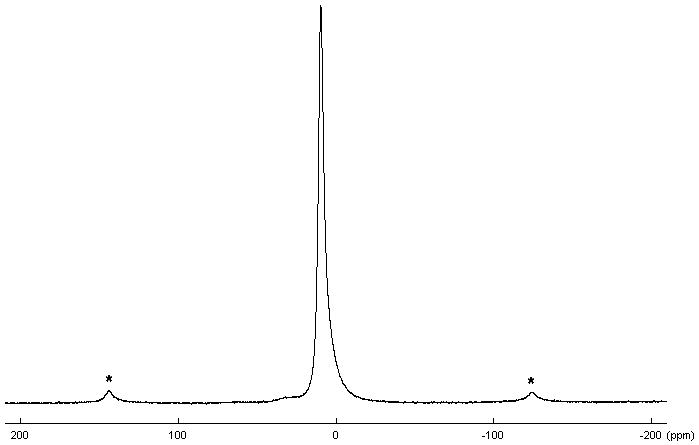

Figure 4.71. ^{27}Al MAS NMR spectrum of **B4.2** (*: spinning side bands).

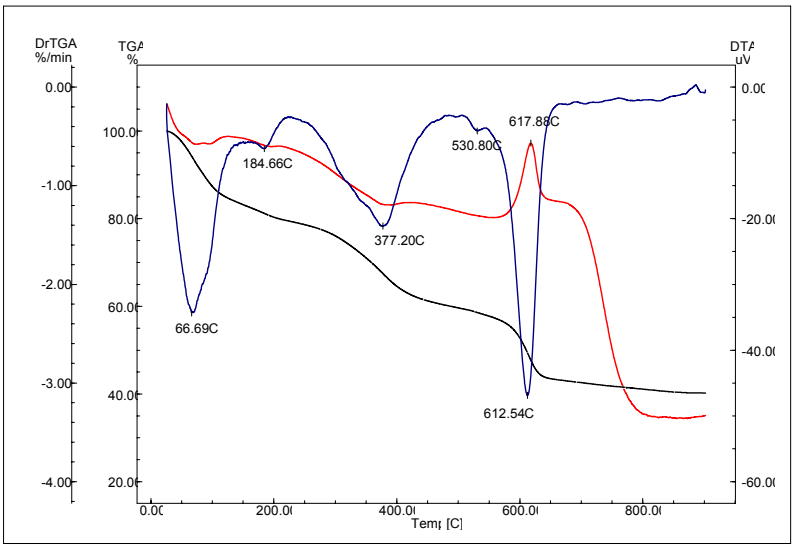

Figure 4.72. TGA(—), DrTGA (—) and DTA (—) curves of the sample **B4.2**.

As described in the previous sections, boron incorporation increased the thermal stability of the LDH. When compared with **B4**, the decomposition and the combustion of the terephthalate anions in **B4.2**, took place at higher temperatures than the samples **B4** and **B4.1** because of the intercalation of borate anions (Figure 4.72).

Table 4.7. Chemical compositions and some properties of borate-LDH samples prepared by boric acid exchange with terephthalate-LDH.

Sample	Formula	d_{003}(Å)	Mg/Al	B%
B4	$[Mg_{0.62}Al_{0.38}(OH)_2](TP)_{0.23}(NO_3)_{0.064}\cdot 0.6H_2O$	14.14	1.65	-
B4.1	$[Mg_{0.59}Al_{0.41}(OH)_2](TP)_{0.20}\cdot 0.7H_2O$	14.25	1.42	-
B4.2	$[Mg_{0.47}Al_{0.21}(OH)_2][Bxx]_{0.11}(NO_3)_{0.009}(TP)_{0.109}\cdot 0.7H_2O$	14.29	2.16	1.06
B4.3	$[Mg_{0.68}Al_{0.32}(OH)_2][B_4O_5.(OH)_4]_{0.033}(TP)_{0.035}(CO_3)_{0.091}\cdot 0.7H_2O$	7.43	2.08	1.47

4.2.5.3. Boric Acid-Exchange with Terephthalate-LDH at pH 12.0

Figure 4.73 shows the PXRD pattern of the sample (**B4.3**) prepared by exchanging **B4** with boric acid solution at pH 12. Highly crystalline carbonate and borate phases were observed in the pattern. The d_{003} reflections of the carbonate and borate phases are 7.43 Å (2θ=11.90°) and 8.51 Å (2θ=10.38°), respectively.

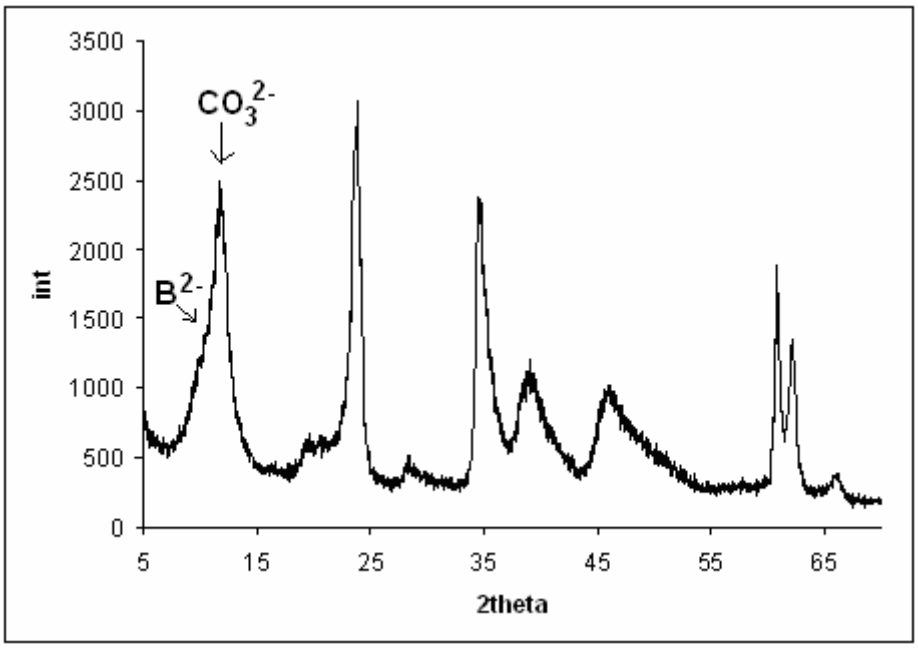

Figure 4.73. PXRD pattern of the sample **B4.3**.

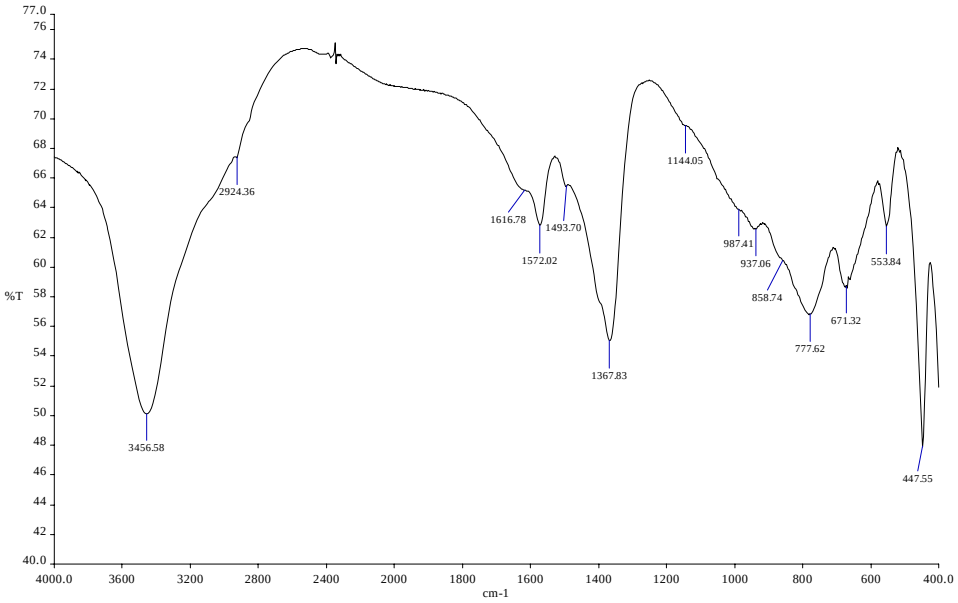

Figure 4.74. FTIR spectrum of the sample **B4.3**.

FTIR spectrum of the sample **B4.3** is shown in Figure 4.74. The strong peak observed at 1564 cm^{-1} in **B4**, which corresponds to the antisymmetric vibration of COO^- , is weakened and shifted to 1572 cm^{-1} because of the elimination of the interlayer terephthalate anions. Atmospheric CO_2 easily contaminates the LDH. The carbonate peak and the ν_3 BO_3 stretching peak together appeared at 1368 cm^{-1}. The peak at 1144 cm^{-1} can be assigned to ν_3 BO_4 stretching and B–OH in plane bending vibration.

^{11}B MAS NMR spectrum revealed that sample **B4.3** contains intercalated TB ions (Figure 4.75). The band at corresponds to the tetrahedrally coordinated boron atom and the band at corresponds to the trigonally coordinated boron atom. The calculated peak ratios of trigonal (14.32 ppm) to tetragonal (2.25 ppm) boron atoms is 1. Since the ion-exchange procedure was conducted at pH 12, monoborate intercalation is expected. With respect to ^{11}B MAS NMR analysis, it is stated that a transformation of borate species occurs after intercalation between the layers.

At high pH values, intercalation of tetraborate ions competes with terephthalate ions. Sample **B4.3**, involves carbonate, tetraborate and terephthalate intercalation

deduced from the analytical results given in Table 4.7 and the results of the PXRD and NMR data.

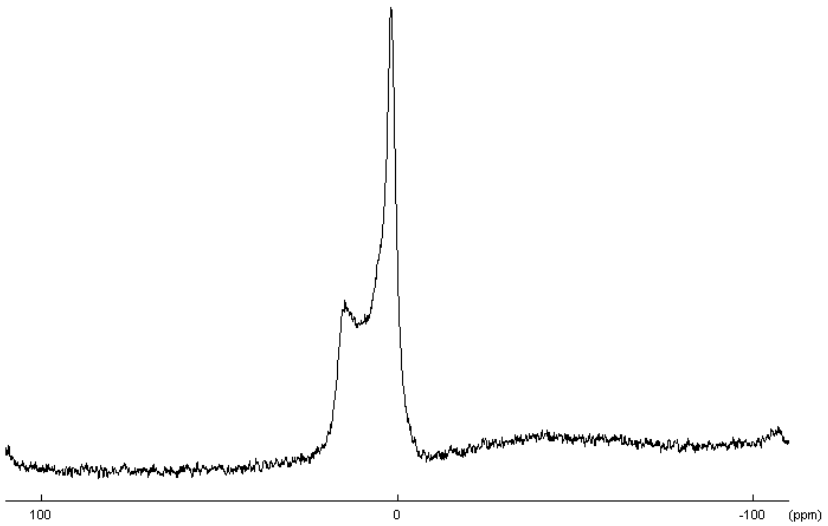

Figure 4.75. ^{11}B MAS NMR spectrum of **B4.3**.

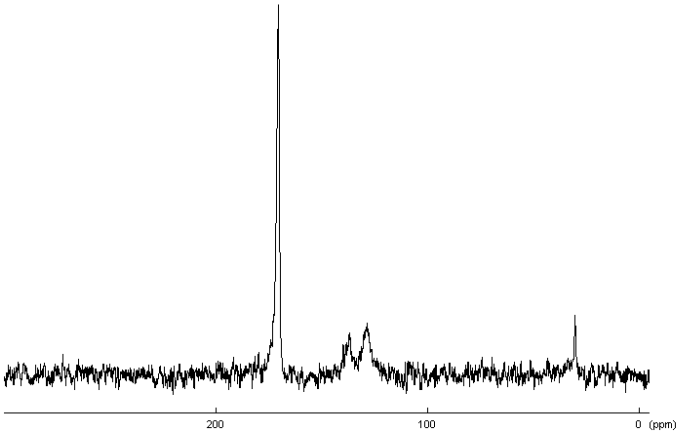

Figure 4.76. ^{13}C CP MAS NMR spectrum of **B4.3**.

Terepthalate intercalation and the carbonate contamination can be seen from the ^{13}C CP MAS NMR spectrum of **B4.3**, shown in Figure 4.76. The sharp and the most intense peak at 170.99 ppm corresponds to the interlayer carbonate ions. The peaks at 137.21 ppm and 128.45 ppm correspond to the C_α and C_β carbon atoms of TP ion. The carboxylate carbon peak of TP at 173.49 ppm was overlapped by the carbonate peak. Much of the terepthalate anions were expelled from the interlayer space by the borate and the carboxylate anions.

4.2.5.4. Tetraborate Anion-Exchange with Terephthalate-LDH

PXRD pattern of the sample **B4.4** is shown in the Figure 4.77. The basal spacing of the borate intercalated LDH is 11.05 Å and gives an interlayer space of 11.05 Å-4.8 Å= 6.25 Å. This space is large enough for the perpendicular intercalation of the tetraborate anion (Li et.al., 1996). Borate anions exchanged with some of the TP anions. This resulted in a disruption in the well-pillared structure of **B4** and a lower crystalline material was obtained.

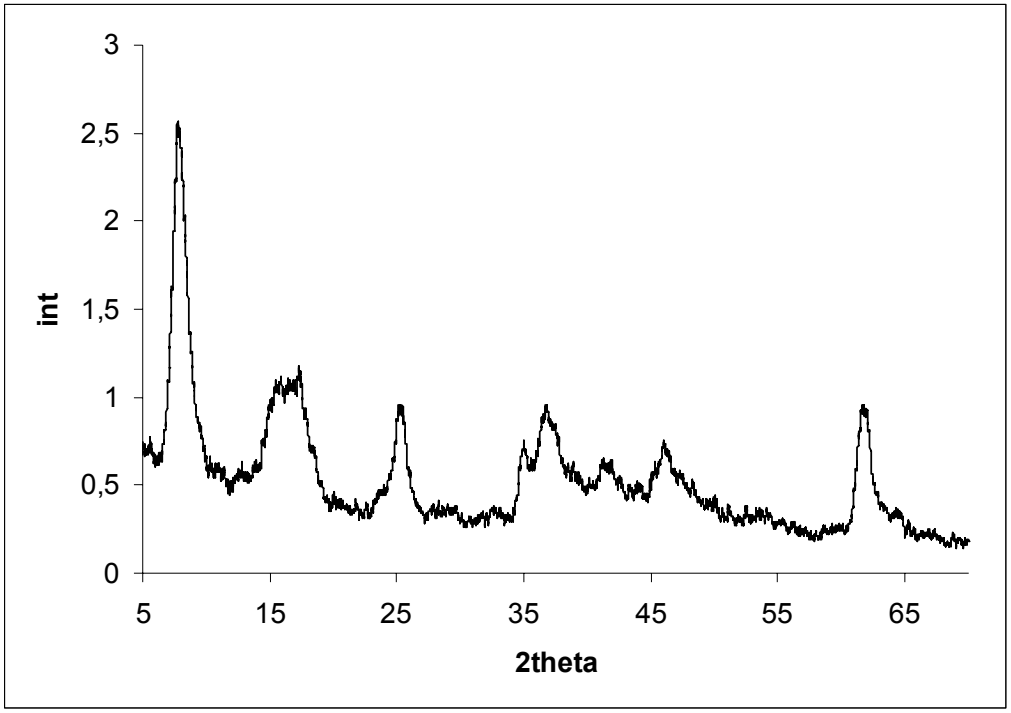

Figure 4.77. PXRD pattern of **B4.4**.

The second evidence of TB intercalation comes from the FTIR spectrum shown in the Figure 4.78. The bands at 1475 cm^{-1} and 1345 cm^{-1} are assigned to ν_3 BO_3 stretching and B–OH plane bending vibrations; at 936 cm^{-1} and 816 cm^{-1} to the ν_1 and ν_2 BO_3, respectively. The peak at 1013 cm^{-1} can be assigned to ν_3 BO_4 stretching and B–OH plane bending vibrations. The bands at 678 cm^{-1}, 574 cm^{-1} and 448 cm^{-1} are the LDH lattice bands (Li et.al., 1996). The weak peak observed at 1564 cm^{-1} corresponds to the antisymmetric vibration of COO^{-} due to the very low amount of remaining, horizontally oriented, interlayer terephthalate anions.

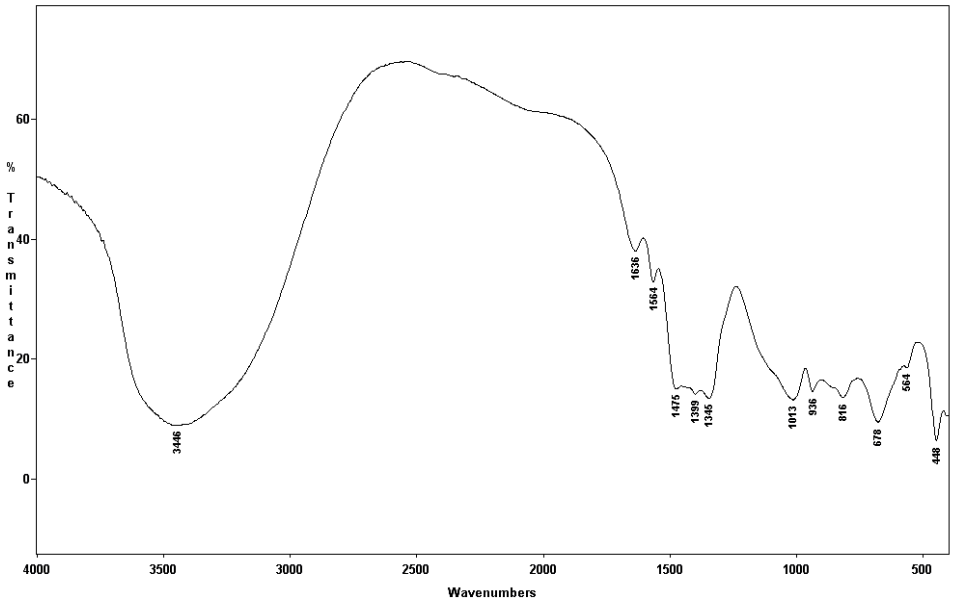

Figure 4.78. FTIR spectrum of **B4.4**.

^{11}B MAS NMR spectrum of the sample **B4.4** is shown on the Figure 4.79. The trigonal to tetragonal peak ratio was calculated from the spectrum as 1 confirming $B_4O_5(OH)_4^{2-}$ intercalation.

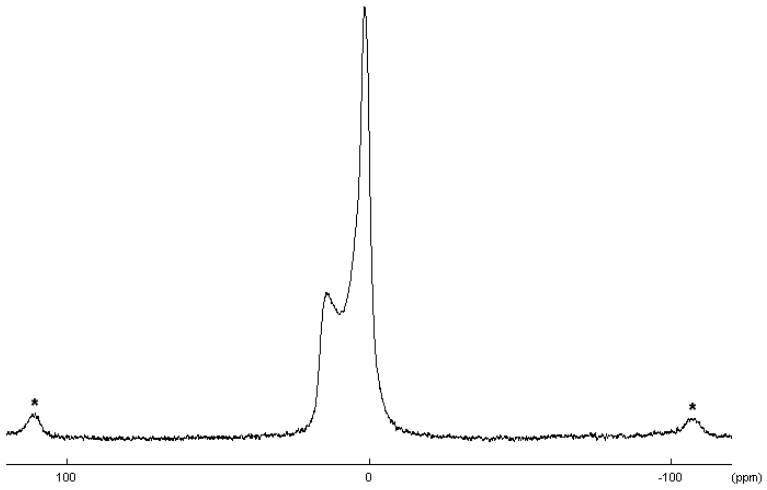

Figure 4.79. ^{11}B MAS NMR spectrum of **B4.4** (*Spinning side bands).

^{27}Al MAS NMR spectrum of the sample **B4.4** is given in Figure 4.80. The sample shows two types of aluminum atoms in the sample. The intense peak at 9.67 ppm is assigned to the octahedrally coordinated aluminum atom while the weak and broad peak observed at 32.99 ppm indicates some disorganization of the layered material (Bechara et.al., 2002).

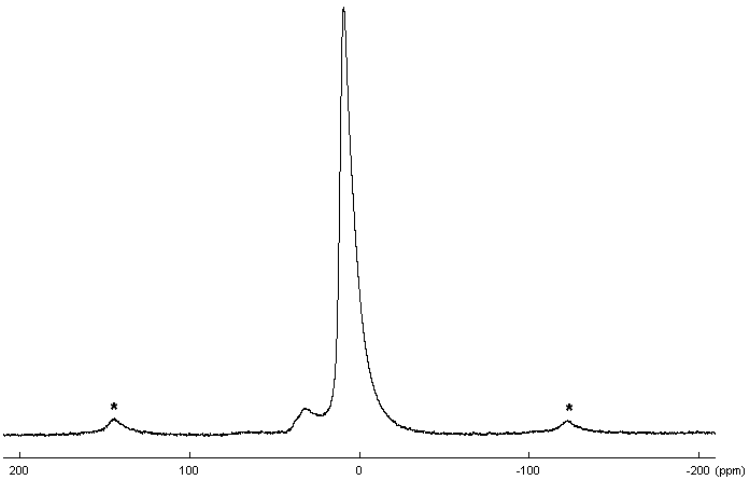

Figure 4.80. ^{27}Al MAS NMR spectrum of **B4.4** (* Spinning side bands).

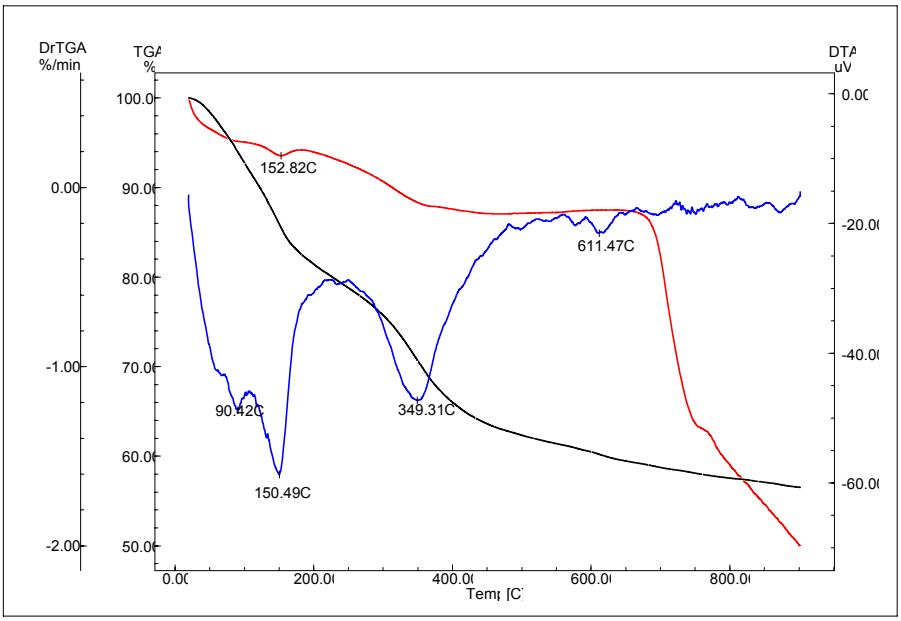

Figure 4.81. TGA (—), DrTGA (—) and DTA (—) curves of **B4.4**.

Thermal decomposition of the sample is seen in Figure 4.81. Dehydration of the sample was observed at 90°C and 150°C. Dehydroxylation of the basal layers and the borate ions took place up to 480°C. The peak around 611°C corresponds the lattice collapse.

4.3. Boron Removal From Aqueous Solutions by Nitrate-LDH

Much of the boron that is present in our environment is naturally occurring. High levels of boron are found in groundwater, in areas associated with geothermal

activity. Boron compounds are used in a wide range of industrial applications and high concentrations are reported in industrial discharges (Okay et al., 1985; Morales et al., 2000). The presence of boron in surface water is additionally a consequence of the discharge of boron-rich sewage arising from the use of some detergents containing boron as an excellent bleaching agent.

Although boron is essential for plant life and small amounts of boron are even claimed to be beneficial for human, high levels may be toxic. Boron concentration recommended for drinking water is 0.5 mg/L (WHO, 2003) and is 0.75 mg/L for irrigation water (Rowe et al., 1995). Since boron is not removed by common water treatment processes, research has focused on the introduction of new techniques for boron removal from water. Recently, Ferreira et al. (2006) reported boron removal from water by using a Mg-Al-NO_3-HT adsorbent synthesized via co-precipitation method. The authors stated that the boron content from solutions containing 5.2 mg/L was reduced to the limit recommended for drinking water, in 120 min. by using 2.5 grams of HT per liter. In the present thesis, boron uptake behavior of a Mg-Al- NO_3-LDH sample which was prepared under CO_2-free conditions has been described. The effects of calcination and contact time on boron removal from water have been investigated. The removal mechanism has been also discussed.

The Mg-Al-NO_3-LDH sample (**B1**) was used in boron removal experiments from boric acid and tetraborate solutions, before and after calcination at different temperatures. **B1** was heated in nitrogen at 400°C for 4 h in order to investigate the effect of calcination on the boron removal capacity. The calcination temperature was determined by the TG/DTA analysis and by following the changes in the XRD patterns on heating (Figure 4.82). TG/DTA analysis showed that interlayer and adsorbed water remove up to 250°C while decomposition of the interlayer anions and dehydroxylation of the layers take place at higher temperatures. This was confirmed by the XRD pattern of the sample calcined at 200°C that the layered structure is preserved at this temperature. Though the relative ratios of the 003 and 006 diffraction lines in the low 2θ values to those in the middle and at higher values of 2θ angles slightly increased, there were no significant change in the XRD pattern indicating that complete dehydration was not

achieved. On further heating; new phases, Mg(Al)O, started to form around 400°C and at 600°C a consequent increase in the oxide phases can be seen. The calcination temperature was chosen high enough to eliminate most of the nitrate ions and low enough to avoid sintering but permit the reconstruction of the original LDH structure by anion sorption. Therefore, boron removal was performed with a sample calcined at 400°C for 4h.

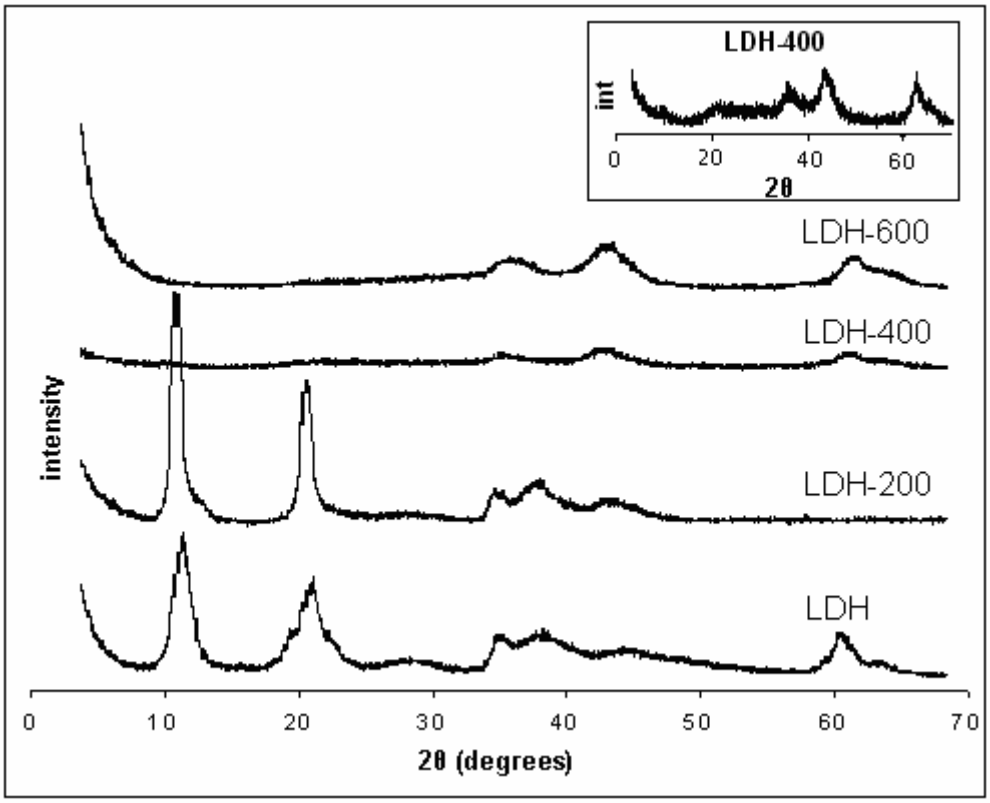

Figure 4.82. PXRD patterns of NO_3-LDH sample calcined at increasing temperatures.

No pH adjustment has been applied through the exchange process. While mixing **B1** or **CA-B1** (calcined B1) with the borate solutions, the suspension pH was noted as 9.0-9.5 with tetraborate and 7.0-7.5 with boric acid. Although the sample preparation was strictly conducted under nitrogen atmosphere, during borate exchange a minor amount of carbonate contamination was inevitable in some cases.

Figure 4.83 gives the adsorption percentages from boric acid and tetraborate solutions as a function of the amount of LDH. The results shown in the figure

demonstrate that adsorption percentage of borate species increases with increasing mass of LDH. Maximum adsorption (>95 %) is at 0.6 g LDH with both types of species. At higher adsorbent doses, the concentration of boron dropped below the detection limits. The experiment of adsorption as a function of contact time was conducted at a fixed dose of LDH with 50 mL 250 ppm boric acid solutions (Figure 4.84). The kinetic curve shows that adsorption is relatively fast in the first two hours then saturation is reached in about six hours.

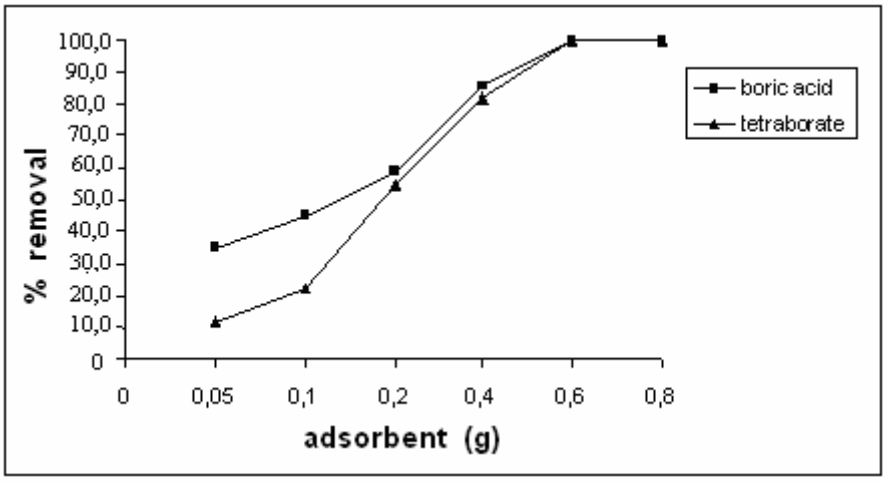

Figure 4.83. Adsorption of boric acid and tetraborate by intercalation as a function of LDH dose.

Table 4.8. Characterization of LDH samples before and after boron intercalation.

Sample	d_{003}(Å)	Surface Area (m^2g^{-1})	ζ pot. (mV)
NO_3-LDH	8.6	17	+0.8
BA-LDH[a]	9.6	-	-
TB-LDH[b]	10.7	48	-

[a] NO_3-LDH sample treated with boric acid solution for 5 h.

[b] NO_3-LDH sample treated with ammonium tetraborate solution for 5 h

A similar behaviour was noted with the CA-B1 sample which uptakes anions from solution through a reconstruction mechanism. Maximum boron removal (>95 %) was again obtained at 0.6 g dose. With respect to the uncalcined sample, the adsorption capacity increased only a smaller amount.

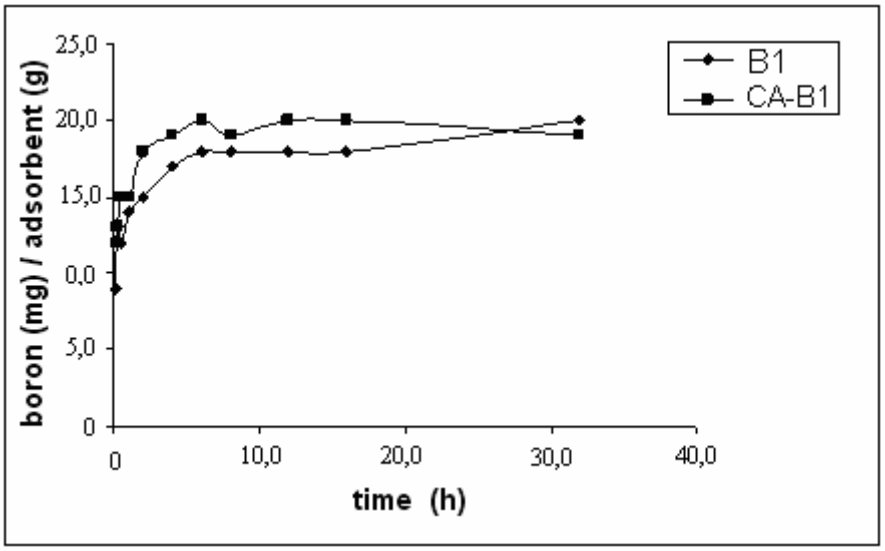

Figure 4.84. Adsorption of boric acid by B1 and CA-B1 samples by intercalation as a function of contact time.

The results showed that, the most possible mechanism of adsorption is anion exchange rather than surface adsorption for the following reasons: First of all, there was a significant increase in the interlayer distance of the LDH material after exchange with the borate ions (Table 4.8). Second, the Zeta potential value of the LDH sample at neutral pH was measured as +0.8 mV which means that the surface possesses no residual positive charge to attract the negatively charged borate anions. Third, assuming that the cross-sectional area of the tetraborate ion is approximately 36 $Å^2$ (Figure 4.24), the total surface area covered by a boron monolayer at 95% adsorption (with 0.6 g of LDH) would be ca. 10 m^2. As the BET surface area was determined to be 17 m^2g^{-1}, the whole surface could be covered by TB as a monolayer at this point. However, the surface area increased up to 48 m^2g^{-1} after tetraborate adsorption. It is clear that LDH transforms into a pillared material by tetraborate intercalation. As is well known, porosity is one of the features that distinguishes pillared compounds from intercalation compounds (Bravo-Suarez, 2004).

Anion exchange mechanism is also important for adsorption from boric acid solution where nonionized boric acid is in equilibrium with the ionized forms (Eqns. 2.1 and 2.2). Assuming that only anionic forms exchange with the interlayer nitrates and that the neutral forms adhere on the surface basic sites, about 40% of the total borate species would be adsorbed on the surface at 95% adsorption, approximating a cross-sectional area of 20 $Å^2$ for the boric acid molecule (Hingston, 1964). The surface adsorption should be much less than 40% since the d-spacing value considerably increased.

It is interesting to compare the relative efficiencies of the uncalcined and calcined-LDH samples towards boron removal. No considerable change was observed when the treatment was made with the CA-B1 sample which intercalates borate ions from solution through a reconstruction mechanism. Considerations based on the surface area are not representative in this case because the surface of the calcined sample will change during the sorption process.

The results revealed that more than 95% boron adsorption can be achieved with HT-like Mg-Al-NO_3-LDH materials.

5. CONCLUSIONS

This study demonstrates that Mg/Al-NO_3-LDH is a suitable host material for the intercalation of borate ions. The choice of the preparation conditions will depend on the desired specific features of the materials as follows:

- A simple and more productive method has been developed to prepare layered double hydroxides, by grinding the hydrated solid precursors manually in a mortar and washing the paste several times. This simple method is a synthetic breakthrough without the needs of heating/refluxing treatment, CO_2-free atmosphere nor solvent. The use of this method seems to be the best way to produce LDHs, not only due to costs involved, but also to their characteristic properties similar to the conventional LDHs, as verified by solid state MAS NMR technique.

The reaction proceeds faster by activating the reagents mechanically and only ten minutes grinding is sufficient to obtain a LDH paste. The role of hydrate water in the initial mixture is fundamental to the reaction. Crystal water of the starting metal salts promotes the reaction. This is assisted by the local heat generated during the grinding process.

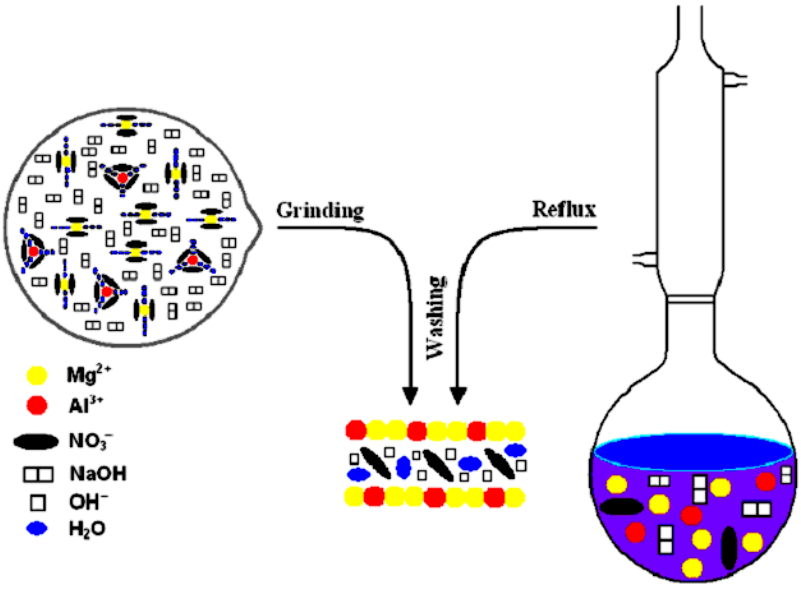

Scheme 5.1. Schematic representation of grinding and reflux methods for the preparation of LDHs.

The use of mechanochemically prepared LDHs in practical applications would be more profitable due to the ease in their synthesis. One possible application would be the removal of boron from aqueous wastes and then the use of thus-obtained boron-intercalated LDH as a flame-retardant agent, a cement/ceramic strengthener or an acid catalyst. The Mg,Al-NO_3-LDH sample prepared via mechanochemical activation was successfully tested for its ion exchange property with tetraborate ions. ^{27}Al MAS NMR analyses revealed that the layers are not disturbed during ion exchange. The borate intercalated derivative thus obtained may well be applied in acid-catalyzed reactions after calcination (Appendix).

- The co-precipitation method at constant pH was found effective in yielding LDHs with intermediate surface areas (30-50 m^2g^{-1}) and boron contents of ca. 3.5%, both with boric acid and tetraborate solutions but with a lower crystallinity in the latter case. Carbonate contamination is an important problem in this technique and also in the ion-exchange process even under CO_2-free conditions.

- The ion-exchange processes performed with boric acid solutions at varying pH values resulted in interesting chemical compositions. ^{11}B MAS NMR analyses revealed that the intercalated borate anions are not exactly the species expected to exist in the applied pH range. The monoborate anions, $B(OH)_4^-$, expected to exist at pH 12, were intercalated in the form of tetraborate anions, B_4^{2-}. The results showed that independently of the applied pH, the borate anions are intercalated as polyborate anions like B_3^-, B_3^{2-} or B_4^{2-}. PXRD results indicated parallel orientation of these polyborate species between the layers. It appears that the high electrostatic interactions between the layers and the interlayer anions and also the interlayer pH, which is different than the solution pH, induce the rearrangement of borate anions to the energetically more favored polyborate anions. Largest boron incorporation into the LDH structure was achieved at pH 9 with boric acid solution.

This new feature of the LDHs is reported the first time in this study. The chemical and physical nature and thus the pH of the interlayer space change during the ion exchange process with the removing and entering ions. The system acts as a nanoreactor in the transformation of borate species.

- The highest borate anion intercalations are achieved with the tetraborate anion exchange because mainly the tetraborate anions present in the solution after dissolving the ammonium tetraborate tetrahydrate. The tetraborate anions penetrate into the interlayer space perpendicular to the layers and two boron atoms intercalate per one plus charge from $[B_4O_5(OH)_4]^{2-}$ solution into the interlayer spaces of the TP- and AD- LDHs.

- The ion-exchange processes with tetraborate solutions, conducted both with nitrate- and carboxylate-LDHs, yielded products with relatively larger gallery heights, surface areas (ca. 80 m^2g^{-1}) and highest boron contents (ca. 6%). Each pillaring tetraborate anion neutralizes two Al^{3+} ions that are on adjacent layers by incorporating four boron atoms. The obtained LDHs displayed the highest thermal stabilities due to the pillaring in the structure by the vertical intercalation of tetraborate anions. The total collapse of the layered structure and transition to mixed oxide phases occurred at temperatures as high as 700°C. This method appears to be more advantageous for obtaining boron-intercalated LDHs to be used for catalytic purposes.

- LDHs expanded with carboxylate ions were shown to have no superiority in exchange with boric acid solution. Exchange reactions with adipate- and terephthalate-pillared LDHs were found effective at pH 9 and even at this pH the products obtained were no better than the products obtained by co-precipitation in terms of their *d* spacings, boron contents and thermal stabilities.

- HT-like Mg-Al-NO_3-LDH materials are environmental-friendly materials and can be successfully applied in boron removal from water for ecological purposes. More than 95% removal was achieved with a nitrate-LDH prepared in CO_2-free conditions. CO_2-free conditions are not strictly necessary for the anion exchange process as for the synthesis of the material itself, since percentage of boron removal was found to be sufficiently high. The products thus obtained contain considerable amounts of boron which makes them available for industrial purposes as well as catalysts for caprolactam conversion.

Boron removal by anion exchange took a long contact time (~6 h) which is indicative of a diffusion-controlled process. Calcination did not affect the removal process to a great extent. Optimum adsorbent doses (~0.6 g) and maximum adsorption capacities (~20 mg of Boron per gram LDH) were nearly the same for uncalcined and calcined samples.

- Finally, the following general conclusions may be drawn:

Co-precipitation method is a quick preparation method for boron-intercalation with LDHs containing small exchangeable nitrate ions.

For specific applications, boron intercalation should be performed via ion-exchange with tetraborate anions to obtain high boron-containing LDHs with well texture properties.

Preparation of LDHs mechanochemically by manual grinding appears to be a promising method in waste treatment processes in terms of green chemistry. This method may also allow the production of tailor-made materials for future biomedical applications since Mg/Al-NO_3-LDHs are biocompatible materials.

REFERENCES

Aamir I. K., O'Hare D., 2002, Intercalation chemistry of layered double hydroxides: recent developments and applications, J. Mater. Chem., 12, 3191-3198.

Adachi-Pagano M., Forano C. and Besse J-P., 2000, Delamination of layered double hydroxides by use of surfactants, Chem. Commun., 91-92.

Aisawa S., Hirahara H., Uchiyama H., Takahashi S. and Narita E., 2002, Synthesis and thermal decomposition of Mn-Al layered double hydroxides Journal of Solid State Chemistry, 167, 152-159.

Allmann R., 1968, Crystal structure of pyroaurite, Acta Crystallographica Section B, 24, 972.

Allmann R., 1970, Double layer structures with layer anions (ME(II)(1-X) ME(III)(X)(OH)2)(X+) of Brucite Type, Chimia, 24(3), 99.

Aramendia M. A., Borau V., Jimenez C., Marinas J.M., Ruiz J. R. and Urbano F.J., 2002, Comparative study of Mg/M(III) (M=Al, Ga, In) layered double hydroxides obtained by coprecipitation and the sol-gel method, Journal of Solid State Chemistry, 168, 156-161.

Battacharyya A. and Hall B. D., 1992, New triborate-pillared hydrotalcites, Inorg. Chem., 31, 3869-3870.

Bechara R., D'Huysser A., Fournier M., Forni L., Fornasari G., Trifiro F. and Vaccari A., 2002, Synthesis and characterization of boron hydrotalcite-like compounds as catalyst for gas-phase transposition of cyclohexanone-oxime, Catalysis Letters, 82, No 1-2, 59-67.

Bravo-Suarez J.J., Paez-Mozo E. A. and Oyama T., 2004, Microtextural properties of layered double hydroxides: a theoretical and structural model, Microporous and Mesoporous Materials 67, 1–17.

Bujd J. and Rode B. M., 1999, The effect of clay structure on peptide bond formation catalysis, Journal of Molecular Catalysis A: Chemical, 144, 129-136.

Burkhardt E.R., Matos K., 2006, Boron reagents in process chemistry: Excellent tools for selective reductions, Chem. Rev., 106(7), 2617-2650.

Cavani F., Trifiro F. and Vaccari A., 1991, Hydrotalcite-type anionic clays: preparation, properties and applications, Catalysis Today, 11, 173-301.

Cervilla A., Corma A., Fombs V.,Llopis E., Paşlanca P., Rey F. and Riberat A.,1994, Intercalation of $[Mo^{VI}O_2(O_2CC(S)Ph_2)_2]^{2-}$ in a Zn(II)-Al(III) layered double hydroxide host : A strategy for the heterogeneous catalysis of the air oxidation of thiols, J. Am. Chem. Soc., 116, 1595-1596.

Cheng S., Lin J.-T., 1992, Preparation and characterization of borate pillared anionic clays, in Expanded Clays and Microporous Solids, Ocelli M. L., and Robson H. E. Eds., van Nostrand Reinhold, New York, 170.

Cheng S., 1999, From layered compounds to catalytic materials, Catalysis Today, 49, 303-312.

Choy J-H, Kwak S-Y., Jeong Y-J. and Park J-S., 2000, Inorganic Layered double hydroxides as nonviral vectors, Angew. Chem. Int. Ed., 39, No.22, 4207-4211.

Crepaldi E. L., Tronto J., Cardoso L. P. and Valim J. V., 2002, Sorption of terephthalate anions by calcined and uncalcined hydrotalcite-like compounds, Colloids and Surfaces A: Physicochem. Eng. Aspects, 211, 103-114.

Cotton F.A. and Wilkinson G., 1980, Boron, Advanced Inorganic Chemistry, 4th Edition, John Wiley & Sons, New York, 289-325.

Coughlin J.R., 1996, Inorganic borates: Chemistry, human exposure, and health and regulatory guidelines, The Journal of Trace Elements in Experimental Medicine, 9, 137-151.

Dahlhoff G., Niederer J.P.M. and Hölderich W.F.,2001, ε-Caprolactam: new by-product free synthesis routes, Catal. Rev. Sci. Eng. 43(4) 381-441.

Del Arco M, Gutierrez S., Martin C., Rives V. And Rocha J., 2000, Effect of the Mg:Al ratio on borate (or slicate)/nitrate exchange in hydrotalcite, Journal of Solid State Chemistry, 151, 272-280.

Drezdzon M.A., 1988, Synthesis of isopolymetalate-pillared hydrotalcite via organic-anion-pillared precursors, Inorg. Chem., 27 (25), 4628-4632.

Feitknecht W. and Gerber M., 1942, Zur kenntnis der doppelhydroxyde und basischen doppelsalze III. über magnesium-aluminumdoppelhydroxyd, Helvetica Chimica Acta, 25, 131-137.

Ferreira O.P., de Moraes S.G., Duran N., Carnejo L., Alves O.L., 2006, Evaluation of boron removal from water by hydrotalcite-like compounds, Chemosphere, 62, 80.

Ferreira A., Ananias D, Carlos L. D., Morais C. M. And Rocha J., 2003, Novel microporous lanthanide silicates with tobermorite-like structure, J. Am. Chem. Soc., 125, 14573-14579.

Hernandez-Moreno M. J., Ulibarri M. A., Rendon J.L. and Serna C. J., 1985, IR characteristics of hydrotalcite-like compounds, Physics and Chemistry of Minerals, 12, 34-38.

Hingston F.J., 1964, Reactions between boron and clays, Aust. J. Soil Res., 2, 83-95.

Isupov V.P., Chupakhine L.E. and Mitrofanova R.P., 2000, Mechanochemical synthesis of double hydroxides, J. Mater. Synth. Process., 8, 251-253.

Khan A.I. and O'Hare D., 2002, Intercalation chemistry of layered double hydroxides: recent developments and applications, J. Matter. Chem., 12, 3191-3198.

Kim N. H., Malhotra S. V. and Xanthos M., 2006, Modification of cationic nanoclays with ionic liquids, Microporous and Mesoporous Materials, 96, 29-35.

Kloprogge J.T., 1998, Synthesis of Smectite and porous pillared clay catalysts: A review, Journal Porous Materials, 5, 5-41.

Kloprogge J. T., Frost R. L., 1999, Fourier transform infrared and raman spectroscopic study of the local structure of Mg-, Ni-, and Co-Hydrotalcites, Journal of Solid State Chemistry, 146, 506-515.

Kloprogge J. T., Hickey L. and Frost R. L., 2004, The effect of synthesis pH and hydrothermal treatment on the formation of zinc aluminum hydrotalcites, Journal of solid state chemistry, 177, 4047-4057.

Kloprogge J. T., 2005, Infrared and raman spectroscopy of naturally occuring hydrotalcites and their stynthetic equivalent: In the application of vibrational spectroscopy to clay minerals and layered double hydroxides, CMS Workshop Lectures, Vol. 13. Kloprogge J. T. ed., The Clay Mineral Society, Aurora, CO, 203-238.

Kooli F., Chisem I. C., Vucelic M. and Jones W., 1996, Synthesis and properties of terepthalate and benzoate intercalates of Mg-Al layered double hydroxides possessing varying layer charge, Chem. Mater., 8, 1969-1977.

Kovanda F., Jiratova K. and Kalouskova R., 2006, Synthetic hydrotalcite-like compounds, Advances in Chemistry Research, Volume I, Gerard F. L. ed., Nova Science Publisher Inc., New York, 89-139.

Kustrowski P., 2005, Influence of thermal treatment conditions on the activity of hydrotalcite-derived Mg-Al oxides in the aldol condensation of acetone, 78, 11-22.

Lee J.D., 1991, Concise Inorganic Chemistry, 4th Edition, Chapman & Hall, London, 359-398.

Li L., Ma S., Liu X., Yue Y., Hui J., Xu R., Bao Y. and Rocha J., 1996, Synthesis and characterization of tetraborate pillared hydrotalcite, Chem. Mater., 8, 204-208.

Liu Z., Ma R., Osada M., Iyi N., Ebina Y., Takada K. and Sasaki T., 2006, Synthesis, anion exchange, and delamination of Co-Al layered double hydroxide: Assembly of the exfoliated nanosheet/polyanion composite films and magneto-optical studies, J. Am. Chem. Soc., 128, 4872-4880.

Lopez T., Bosch P., Ramos E.,. Gomez R, Novaro O., Acosta D., and Figueras F., 1996 Synthesis and characterization of sol-gel hydrotalcites: structure and texture, Langmuir, 12, 189-192.

Malickia N., Mafra L., Quoineaud A.A., Rocha J., Thibaut-Starzyk F. and Fernandez C., 2005, Multiplex MQMAS NMR of quadrupolar nuclei, Solid State Nuclear Magnetic Resonance, 28, 13-21.

Meyn M., Beneke K and Lagaly G., 1990, Anion-exchange reactions of layered double hydroxides, Inorg. Chem., 29, 5201-5207.

Miyata S. and Kumura T., 1973, Synthesis of new hydrotalcite-like compounds and their physico-chemical properties, Chemistry Letters, 843-848.

Miyata S., 1983, Anion-exchange properties of hydrotalcite-like compounds, Clays And Clay Minerals, 31, No.4, 305-311.

Mohanambe L. and Vasudevan S., 2005, Anionic clays containing anti-inflammatory drug molecules: comparison of molecular dynamics simulation and measurements, J. Phys. Chem. B, 109, 15651-15658.

Morales G.V., Capretto M.E., Mercado Fuentes L. and Quiroga O.D., 2000, Dissolution kinetics of hydroboracite in water saturated with carbon dioxide, Hydrometallurgy, 58, 127-133.

Möhmel S., Kurzawski I., Uecker D., Müler D. And Geßner W., 2002, The influence of a hydrothermal treatment using microwave heating on the crystallinity of layered double hydroxides, Cryst. Res. Technol., 37, 4, 359-369.

Nascimento G. M., Barbosa P. S. M., Constantino V. R. L. and Temperini L. A., 2006, Benzidine oxidation on cationic clay surfaces in aqueous suspension monitored by in situ resonance raman spectroscopy, Colloids and Surfaces A: Physicochem Eng. Aspects, 289, 39-46.

Okay O., Güçlü H., Soner E. and Balkaş T., 1985, Boron pollution in the Simav River, Turkey and various methods of boron removal, Water. Res., 19, 857-862.

O'Leary S., O'Hare D. and Seeley G., 2002, Delamination of layered double hydroxides in polar monomers: new LDH-acrylate nanocomposites, Chem. Commun, 1506-1507.

Parker L.M., Milestone N.B., Newman R.H., 1995, The use of hydrotalcite as an anion absorbent, Ind. Eng. Chem. Res., 34, 1196.

Pinnavaia T. J., 1995, Nanoporous layered materials, Materials Chemistry, An Emerging Discipline, Ed. by Interrante L. V., Casper L. A. and Ellis A. B., Advances in Chemistry Series 245, American Chemical Society, Washinhton DC, 283-300.

Rao C.N.R., 1993, Chemical synthesis of solid inorganic materials, Materials Science and Engineering, B18, 1-21.

Reichle W. T., 1986, Anionic clay minerals, Chemtech, January 58-63.

Rowe D.R. and Abdel-Magid I.M., 1995, Handbook of Wastewater Reclamation and Reuse, , Lewis Publishers, Boca Raton, Florida, 550 pp.

Rives V., 2002, Characterization of layered double hydroxides and their decomposition products, Materials Chemistry and Physics, 75, 19-25.

Rives V. And Ulibarri M. A., 1999, Layered double hydroxides (LDH) intercalated with metal coordination compounds and oxometalates, Coordination Chemistry Reviews, 181, 61-120.

Roy D. R., Roy R. And Osburn E. F., 1953, The system MgO-Al_2O_3-H_2O and influence of carbonate and nitrate ions on the phasa equilibria, american Journal of Science, 251, 337-361.

Salentine C. G., 1983, High-field boron-11 NMR of alkali borates. Aqueous polyborate equilibria, 22 (26), 3920-3924.

Shi L., Li D., Wang J., Li S., Evans D.G., Duan X., 2005, Synthesis and smoke-suppressant properties of a borate-intercalated layered double hydroxide, Clays and Clay Minerals, 53, 294.

Simon J. M., Smith R. A., 2000, Borate Raw Materials, Glass Tech, 41 (6), 169-173.

Soofin C. and Lin J-T, 1992, Preparation and characterization of borate pillared anionic clays, Mario L. Ocelli, Harry E. Robson editors, Expanded Clays and Other Microporous Solids, Van Nostrad Reinhold, New York, 170.

Szwacki N.G., Sadrzadeh A. and Yakobson B.I., 2007, B_{80} fullerene:An *Ab Initio* prediction of geometry, stability, and electronic structure, Phys. Rev. Lett., 98, 166804.

Taylor H.F.W., 1969, Segregation and cation-ordering in sjogrenite and pyroaurite, Mineralogical Magazine, 37 (287), 338.

Ulibarri, M.A., Pavlovic I., Barriga C., Hermosin M.C., Carnejo J., 2001, Adsorption of anionic species on hydrotalcite-like compounds: effect of interlayer anion and crystallinity Appl. Clay Sci., 18, 17.

Vaccari A., 1998, Preparation and catalytic properties of cationic and anionic clays, Catalysis Today, 41, 53-71.

Vaccari A., 1999, Clays and catalysis: a promising future, Applied Clay Science, 14, 161-198.

Woods W.G., 1996, Review of possible boron speciation relating to its essentiality, The Journal of Trace Elements in Experimental Medicine, 9, 153-163.

Weaver C. E., 1989, Clays, Muds, and Shales, (Developments in Sedimentology 44), Elsevier Science Publishers, Amsterdam-Oxford-New York-Tokyo, 1.

Weicher F.H., Standard Methods of Chemical Analysis, Part B, sixth ed., Van Nostrand, Princeton, New Jersey, 1963, 2406– 2407.

Weir M.R. and Kydd R.A., 1998, Synthesis of metatungstate pillared layered double hydroxides with variable layer composition. Effect of the Mg:Al ratio on the microporous structure, Micropor. Mesopor. Mater., 20, 339-347.

Weir M. R., Moore J. and Kydd R. A., 1997, Effects of pH and Mg:Ga ratio on the synthesis of gallium-containing layered double hydroxides and their polyoxometalate anion exchanged products, Chem. Mater., 9, 1686-1690.

WHO, 2003, Guidelines for drinking water quality, Geneva, World Health Organization (WHO/SDE/WSH/03.04/54).

Yıldız A. and Genç Ö., 1993, Enstrümantal Analiz, Hacettepe Üniversitesi Yayınları A-64, Ankara, 111-117.

APPENDIX

Catalytic Applications of Borate-LDHs in Octanol Decomposition Reaction

The use of mechanochemically prepared LDHs in practical applications would be more profitable due to the ease in their synthesis. One possible application may be their use in waste treatment processes to remove anionic pollutants and the subsequent materials may be further used for miscellaneous purposes. For example, removal of boron from aqueous wastes by a LDH simply prepared as described in Section **3.5** and then the use of thus-obtained boron-intercalated LDH as a flame-retardant agent or an acid catalyst is expected to be beneficial in both ecological and industrial aspects.

HT-type LDHs have been reported to be basic catalysts (Reichle, 1985). On the other hand, borate pillared LDHs contain acid sites suitable for the acid catalysed reactions such as Beckmann rearrangement of cyclohexanone oxime to caprolactam and alcohol conversion reactions (Lin et al., 1999; Bechara et al., 2002). In order to verify the usability of mechanochemically prepared LDH sample in catalytic reactions, LDH samples prepared by co-precipitation (**B1**) and by mechanochemical activation (**B2**) were first tested for their anion exchange properties with borate ions as described in Sections **3.4.1.4** and **3.5.1**. The boron intercalated derivatives thus obtained (**B1.4** and **B2.1**) and the plain **B1** were then applied in alcohol conversion reaction comparatively, after being calcined under N_2 atmosphere at 450°C for 3 hours*.

Octanol conversion reaction was conducted as an indicator reaction. 0.1g **B1.4** (**B2.1** or **B1**) was refluxed with 2.6 mL 2-octanol at 175°C for 12 hours. The resulting suspension was shaked with 1 mL 1 M Na_2CO_3 in order to release the products/reactants immobilized on the catalyst surface and in the interlayer regions. 2.5 mL ether was then added to extract the organic substances and the ether phase was analyzed by a GC-MS instrument.

As shown in Table, the catalytic performances of boron-intercalated samples in the dehydration of octanol to octene are comparatively low with respect to the LDH

sample which does not contain boron (**B1**). The average low activities of **B2.1** and **B1.4** in octanol conversion and octene selectivity can be attributed to the strong electrostatic interactions between the anionic and cationic layers in the boronated LDHs that result in a grafting in the structure during thermal treatment and a reduction in the acidity of the system.

Table. Results of Catalytic Octanol Decomposition Reaction

Catalyst	Octene (%)	Octanone (%)
B2.1	12.2	-
B1.4	1.05	4.99
B1	34.7	1.03

Highest conversion in the catalytic reaction was obtained with the plain LDH (**B1**) under the applied reaction conditions. Apparently, the calcined **B1** undergoes a rapid uptake of octanol molecules and a reconstruction of the LDH structure by making hydrogen bonds through the octanol molecules in the interlayer region where the catalytic reaction proceeds over interlayer acid sites more effectively. Although the boron incorporated into the mechanochemically synthesized LDH sample (**B2.1**) worked with a lower conversion, it showed a significant selectivity in octene formation. This finding deserves further analysis and optimization of catalytic reaction parameters for a better performance.

*****Thermal analyses of the LDHs revealed that dehydroxylation of the layers continue up to 600°C. Small exothermic peaks were detected on the DTA curves around 700°C due to the complete lattice collapse and transition to mixed oxide phases. Therefore, the samples were calcined at 450°C for three hours to ensure only dehydration. Catalytic reactions were started immediately after calcination to prevent carbonate poisoning.